PATHOPHYSIOLOGY OF INTERLEUKIN-TWO INDUCED NEUROLOGIC TOXICITY

by

Yetty Yennawati Irwan

A dissertation submitted to the faculty of
The University of Utah
in partial fulfillment of the requirements for the degree of

Doctor of Philosophy

in

Experimental Pathology

Department of Pathology

The University of Utah

December 2010

Copyright © Yetty Yennawati Irwan 2010

All Rights Reserved

The University of Utah Graduate School

STATEMENT OF DISSERTATION APPROVAL

The dissertation of **Yetty Yennawati Irwan**

has been approved by the following supervisory committee members:

Wolfram E. Samlowski	, Chair	**9/29/2009** Date Approved
John H. Weis	, Member	**9/29/2009** Date Approved
Lorise C. Gahring	, Member	**9/29/2009** Date Approved
Glen R. Hanson	, Member	**9/29/2009** Date Approved
Matthias Schabel	, Member	**9/29/2009** Date Approved

and by **Peter E. Jensen** , Chair of the Department of **Pathology**

and by Charles A. Wight, Dean of The Graduate School.

ABSTRACT

Interleukin-2 (IL-2) induces neuropsychiatric toxicity in patients, which is often dose-limiting and currently not well understood due to lack of suitable experimental methods. We therefore evaluated a number of experimental techniques to quantify changes in the brain vasculatures in a well-characterized IL-2 treatment murine model. Direct measurement of small molecule accumulation, wet versus dry brain weight comparison, and proton density MRI lacked sensitivity and reliability to detect small changes in the brain water content. Successful methods included dynamic contrast enhanced (DCE) MRI and immunohistochemistry using specific endothelial markers to identify vasodilation in carefully matched regions of the mouse brain. Both methods demonstrated significant vasodilation of the brain blood vessels following IL-2 treatment. DCE MRI further indicated that IL-2 increased brain blood vessel permeability to the contrast agent. Using these techniques, we evaluated the mechanism involved in IL-2-induced neuropsychiatric toxicity. We initially established that mice exhibited behavioral changes following IL-2 treatment, indicating that IL-2 affected the brain in the murine model as in patients. The spontaneous movement, rearing, and grooming significantly decreased by day 2 following IL-2 treatment in the C3H/HeN mice, while the motor strength and coordination of these mice were affected by day 4. Vasodilation and microvascular permeability evaluated by immunohistochemistry and DCE MRI were not

observed until day 4, suggesting that IL-2-induced behavioral changes occurred before detectable vasodilation and microvascular permeability. Further experiments established that IL-2 mediates its cardiovascular toxicity via its receptor on leukocytes, instead of a direct action on endothelial cells. This finding supports the concept that the dose-limiting toxicities associated with IL-2 therapy are mediated by the secondary inflammatory cytokine storm. We therefore evaluated the role of nitric oxide (NO) produced by endothelial NO synthase (eNOS) in vascular changes in the brain following IL-2 treatment. The data indicated that activation of eNOS-mediated changes in vascular permeability and vasodilation correlate with motor function changes induced by IL-2, while changes in spontaneous behavior following IL-2 treatment are not mediated by NO.

To my father who always believed in me

TABLE OF CONTENTS

LIST OF FIGURES

LIST OF ABBREVIATIONS

IL	Interleukin
NK	Natural killer
IL-2R	IL-2 receptor
IL-2Rα	IL-2R alpha chain
IL-2Rβ	IL-2R beta chain
γc	Gamma chain
JAK	Janus kinases
STAT	Signal transducers and activators of transcription
LAK	Lymphokine-activated killer
TNF	Tumor necrosis factor
IFN	Interferon
GM-CSF	Granulocyte-macrophage colony-stimulating factor
VLS	Vascular leak syndrome
NO	Nitric oxide
cGMP	Cyclic guanosine monophosphate
sGC	Soluble guanylate cyclase
iNOS	Inducible nitric oxide synthase
CNS	Central nervous system

NOS	Nitric oxide synthase
nNOS	Neuronal NOS
eNOS	Endothelial NOS
mtNOS	Mitochondrial NOS
NADPH	Nicotinamide adenine dinucleotide phosphate
FAD	Flavin adenine dinucleotide
FMN	Flavin mononucleotide
BH_4	Tetrahydrobiopterin
O_2	Oxygen
CaM	Calmodulin
Ca^{2+}	Calcium
Ser	Serine
Thr	Threonine
O_2^-	Superoxide
$ONOO^-$	Peroxynitrite
MRI	Magnetic resonance imaging
BBB	Blood-brain barrier
DCE	Dynamic contrast enhanced
ICU	Intensive care unit
NaFl	Sodium fluorescein
Iso-B4	Isolectin GS-IB_4
vWF	von Willebrand Factor
ROI	Region of interest

SI	Signal intensity
PD	Proton density
f^{PV}	Fractional plasma volume
K^{PS}	Endothelial transfer coefficient
PS	Permeability surface area product
SEM	Standard error of the mean
WT	Wild-type
BM	Bone marrow
KO	Knockout

ACKNOWLEDGMENTS

First and foremost, I would like to thank Dr. Wolfram Samlowski, my PI, for his mentorship. I am grateful for the opportunity to do this research in his lab. It has been a very challenging project and a tough journey, but we made it. I thank him for all his support and advice, and for reviewing all my papers. His work ethic is definitely an inspiration to me.

I want to thank John McGregor, our lab manager, for all his consultations whether in research or in life. I thank him for his support throughout my many difficult times. His jokes always make me laugh and he taught me so many American metaphors. I also thank him for ordering all my research reagents and necessities, for helping me in some experiments, and for proofreading all my writings. I could not have asked for a better lab manager than him. Next I want to thank Shweta Tharkar, our current research assistant in the lab, for all her help. She is very organized and it is good to have her in the lab. I also would like to thank the previous members of the lab, Courtney McKinney and Muralidhar Kondapaneni. Courtney was our previous lab technician. She is an expert in immunohistochemistry and taught me the technique. Murali was a previous graduate student in our lab. He laid down the ground work for nitric oxide's contribution in IL-2 induced toxicities. Both Courtney and Murali were good coworkers and friends to me.

I would like to thank my supervisory committee members – Dr. Glen Hanson, John Weis, Lorise Gahring, and Matthias Schabel – for their constructive criticisms and

experimental ideas. I thank Dr. Gach, who operates the MRI scanner at the Nevada Cancer Institute and Gopalkrishna Veni, who used to work for him. Gopal helped me analyzing the proton density MRI images and later helped me getting my DCE MRI images from the scanner. I also thank Yi Feng for his technical advice in DCE MRI and his MATLAB codes to analyze the DCE MRI data. I would like to thank Dr. James Symanowski, the Head of Biostatistics at the Nevada Cancer Institute, for his help in statistical analysis of the immunohistochemistry and behavioral data. I thank Dr. Victor Laubach for his generous donation of iNOS knockout mice and Novartis for its donation of IL-2 to our lab.

Last but not least, I would like to thank my family and friends for their support throughout my graduate school journey. I would not have made it without them. My father, who passed away 5 years ago, remains my constant motivation to get this PhD degree. I cannot be more thankful to my mother, who always makes the long trip from Indonesia to the US at least once a year to keep me company, cook for me, and do all the housework so I can focus with the lab work. I also thank my American families: Dad (Harry), Mom (Cathy), Molly, Lee, and Sandy Stoltzfus. They were my host families when I arrived in the US 12 years ago, but they always treat me like their own. Without them, I may not have stayed in the US and obtained this higher education. Finally, I would like to thank God for all His blessings, especially a beautiful daughter, who kept me company during the final stage of achieving this degree and became an extra motivation for me. I love you very much, Fei Fei.

CHAPTER 1

INTRODUCTION

Interleukin-2

Interleukin-2 (IL-2) was first identified in 1976 as the active component of a lymphocyte conditioned medium that supported the long-term growth of T lymphocytes *in vitro* (1) and hence named T-cell growth factor (TCGF). In 1981, it was characterized as a variably glycosylated 15,500 Dalton protein (2). IL-2 was then purified to homogeneity (3) and its cDNA was cloned in 1983 (4). The gene that expresses IL-2 spans four exons and is located on chromosome 4q26–q27 in human or chromosome 3 in mouse (5). The human cDNA encodes a polypeptide composed of 153 amino acids, with the first 20 amino acids serving as a signal sequence and are cleaved prior to secretion. The murine amino acid sequence is about 60% homology to the human sequence. Both are secreted as single polypeptides with molecular weights of 15–17 kDa (6). The size and charge variability of IL-2 depends on the degrees of glycosylation, which have no effect on activity (6). Therefore, recombinant IL-2 is equally effective in stimulating T-cells proliferation as glycosylated IL-2. Recombinant human IL-2 has been found to be effective in mice.

The crystal structure of IL-2 was determined in 1991 (7), which showed that IL-2 folds into four α (alpha) helical domains (named A, B, C, and D) connected by 3 loops (A–B, B–C, and C–D loops) and has a single disulfide bridge (Fig. 1.1). The first and last two α helices are each connected by a long crossover loop, resulting in an “up-up-down-down” topological structure because the first two α helices (the A and B helices) appear to orient in an upward direction while the last two α helices (C and D) can be oriented in a downward direction as viewed from the NH_2- to COOH-terminal. IL-2 also has two more small α helices, named A’ and B’.

Figure 1.1

The crystal structure of IL-2 generated using RasMol software.

In the immune system, a small amount of IL-2 is mainly secreted by antigen-activated T-helper (Th1) lymphocytes. Additionally, dendritic cells, monocytes, natural killer (NK) cells, and activated $CD8^+$ T-cells can also produce IL-2. In the normal brain, IL-2 expression is extremely low and regionally restricted. IL-2 in the brain is produced by the glial cells, which include microglial cells, oligodendrocytes, astrocytes, and ependymal cells.

IL-2 Receptor

IL-2 was the first cytokine identified to mediate its effects via a cell surface receptor that has similar characteristics to those of classic hormone receptors, including stereospecificity, saturability, and high affinity (8). IL-2 binds to a well-characterized heterotrimeric receptor on its target cells (9). The IL-2 receptor (IL-2R) is composed of three noncovalently linked distinct chains: 1) the alpha chain (IL-2Rα, CD25), 2) beta chain (IL-2Rβ, CD122), and 3) a common cytokine receptor gamma chain (γc, CD132) (10-18). IL-2Rα is essential for specific binding of IL-2. By itself, IL-2Rα binds to IL-2 with a low affinity (binding affinity $K_d \approx 10$ nM) and does not play a role in signal transduction (19). IL-2Rβ alone also has a very low affinity ($K_d \approx 100$ nM) whereas isolated γc has no detectable binding affinity to IL-2, but the complex of IL-2Rβ and γc binds to IL-2 with an intermediate affinity ($K_d \approx 1$ nM) (20). This two-part receptor complex is found on macrophages, NK cells, and resting T cells (9). Upon IL-2 binding, IL-2Rβ and γc complex is sufficient and necessary for effective signal transduction via the heterodimerization of their cytoplasmic domains (21-22). A complex of all three IL-2R subunits (IL-2Rα, IL-2Rβ, and the γc) binds to IL-2 with high affinity ($K_d \approx 10$ pM)

and is the receptor form found on activated T cells (18) that mediates most biological activities of IL-2 *in vivo* (9). There is homology between the mouse IL-2R and human IL-2R. In the mouse brain, IL-2 receptors have been found on microglial cells and on myelin (23-24), mainly in the hippocampus, frontal cortex, and striatum regions (25).

The recently elucidated structure of the IL-2 and IL-2R quaternary complex revealed many details of the interactions between IL-2 and its various receptor complexes. The structure of IL-2Rα and its mode of interaction with IL-2 differ from the typical cytokine receptor (26). IL-2Rα folds into two "sushi-like" domains, which form five-stranded β-sheet sandwiches (27). A long connecting peptide of the IL-2Rα, between its globular head and the transmembrane segment, allows its binding domain to extend away from the cell surface and reach the dorsally located binding site on IL-2 (28), capturing the IL-2 molecule and setting it against the βγ complex. IL-2Rβ and γc, on the other hand, contain a "WSXWS" motif in the C-terminal domain and two disulfide bonds in the N-terminal domain that are characteristics of the class I cytokine receptor superfamily (29). They consist of N- and C-terminal fibronectin-III domains, which are characterized by a β-sandwich sheet containing seven antiparallel strands arranged in a three-on-four topology, and their bases converge to form a Y shape where IL-2 binds to (28). The formation of the IL-2 and IL-2R quaternary complex is mediated by four binding sites: IL-2/IL-2Rα, IL-2/IL-2Rβ, IL-2/γc, and IL-2Rβ/γc (28). IL-2/IL-2Rα interface is the largest of the three interfaces with a hydrophobic center, a polar periphery featuring five ion pairs, and seven hydrogen bonds between IL-2 and IL-2Rα (27). Interestingly, IL-2Rα does not associate with IL-2Rβ or γc and the three contact sites on IL-2 normally do not overlap with each other, except for a small region of helix A that

wedges tightly between IL-2Rβ and γc to form a three-way junction for a composite binding site for the final γc recruitment (27). There are only minor conformational changes observed in the IL-2 structure upon forming a quaternary complex with IL-2R, the most significant is the arrangement of the BC loop due to crystal-packing interactions (27).

Whereas IL-2Rα chain (CD25) is specific to the IL-2 receptor, IL-2Rβ is also a subunit of the IL-15 receptor while the γc is shared by IL-4, IL-7, IL-9, IL-15, and IL-21 receptors (30). Hence the redundancy of IL-2 functions with those of other cytokines sharing a common γc in their receptors. IL-2 exerts its diverse activities by binding to different receptor complexes of IL-2R depending on which components of the receptor are expressed on the cell surface. A crucial number of IL-2 receptors must be activated before a single T cell will make the irreversible, all-or-none commitment to pass through the G_1 restriction point to undergo proliferation (31-32). A number of other cells (i.e.,monocytes, fibroblasts, keratinocytes, and perhaps endothelial cells) express IL-2Rβ and γc on their cell surface, but it is not clear whether IL-2 binds to these receptors and plays a physiological role in these cells.

Signaling Pathways and Biological Activities of IL-2

IL-2 binding to IL-2R activates numerous intracellular tyrosine kinases, leading to a rapid increase in tyrosine phosphorylation of many cellular proteins and subsequent increase in expression of several nuclear proto-oncogenes critical for proliferation (33). The cytoplasmic domains of IL-2Rβ and γc associate with Janus kinases JAK1 and JAK3, respectively (34-35). IL-2 binding to IL-2R activates these Janus kinases, leading

to phosphorylation and concurrent induction of STAT (signal transducers and activators of transcription) proteins (36). Although several STAT-like DNA binding activities seem to be involved in the IL-2 signaling pathway (37-38), activation of STAT5 protein in particular has been functionally linked to the IL-2Rβ subunit via a redundant tyrosine-containing motif found in several cytokine receptors (39-41). Upon phosphorylation, STAT5 proteins dissociate from the IL-2Rβ, dimerize, and translocate to the nucleus where they promote the transcription of IL-2 specific genes. Additionally, IL-2 binding to IL-2R also triggers other signaling pathways, such as phosphorylation of the Src-family protein tyrosine kinases Lck (leukocyte-specific protein tyrosine kinase) and Syk (spleen tyrosine kinase), expression of the anti-apoptotic protein B-cell lymphoma 2 (Bcl-2), stimulation of the phosphatidylinositol-3-kinase–AKT pathway, and stimulation of the Ras–Raf-mitogen-activated-protein-kinase pathway, leading to the activation of Fos- and Jun-containing transcription factor complexes (42).

IL-2 plays a key role in cell-mediated immunity (43). At low concentrations (10-100 IU/ml), IL-2 is a potent autocrine T-cell growth factor and is the key cytokine responsible for rapid activation, clonal expansion, and differentiation of antigen-activated T-cells (44). It also plays a role in the proliferation and survival of mature B-cells, and in enhancing the phagocytic capability, oxidative burst, and microbicidal activities of monocytes (i.e., macrophages and neutrophils). Moreover, IL-2 promotes the proliferation of NK cells and activates their cytotoxic function. High concentrations of IL-2 (> 600 IU/ml) rapidly activate a population of NK cell-derived cytotoxic lymphocytes named lymphokine-activated killer (LAK) cells (45). These cells are termed “nonspecific” killer cells because their cytotoxicity does not require antigen presentation

in the context of self-MHC on target cells (46). Thus LAK cells demonstrate killing against almost all cultured and freshly isolated malignant cells (47-48), including multidrug-resistant cancer cells (49). Activation of lymphocytes by IL-2 also strongly induces production of inflammatory cytokines. These secondarily released cytokines include IL-2, IL-3, IL-4, IL-5, IL-6, IL-9, IL-10, IL-12, IL-13, tumor necrosis factor (TNF), interferon (IFN)-γ, lymphotoxin (LT), and granulocyte-macrophage colony-stimulating factor (GM-CSF) (44). Lastly, both IL-2 and IL-2R knockout mice have been found to suffer from lymphoproliferation followed by lethal autoimmunity, indicating that IL-2 also has a crucial role in the termination of T-cell responses and maintenance of self-tolerance (50). IL-2 regulates the T-cell tolerance via a group of cells called T regulatory cells (T_{reg}) and this function is the only known nonredundant activity of IL-2.

Preclinical Studies and Clinical Uses of IL-2

Activation of cytolytic T-cells and LAK cells cytotoxicity against tumor cells *in vitro* by IL-2 led to the evaluation of this cytokine as an anti-cancer drug. In preclinical studies, concurrent administrations of IL-2 and LAK cells on tumor-bearing mice resulted in the regressions of liver and lung metastases (51-52). These tumor regressions were associated with prolonged survival of the experimental mice (53-54), and correlated with both increasing doses of LAK cells (up to 10^8 cells/mouse) and IL-2 (up to 10^5 IU every 8 hours) (51, 55-56). Higher doses of IL-2 were lethal to experimental mice due to the development of cardiovascular toxicities.

In clinical studies, cancer therapy using a high-dose i.v bolus of IL-2 induced 10-15% partial and 5-7% complete responses in patients with metastatic renal cell carcinoma

and malignant melanoma (57-58). About 60% of the complete responses proved durable with up to 20 years of follow-up (59). IL-2 therapy was consequently approved by the FDA for treatment of metastatic renal cell carcinoma and melanoma in 1992 and 1998, respectively. To date, IL-2 remains the only clinically available agent that can induce durable complete remissions of metastatic melanoma and renal cell carcinoma in patients despite the dramatic increase in treatment options in the past 4 years. Other agents, such as V600E B-raf specific inhibitor for treatment of melanoma (60) or inhibitors of mTOR (mammalian target of rapamycin) and VEGF (vascular endothelial growth factor) pathways for treatment of renal cancer (61), predominantly induce tumor growth arrest, requiring ongoing administration of these expensive drugs to maintain clinical responses. Attempts to improve IL-2 based immunotherapy include concomitant adoptive transfer of *in vitro* activated LAK cells (62-64) or tumor specific $CD8^+$ T-cells (termed tumor infiltrating lymphocytes or TILs) or vaccines directed against the cancer cells. These modifications were performed to enhance the immune activities towards the tumor, but have not been proven superior to the treatment with IL-2 alone (57, 65).

Dose-limiting Cardiovascular Toxicities of IL-2 Therapy

The effectiveness as well as a broader utilization of IL-2 therapy as a cancer treatment is limited by its severe dose-limiting toxicities, which include cardiovascular and neuropsychiatric toxicities (64, 66-67). The two most prominent cardiovascular toxicities of IL-2 administration are vascular leak syndrome (VLS) and hypotension. IL-2 induced VLS is characterized by generalized extravasations of intravascular fluid into interstitial tissues. It is associated with marked fluid retention (weight gain), noncardiac

pulmonary edema, and reversible renal dysfunction (68). In conjunction with VLS and intravascular volume depletion, IL-2 also induces hypotension, due to a marked decrease in systemic vascular resistance and hypoperfusion of vital organs, such as the heart and kidneys (69).

These IL-2 induced cardiovascular toxicities are thought to be indirectly mediated by the inflammatory cytokines released upon IL-2 administration, termed a “cytokine storm” (70). These secondarily released cytokines, particularly IL-5, IL-6, IFNγ, GM-CSF, and TNFα (71-74), reach high levels in patient serum. High dose of steroids can block IL-2 induced cardiovascular toxicity, but also completely abrogate therapeutic responses, indicating that these secondarily released cytokines may also contribute to the IL-2 treatment response (75). These secondary inflammatory cytokines, mainly IFNγ and TNF, can induce the production of nitric oxide (NO) through activation of the inducible L-arginine:NO synthesis pathway (76-80). The levels of nitrate (metabolites of NO) in the serum and urine of patients have been shown to be elevated 6–10-fold on days 5–7 after a 5-day treatment course of IL-2 (81). Studies in our lab have shown that the mechanism of IL-2 induced VLS is via induction of NO synthesis by endothelial NO synthase (82) whereas the hypotension appears to be due to catecholamine oxidation by superoxide and/or peroxynitrite (83).

Nitric Oxide

In 1980, a small molecule released by the endothelial cells that diffuses to and relaxes the adjacent muscle was identified (84) and named endothelial derived relaxing factor (EDRF). This vasodilator was later demonstrated to be NO (85-87). There are

various stimuli that can act on the endothelial cells to cause relaxation of vascular smooth muscle and therefore vasodilation. A few stimuli, such as adenosine, histamine (via H_2 receptors), and atrial natriuretic peptide, cause vasodilation independent of the endothelium whereas acetylcholine, substance P, vasoactive intestinal peptide, histamine, bradykinin, and some other vasodilators act via endothelium by causing the release of NO (88). Many additional endothelium-derived vasodilator and vasoconstrictor players have also been identified (i.e., prostaglandin H_2, endothelin-1, and the endothelium-derived hyperpolarizing factor), but none of these molecules play such a crucial role in the regulation of vascular tone and homeostasis as NO. The fluid shear stress (shear stretch) exerted on the endothelium by the flowing blood is the main stimulus for a continuous synthesis of NO *in vivo* (89-90). Changes in shear stress are detected by the stretch receptors on endothelial cells, which are connected to the endothelial cytoskeleton by cell membrane adaptor proteins (i.e., integrins). Activation of the endothelial cytoskeleton results in the release of NO from endothelial cells that diffuses to the vascular smooth muscle cells and induces vasodilation and increased blood flow.

Nitric oxide, with a chemical formula of NO, is a small gas molecule under ambient conditions. It is extremely labile, with a half-life of only about 3–5 seconds, after which it is oxidized into nitrites and nitrates by water or oxygen (91). NO is also highly lipophilic and readily diffusible, and therefore can diffuse and traverse multiple cell membranes to reach its numerous targets, making it an ideal signaling messenger. The known repertoire of NO functions in physiologic and pathological processes has steadily increased in recent years along with a better understanding of its diverse biochemical targets (91-92). NO interacts with various types of protein bound metal centers and has a

susceptibility to interact with cysteine thiol groups and other nucleophilic amino acids, such as tyrosine residues in a process called nitrosation. It also has several molecular targets, which upon interaction can modulate gene expression, mRNA stability and translation, as well as intracellular signaling (93).

NO relaxes smooth muscle by stimulating the synthesis of cGMP (cyclic guanosine monophosphate) (94). It augments cGMP levels by interacting with the heme-containing soluble guanylate cyclase (sGC) (95-96), displacing the iron from the plane of the heme molecule (97). This interaction leads to sGC structural change and activation, resulting in increased intracellular cGMP production (98). Subsequent events include the activation of calcium activated potassium channels (99), activation of cGMP-dependent protein kinases (100), and decreases in cytosolic calcium (Ca^{2+}) concentration in cardiac and endothelial smooth muscle cells via alterations in calcium transporter function (101-103). The final result of these events is decreased phosphorylation of myosin light chain, resulting in smooth muscle relaxation (104).

The mechanism of action of most pharmacologically useful vasodilators involves either direct release of NO or indirect metabolism of nitrates to NO (105). Nitroglycerin and the organic nitrates, which are potent treatments of cardiac angina, act by stimulating guanylate cyclase after they are converted to NO, resulting in blood vessel relaxation (106-107). In contrast, when various derivatives of arginine that inhibit NO synthase are administered to humans (108-109) or experimental animals (110-112), they result in a rapid rise in blood pressure, suggesting that NO plays a direct role in the regulation of blood pressure. NO is also involved in vascular remodeling and angiogenesis, and has been implicated in atherosclerosis, a pathological damage of endothelium resulting in

stroke. NO can inhibit blood clotting by preventing platelet aggregation (113-115) and adhesion (116-117). Moreover, NO is thought to play a key role in diffusion across endothelium as it has been shown to regulate focal adhesion integrity via FAK (focal adhesion kinase) phosphorylation in endothelial cells, which is important in the regulation of tight junction and of macromolecule transport across endothelium (118). NO has also been suggested to interact with hemoglobin (Hb) when Hb is in the oxygen partial pressure (pO_2)-dependent allosteric transition, be carried away by the red blood cells, and then released in the relatively ischemic tissues (119). NO subsequently induces vasodilation in oxygen-poor loci, diverting blood flow and thus increasing oxygen delivery to where it is most needed (120). Abnormalities in this process are associated with sickle cell anemia (121).

In the immune system, NO plays a key role in mediating the bactericidal and tumoricidal actions of macrophages (79, 122-124). Inflammatory stimuli, such as endotoxin, stimulate the production of very large amounts of NO by the inducible NO synthase (iNOS), enabling macrophages to kill tumor cells and bacteria. Besides killing bacteria, NO also can inhibit viral replication (125-126).

In the central nervous system (CNS), beginning with influential works of Garthwaite (127-128) and Snyder (129-131), NO has been identified as an important messenger molecule (132-136). The brain is capable of synthesizing NO (137-139). NO has been proposed to mediate neuronal plasticity, which underlies both development and information storage in the brain, by potentiating neurotransmitter release (91). NO signaling in the CNS appears to be essential for two forms of neuronal plasticity: 1) long-term depression (LTD) in the cerebellum (138) and 2) long-term potentiation (LTP) in

the hippocampus (140). Via its regulation of synaptic plasticity and neurotransmitter release, NO contributes to brain development, memory formation, and behavior (91). Excess levels of NO are neurotoxic and have been implicated in stroke and other neurodegenerative diseases *in vivo* (141).

Nitric Oxide Synthase

The specific action of NO depends on its enzymatic source, namely the nitric oxide synthase (NOS) enzyme family. Because NO cannot be released, stored, or inactivated by conventional regulatory mechanisms, NOS is one of the most highly regulated enzymes in biology. There are four major isoforms of NOS named after the tissue, cell source, and the order of which the isoform was characterized: 1) neuronal NOS (nNOS or NOS-1) (130, 142-143), 2) inducible NOS (iNOS or NOS-2) (144-147), 3) endothelial NOS (eNOS or NOS-3) (148), and, more recently, 4) mitochondrial NOS (mtNOS) (149-152).

All NOS isoforms are self-sufficient enzymes with two main functional domains fused into a single polypeptide (153). The C-terminal reductase domain contains the binding sites for NADPH (nicotinamide adenine dinucleotide phosphate), FAD (flavin adenine dinucleotide), and FMN (flavin mononucleotide). The N-terminal catalytic or oxygenase domain binds the redox cofactor, tetrahydrobiopterin (BH_4), the heme prosthetic group, and the substrates L-arginine and oxygen (O_2). This architecture is similar to that of cytochrome P-450BM-3 (154). Two NOS peptides dimerized in a head-to-tail manner (Fig. 1.2) to ensure proper transfer of electrons from the reductase domain of one monomer to the oxygenase domain of the second monomer (155).

Figure 1.2

The structure of nitric oxide synthase (NOS) dimer. Arrows indicate the reaction mechanism of NO synthesis by the enzyme.

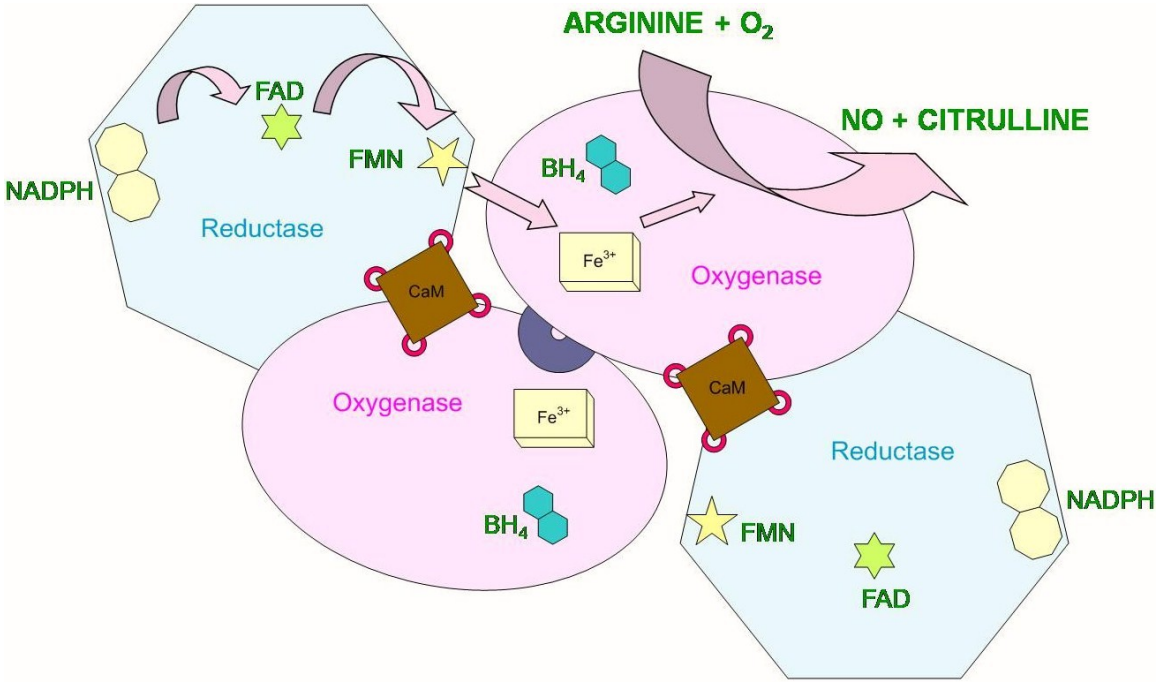
ARGININE + O_2
NO + CITRULLINE
FAD
FMN
NADPH
Reductase
BH_4
Fe^{3+}
Oxygenase
CaM
Oxygenase
Fe^{3+}
CaM
Reductase
NADPH
BH_4
FMN
FAD

NOS oxidizes the guanidine group of L-arginine, in the presence of NADPH and O_2, and in a process that consumes five electrons to produce NO with stoichiometric formation of L-citrulline. Thus, L-N^{ω}-substituted arginine analogs, such as L-N^{ω}-methyl-arginine (L-NMA) and L-N^{ω}-nitro-arginine (L-NNA), serve as NOS inhibitors (156). The catalysis process from arginine to NO takes two independent monooxygenase reaction steps. The first step is a two-electron oxidation of L-arginine to L-N^{ω}-hydroxyarginine (LHA), utilizing 1 equivalents of NADPH and 1 equivalents O_2, and releasing one molecule of water (157-158). The reducing equivalents from NADPH are transferred through FAD to FMN and finally to the heme (159). This hydroxylation reaction is accelerated by BH_4, requires calmodulin (CaM) and Ca^{2+} as activators, and is blocked by carbon monoxide (CO) (157, 160-161). CaM is believed to facilitate the flow of electrons from the reductase domain to the monooxygenase domain and also from FAD to FMN (162). In the second step, one electron (or 0.5 equivalents of NADPH) is essential to form a second equivalent of reduced oxygen molecule (163), which then attacks the guanidine carbon of LHA to form a tetrahedral intermediate. This tetrahedral intermediate collapses to form the carbonyl group of L-citrulline with simultaneous expulsion of NO. The complete stoichiometry of NO synthesis by NOS therefore utilizes 1 mole of L-arginine, 1.5 moles of NADPH, and 2 moles of O_2 and produces 2 moles of water, 1 mole of L-citrulline, and1 mole of NO (164).

The involvement of BH_4 and CaM is unique to NOS. The CaM/Ca^{2+} binding domain lies in the center of the enzyme. nNOS, eNOS, and mtNOS are expressed constitutively in mammals and their activities are regulated by CaM binding in a Ca^{2+} concentration dependent manner (165-166). Conversely, iNOS has CaM bound

permanently as an additional subunit and thus is not controlled by CaM binding nor it is Ca^{2+} concentration dependent, but is under transcriptional regulation instead (167).

The mammalian NOS enzymes are products of distinct genes located on different chromosomes but they exhibit about 50 to 60% sequence homology with each other (164). nNOS is 155 kDa and found in peripheral and central neurons, noncholinergic and nonadrenergic neurons, endometrium, pancreatic islets, skeletal and smooth muscle, neutrophils and epithelium (92, 168). It has four splice variants and accounts for the majority of physiologic processes attributed to NO in the nervous system (169). iNOS is a 125 kDa protein expressed in macrophages, NK cells, neutrophils, smooth muscle, liver, heart, endothelium and other cell types (168). It is crucial for immune function and is inducible in response to glucocorticoids, cytokines, which include IL-1, TNF-α, IFNγ, and lipopolysaccharide (LPS), a bacterial cell-wall component that elicits symptoms of sepsis (170). eNOS is 125 kDa (168) and is the main isoform found in the endothelium. It is also found in smooth muscle, heart, brain, and other sites (168). mtNOS is 144-kDa and associates with the mitochondrial inner membrane (171). It produces NO to regulate mitochondrial respiration (172).

Unlike nNOS and iNOS, which are mainly cytosolic, eNOS is predominantly localized to the plasma membrane (148). eNOS bioactivity and mobilization to specific organelles are highly regulated by multiple posttranslational modifications, such as acylation and phosphorylation. eNOS is irreversibly myristoylated at its N-terminal glycine (173). Myristoylation targets the enzyme to the cell membrane, where it is doubly palmitoylated at the N-terminal cysteine residues 15 and 26, a modification that further anchors eNOS to the plasmalemmal caveolae of endothelial cells (174). The N-

myristoylation is sufficient and necessary for eNOS membrane association (175-176), palmitoylation (177-178), compartmentalization to the Golgi complex of cells, and most importantly, efficient NO synthesis (179). Palmitoylation is required for localization of eNOS in caveolae (180-181) and regulation of the frequency and magnitude of NO release *in vivo* in response to stimuli (182). In contrast to the myristoylation, palmitoylation and the consequential caveolar targeting are reversible and controllable as the thiopalmitoyl bonds are labile, hence creating an additional level of dynamic regulation of eNOS activity (183). Another dynamic control of eNOS involves various pathways of phosphorylation and dephosphorylation. eNOS phosphorylation is usually associated with its agonist-triggered translocation to the cytosol (184). eNOS has multiple phosphorylation sites, including Ser (Serine) 635 and Ser 1177, which are stimulatory, and Thr (Threonine) 495 and Ser 116, which are inhibitory (164). (Note that the numbering system refers to phosphorylation sites of human eNOS isoform.) The protein kinase Akt (protein kinase B) is a key enzyme that phosphorylates eNOS at Ser 1177 in response to agonists, resulting in eNOS released into the cytosol and activation at basal levels (185). Kinase Akt is activated by phosphoinositide-3-kinase (PI3K) (186), which in turn is activated by many eNOS agonists (i.e., vascular endothelial growth factor). eNOS Ser 635 represents a second stimulatory phosphorylation in respond to basal stimuli, such as shear stress, and agonists downstream of protein kinase A (187). In contrast, phosphorylation of eNOS at Thr 945 inhibits enzyme activity by preventing CaM binding (188).

When eNOS is uncoupled from essential cofactors or is in the oxidized state, it produces superoxide (O_2^-) instead of NO (189). This situation has been demonstrated in

diseases, such as atherosclerosis, hypertension, hypercholesterolemia, and diabetes (189-191). O_2^- and NO react rapidly, generating peroxynitrite ($ONOO^-$), a potent oxidizing agent (192-194). This reaction further decreases NO availability while promoting lipid and protein oxidation (195). $ONOO^-$ itself plays a crucial role in eNOS uncoupling (196) by oxidizing the essential cofactor BH_4 to the inactive pterin, 7,8-dihydrobiopterin (BH_2) and removing zinc from the zinc-thiolate cluster (197).

Dose-limiting Neuropsychiatric Toxicity of IL-2 Therapy

When clinical cardiovascular toxicities of IL-2 are attenuated with pressor agents and fluid administration, the effective dose escalation of IL-2 therapy is further limited by the onset of neuropsychiatric toxicity. In data reported in 1987, a large percentage of patients were found to develop striking neuropsychiatric changes after the onset of IL-2 treatment, with 30–50% of patients experienced cognitive and behavioral changes (67). All of these patients returned to their baseline cognitive scores at follow-up. Based on our clinical experiences, perhaps as high as 40% of patients receiving IL-2 therapy have subtle neuropsychiatric changes, such as mental slowing or confusion, and approximately 10–20% of patients develop more severe manifestations, such as agitation, hallucinations, or delusions. IL-2 induced neuropsychiatric toxicity is the least predictable and treatable compared to the cardiovascular toxicities. Management is generally by holding further doses of IL-2 and allowing patients to recover spontaneously.

In 1989, a study was conducted to look at the effects of IL-2 in the brain of patients with extracranial cancer without evidence of intracranial metastases using T_2-weighted MRI before and after IL-2 therapy (198). The results suggested a massive

increase of cerebral water content after IL-2 therapy in both the gray matter (12.6±7.3%) and white matter (17±6.2%). However, the range of these measurements actually varied from 3–48% and only 3 out of these 7 patients were mildly lethargic, raising questions concerning the accuracy of these data. The magnitude of these apparent cerebral water content increases are far greater than the magnitude of VLS measured in any other organ or even compared to the overall weight changes in the intact IL-2 treated animals or patients (approximately 6–8%), and thus are difficult to believe.

Previous studies in animal models showed increased permeability of horseradish peroxidase into the brain of cats and rats after a single bolus intravenous injection of recombinant IL-2, suggesting that IL-2 disrupted the blood-brain barrier (BBB) and cerebrovascular morphological integrity (199-200). Another study in a rat gliosarcoma model suggested that IL-2 increased the permeability of carbon-14-labeled aminoisobutyric acid from the BBB into the brain of tumor-bearing rat brains, but not in normal brains (201). Since tumors are known to have abnormal blood vessel permeability and accordingly could have contributed to the increased brain edema following IL-2 treatment, the significance of this finding is uncertain.

The pathophysiology of IL-2 induced neuropsychiatric toxicity therefore remains poorly understood to date. Further efforts to study this toxicity have been limited by the availability of suitable experimental techniques and the technical challenges of performing dynamic contrast enhanced (DCE) MRI (magnetic resonance imaging) studies in critically ill patients, who normally are hospitalized in the ICU (intensive care unit). It would be quite difficult to perform DCE MRI studies once these patients display neuropsychiatric toxicity (delirium) as they are frequently receiving intravenous pressor

agents, intubated, and would not be stable enough to undergo lengthy MRI scans. Additionally, the gadolinium-based contrast agent used for DCE MRI may have an adverse effect for IL-2 treated patients, who usually develop a certain degree of acute renal dysfunction, as this agent has been shown to be associated with the development of nephrogenic fibrosing dermopathy (NFD) and nephrogenic systemic fibrosis (NSF) in patients with kidney dysfunction (202-204).

It is likely that the "cytokine storm" released following IL-2 therapy induces changes in brain microvasculature, such as vascular leak and brain edema, which correlate to changes in the CNS function and thus trigger neuropsychiatric toxicity. Therefore, development and evaluation of a number of potential experimental methods to quantify changes on the brain blood vessels in a well-characterized IL-2 treatment murine model (83, 205) are required to delineate IL-2 induced neuropsychiatric toxicity. Once successful assays have been identified, the mechanisms of this toxicity can be determined. The role of NO and superoxide, the major players in systemic IL-2 induced VLS and hypotension, respectively, in IL-2 induced CNS changes is currently unknown. Detailed understanding of the mechanisms by which IL-2 induces neuropsychiatric toxicity will be useful in identifying possible pharmacologic inhibitors of this process to be used in patients, which may enable dose escalation of IL-2 treatment to achieve the effective high dose. In addition, this knowledge may also be broadly applicable to other conditions that give rise to an inflammatory "cytokine storm," such as clinical administration of cytokines IL-1, TNF, and IFNγ, as well as endotoxin and bacterial sepsis syndromes.

Sepsis

A potential implication of this study in other area of Biology is sepsis. Sepsis is a clinical syndrome characterized by a systemic response to an infection. There are roughly 750,000 cases of sepsis annually in the United States (206-207). It is the leading cause of death among hospitalized patients in noncoronary ICU (208-209), causing an estimated 215,000 deaths (9.3% of all deaths) in the United States and considerable morbidity, health care utilization, and cost (210). At the initial stages of sepsis, patients develop very similar clinical symptoms to the side effects of IL-2 therapy, particularly hypotension, VLS, and delirium (neuropsychiatric toxicity) (69). This is also associated with a very similar inflammatory "cytokine storm" (211-213). However, as sepsis progresses, patients experience irreversible organ failure, with a high incidence of acute tubular necrosis and irreversible hypotension, leading to death. In contrast, IL-2 dose limiting toxicities are reversible (i.e., complete resolution of renal function changes) following completion of IL-2 therapy and therefore may provide useful to model the early cardiovascular and neuropsychiatric effects of sepsis.

References

1. Morgan DA, Ruscetti FW, Gallo R. 1976. Selective in vitro growth of T lymphocytes from normal human bone marrows. *Science* 193: 1007-8.

2. Robb RJ, Smith KA. 1981. Heterogeneity of human T-cell growth factor(s) due to variable glycosylation. *Mol Immunol* 18: 1087-94.

3. Smith KA, Favata MF, Oroszlan S. 1983. Production and characterization of monoclonal antibodies to human interleukin 2: strategy and tactics. *J Immunol* 131: 1808-15.

4. Taniguchi T, Matsui H, Fujita T, Takaoka C, Kashima N, Yoshimoto R, Hamuro J. 1983. Structure and expression of a cloned cDNA for human interleukin-2. *Nature* 302: 305-10.

5. Fitzgerald KA, O'Neill LAJ, Gearing AJH, Callard RE. 2001. IL-2. In *The Cytokine Factsbook*, pp. 44-50. London: Academic Press.

6. Robb RJ, Kutny RM, Panico M, Morris HR, Chowdhry V. 1984. Amino acid sequence and post-translational modification of human interleukin 2. *Proc Natl Acad Sci U S A* 81: 6486-90.

7. Bazan JF. 1992. Unraveling the structure of IL-2. *Science* 257: 410-3.

8. Robb RJ, Munck A, Smith KA. 1981. T cell growth factor receptors. Quantitation, specificity, and biological relevance. *J Exp Med* 154: 1455-74.

9. Nelson BH, Willerford DM. 1998. Biology of the interleukin-2 receptor. *Adv Immunol* 70: 1-81.

10. Leonard WJ, Depper JM, Uchiyama T, Smith KA, Waldmann TA, Greene WC. 1982. A monoclonal antibody that appears to recognize the receptor for human T-cell growth factor; partial characterization of the receptor. *Nature* 300: 267-9.

11. Leonard WJ, Depper JM, Crabtree GR, Rudikoff S, Pumphrey J, Robb RJ, Kronke M, Svetlik PB, Peffer NJ, Waldmann TA, et al. 1984. Molecular cloning and expression of cDNAs for the human interleukin-2 receptor. *Nature* 311: 626-31.

12. Nikaido T, Shimizu A, Ishida N, Sabe H, Teshigawara K, Maeda M, Uchiyama T, Yodoi J, Honjo T. 1984. Molecular cloning of cDNA encoding human interleukin-2 receptor. *Nature* 311: 631-5.

13. Cosman D, Cerretti DP, Larsen A, Park L, March C, Dower S, Gillis S, Urdal D. 1984. Cloning, sequence and expression of human interleukin-2 receptor. *Nature* 312: 768-71.

14. Sharon M, Klausner RD, Cullen BR, Chizzonite R, Leonard WJ. 1986. Novel interleukin-2 receptor subunit detected by cross-linking under high-affinity conditions. *Science* 234: 859-63.

15. Teshigawara K, Wang HM, Kato K, Smith KA. 1987. Interleukin 2 high-affinity receptor expression requires two distinct binding proteins. *J Exp Med* 165: 223-38.

16. Tsudo M, Kozak RW, Goldman CK, Waldmann TA. 1987. Contribution of a p75 interleukin 2 binding peptide to a high-affinity interleukin 2 receptor complex. *Proc Natl Acad Sci U S A* 84: 4215-8.

17. Hatakeyama M, Tsudo M, Minamoto S, Kono T, Doi T, Miyata T, Miyasaka M, Taniguchi T. 1989. Interleukin-2 receptor beta chain gene: generation of three receptor forms by cloned human alpha and beta chain cDNA's. *Science* 244: 551-6.

18. Takeshita T, Ohtani K, Asao H, Kumaki S, Nakamura M, Sugamura K. 1992. An associated molecule, p64, with IL-2 receptor beta chain. Its possible involvement in the formation of the functional intermediate-affinity IL-2 receptor complex. *J Immunol* 148: 2154-8.

19. Wang HM, Smith KA. 1987. The interleukin 2 receptor. Functional consequences of its bimolecular structure. *J Exp Med* 166: 1055-69.

20. Rickert M, Boulanger MJ, Goriatcheva N, Garcia KC. 2004. Compensatory energetic mechanisms mediating the assembly of signaling complexes between interleukin-2 and its alpha, beta, and gamma(c) receptors. *J Mol Biol* 339: 1115-28.

21. Nakamura Y, Russell SM, Mess SA, Friedmann M, Erdos M, Francois C, Jacques Y, Adelstein S, Leonard WJ. 1994. Heterodimerization of the IL-2 receptor beta- and gamma-chain cytoplasmic domains is required for signalling. *Nature* 369: 330-3.

22. Nelson BH, Lord JD, Greenberg PD. 1994. Cytoplasmic domains of the interleukin-2 receptor beta and gamma chains mediate the signal for T-cell proliferation. *Nature* 369: 333-6.

23. Hanisch UK, Lyons SA, Prinz M, Nolte C, Weber JR, Kettenmann H, Kirchhoff F. 1997. Mouse brain microglia express interleukin-15 and its multimeric receptor complex functionally coupled to Janus kinase activity. *J Biol Chem* 272: 28853-60.

24. Chakraborty G, Reddy R, Drivas A, Ledeen RW. 2003. Interleukin-2 receptors and interleukin-2-mediated signaling in myelin: activation of diacylglycerol kinase and phosphatidylinositol 3-kinase. *Neuroscience* 122: 967-73.

25. Petitto JM, Huang Z. 1994. Molecular cloning of a partial cDNA of the interleukin-2 receptor-beta in normal mouse brain: in situ localization in the hippocampus and expression by neuroblastoma cells. *Brain Res* 650: 140-5.

26. Rickert M, Wang X, Boulanger MJ, Goriatcheva N, Garcia KC. 2005. The structure of interleukin-2 complexed with its alpha receptor. *Science* 308: 1477-80.

27. Stauber DJ, Debler EW, Horton PA, Smith KA, Wilson IA. 2006. Crystal structure of the IL-2 signaling complex: paradigm for a heterotrimeric cytokine receptor. *Proc Natl Acad Sci U S A* 103: 2788-93.

28. Wang X, Rickert M, Garcia KC. 2005. Structure of the quaternary complex of interleukin-2 with its alpha, beta, and gammac receptors. *Science* 310: 1159-63.

29. Bazan JF. 1990. Structural design and molecular evolution of a cytokine receptor superfamily. *Proc Natl Acad Sci U S A* 87: 6934-8.

30. Ozaki K, Leonard WJ. 2002. Cytokine and cytokine receptor pleiotropy and redundancy. *J Biol Chem* 277: 29355-8.

31. Smith KA. 1995. Cell growth signal transduction is quantal. *Ann N Y Acad Sci* 766: 263-71.

32. Smith KA. 2004. The quantal theory of how the immune system discriminates between "self and non-self". *Med Immunol* 3: 3.

33. Mills GB, Schmandt R, Gibson S, Leung B, Hill M, May C, Shi YF, Branch DR, Radvanyi L, Truitt KE, et al. 1993. Transmembrane signaling by the interleukin-2 receptor: progress and conundrums. *Semin Immunol* 5: 345-64.

34. Miyazaki T, Kawahara A, Fujii H, Nakagawa Y, Minami Y, Liu ZJ, Oishi I, Silvennoinen O, Witthuhn BA, Ihle JN, et al. 1994. Functional activation of Jak1 and Jak3 by selective association with IL-2 receptor subunits. *Science* 266: 1045-7.

35. Russell SM, Johnston JA, Noguchi M, Kawamura M, Bacon CM, Friedmann M, Berg M, McVicar DW, Witthuhn BA, Silvennoinen O, et al. 1994. Interaction of IL-2R beta and gamma c chains with Jak1 and Jak3: implications for XSCID and XCID. *Science* 266: 1042-5.

36. Darnell JE, Jr., Kerr IM, Stark GR. 1994. Jak-STAT pathways and transcriptional activation in response to IFNs and other extracellular signaling proteins. *Science* 264: 1415-21.

37. Beadling C, Guschin D, Witthuhn BA, Ziemiecki A, Ihle JN, Kerr IM, Cantrell DA. 1994. Activation of JAK kinases and STAT proteins by interleukin-2 and interferon alpha, but not the T cell antigen receptor, in human T lymphocytes. *EMBO J* 13: 5605-15.

38. Gilmour KC, Reich NC. 1994. Receptor to nucleus signaling by prolactin and interleukin 2 via activation of latent DNA-binding factors. *Proc Natl Acad Sci U S A* 91: 6850-4.

39. Gaffen SL, Lai SY, Xu W, Gouilleux F, Groner B, Goldsmith MA, Greene WC. 1995. Signaling through the interleukin 2 receptor beta chain activates a STAT-5-like DNA-binding activity. *Proc Natl Acad Sci U S A* 92: 7192-6.

40. Hou J, Schindler U, Henzel WJ, Wong SC, McKnight SL. 1995. Identification and purification of human Stat proteins activated in response to interleukin-2. *Immunity* 2: 321-9.

41. Lin JX, Migone TS, Tsang M, Friedmann M, Weatherbee JA, Zhou L, Yamauchi A, Bloom ET, Mietz J, John S, et al. 1995. The role of shared receptor motifs and common Stat proteins in the generation of cytokine pleiotropy and redundancy by IL-2, IL-4, IL-7, IL-13, and IL-15. *Immunity* 2: 331-9.

42. Miyazaki T, Liu ZJ, Kawahara A, Minami Y, Yamada K, Tsujimoto Y, Barsoumian EL, Permutter RM, Taniguchi T. 1995. Three distinct IL-2 signaling pathways mediated by bcl-2, c-myc, and lck cooperate in hematopoietic cell proliferation. *Cell* 81: 223-31.

43. Mertelsmann R, Welte K. 1986. Human interleukin 2: molecular biology, physiology and clinical possibilities. *Immunobiology* 172: 400-19.

44. Weiss A. 1993. T lymphocyte activation. In *Fundamental Immunology.*, ed. WE Paul, pp. 467-504. New York: Raven Press.

45. Lotze MT, Grimm EA, Mazumder A, Strausser JL, Rosenberg SA. 1981. Lysis of fresh and cultured autologous tumor by human lymphocytes cultured in T-cell growth factor. *Cancer Res.* 41: 4420-5.

46. Grimm EA, Wilson DJ. 1985. The human lymphokine-activated killer cell system. V. Purified recombinant interleukin 2 activates cytotoxic lymphocytes which lyse both natural killer-resistant autologous and allogeneic tumors and trinitrophenyl-modified autologous peripheral blood lymphocytes. *Cell Immunol* 94: 568-78.

47. Hank JA, Kohler PC, Weil-Hillman G, Rosenthal N, Moore KH, Storer B, Minkoff D, Bradshaw J, Bechhofer R, Sondel PM. 1988. In vivo induction of the lymphokine-activated killer phenomenon: interleukin 2-dependent human non-major histocompatibility complex-restricted cytotoxicity generated in vivo during administration of human recombinant interleukin 2. *Cancer Res.* 48: 1965-71.

48. Rayner AA, Grimm EA, Lotze MT, Wilson DJ, Rosenberg SA. 1985. Lymphokine-activated killer (LAK) cell phenomenon. IV. Lysis by LAK cell clones of fresh human tumor cells from autologous and multiple allogeneic tumors. *J. Natl. Cancer Inst.* 75: 67-75.

49. Harker WG, Tom C, McGregor JR, Slade L, Samlowski WE. 1990. Human tumor cell line resistance to chemotherapeutic agents does not predict resistance to natural killer or lymphokine-activated killer cell-mediated cytolysis. *Cancer Res.* 50: 5931-6.

50. Malek TR, Bayer AL. 2004. Tolerance, not immunity, crucially depends on IL-2. *Nat Rev Immunol* 4: 665-74.

51. Lafreniere R, Rosenberg SA. 1985. Successful immunotherapy of murine experimental hepatic metastases with lymphokine-activated killer cells and recombinant interleukin 2. *Cancer Res.* 45: 3735-41.

52. Papa MZ, Mule JJ, Rosenberg SA. 1986. Antitumor efficacy of lymphokine-activated killer cells and recombinant interleukin 2 in vivo: successful immunotherapy of established pulmonary metastases from weakly immunogenic

and nonimmunogenic murine tumors of three district histological types. *Cancer Res.* 46: 4973-8.

53. Mule JJ, Shu S, Rosenberg SA. 1985. The anti-tumor efficacy of lymphokine-activated killer cells and recombinant interleukin 2 in vivo. *J. Immunol.* 135: 646-52.

54. Eberlein TJ, Rosenstein M, Rosenberg SA. 1982. Regression of a disseminated syngeneic solid tumor by systemic transfer of lymphoid cells expanded in interleukin 2. *J. Exp. Med.* 156: 385-97.

55. Rosenberg SA, Mule JJ, Spiess PJ, Reichert CM, Schwarz SL. 1985. Regression of established pulmonary metastases and subcutaneous tumor mediated by the systemic administration of high-dose recombinant interleukin 2. *J Exp Med* 161: 1169-88.

56. Ettinghausen SE, Rosenberg SA. 1986. Immunotherapy of murine sarcomas using lymphokine activated killer cells: optimization of the schedule and route of administration of recombinant interleukin-2. *Cancer Res* 46: 2784-92.

57. Rosenberg SA, Yang JC, Topalian SL, Schwartzentruber DJ, Weber JS, Parkinson DR, Seipp CA, Einhorn JH, White DE. 1994. Treatment of 283 consecutive patients with metastatic melanoma or renal cell cancer using high-dose bolus interleukin 2. *Jama* 271: 907-13.

58. Atkins MB, Lotze MT, Dutcher JP, Fisher RI, Weiss G, Margolin K, Abrams J, Sznol M, Parkinson D, Hawkins M, Paradise C, Kunkel L, Rosenberg SA. 1999. High-dose recombinant interleukin 2 therapy for patients with metastatic melanoma: analysis of 270 patients treated between 1985 and 1993. *J Clin Oncol* 17: 2105-16.

59. Atkins MB, Kunkel L, Sznol M, Rosenberg SA. 2000. High-dose recombinant interleukin-2 therapy in patients with metastatic melanoma: long-term survival update. *Cancer J. Sci. Am.* 6 Suppl 1: S11-4.

60. Menard D, Niculescu-Duvaz I, Dijkstra HP, Niculescu-Duvaz D, Suijkerbuijk BM, Zambon A, Nourry A, Roman E, Davies L, Manne HA, Friedlos F, Kirk R, Whittaker S, Gill A, Taylor RD, Marais R, Springer CJ. 2009. Novel potent BRAF inhibitors: toward 1 nM compounds through optimization of the central phenyl ring. *J Med Chem* 52: 3881-91.

61. Samlowski WE, Wong B, Vogelzang NJ. 2008. Management of renal cancer in the tyrosine kinase inhibitor era: a view from 3 years on. *BJU Int.* 102: 162-5.

62. Fisher RI, Coltman CA, Jr., Doroshow JH, Rayner AA, Hawkins MJ, Mier JW, Wiernik P, McMannis JD, Weiss GR, Margolin KA, et al. 1988. Metastatic renal cancer treated with interleukin-2 and lymphokine-activated killer cells. A phase II clinical trial. *Ann Intern Med* 108: 518-23.

63. Dutcher JP, Creekmore S, Weiss GR, Margolin K, Markowitz AB, Roper M, Parkinson D, Ciobanu N, Fisher RI, Boldt DH, et al. 1989. A phase II study of interleukin-2 and lymphokine-activated killer cells in patients with metastatic malignant melanoma. *J Clin Oncol* 7: 477-85.

64. Margolin KA, Rayner AA, Hawkins MJ, Atkins MB, Dutcher JP, Fisher RI, Weiss GR, Doroshow JH, Jaffe HS, Roper M, et al. 1989. Interleukin-2 and lymphokine-activated killer cell therapy of solid tumors: analysis of toxicity and management guidelines. *J Clin Oncol* 7: 486-98.

65. Yang JC, Topalian SL, Parkinson D, Schwartzentruber DJ, Weber JS, Ettinghausen SE, White DE, Steinberg SM, Cole DJ, Kim HI, et al. 1994. Randomized comparison of high-dose and low-dose intravenous interleukin-2 for the therapy of metastatic renal cell carcinoma: an interim report. *J Clin Oncol* 12: 1572-6.

66. Siegel JP, Puri RK. 1991. Interleukin-2 toxicity. *J Clin Oncol* 9: 694-704.

67. Denicoff KD, Rubinow DR, Papa MZ, Simpson C, Seipp CA, Lotze MT, Chang AE, Rosenstein D, Rosenberg SA. 1987. The neuropsychiatric effects of treatment with interleukin-2 and lymphokine-activated killer cells. *Ann Intern Med* 107: 293-300.

68. Mann H, Ward JH, Samlowski WE. 1990. Vascular leak syndrome associated with interleukin-2: chest radiographic manifestations. *Radiology* 176: 191-4.

69. Ognibene FP, Rosenberg SA, Lotze M, Skibber J, Parker MM, Shelhamer JH, Parrillo JE. 1988. Interleukin-2 administration causes reversible hemodynamic changes and left ventricular dysfunction similar to those seen in septic shock. *Chest* 94: 750-4.

70. Panelli MC, White R, Foster M, Martin B, Wang E, Smith K, Marincola FM. 2004. Forecasting the cytokine storm following systemic interleukin (IL)-2 administration. *J. Transl. Med.* 2: 17.

71. Gemlo BT, Palladino MA, Jr., Jaffe HS, Espevik TP, Rayner AA. 1988. Circulating cytokines in patients with metastatic cancer treated with recombinant interleukin 2 and lymphokine-activated killer cells. *Cancer Res.* 48: 5864-7.

72. Mier JW, Vachino G, van der Meer JW, Numerof RP, Adams S, Cannon JG, Bernheim HA, Atkins MB, Parkinson DR, Dinarello CA. 1988. Induction of circulating tumor necrosis factor (TNF alpha) as the mechanism for the febrile response to interleukin-2 (IL-2) in cancer patients. *J. Clin. Immunol.* 8: 426-36.

73. Jablons DM, Mule JJ, McIntosh JK, Sehgal PB, May LT, Huang CM, Rosenberg SA, Lotze MT. 1989. IL-6/IFN-beta-2 as a circulating hormone. Induction by cytokine administration in humans. *J. Immunol.* 142: 1542-7.

74. Schaafsma MR, Falkenburg JH, Landegent JE, Duinkerken N, Osanto S, Ralph P, Kaushansky K, Wagemaker G, Van Damme J, Willemze R, et al. 1991. In vivo production of interleukin-5, granulocyte-macrophage colony-stimulating factor, macrophages colony-stimulating factor, and interleukin-6 during intravenous administration of high-dose interleukin-2 in cancer patients. *Blood* 78: 1981-7.

75. Papa MZ, Vetto JT, Ettinghausen SE, Mule JJ, Rosenberg SA. 1986. Effect of corticosteroid on the antitumor activity of lymphokine-activated killer cells and interleukin 2 in mice. *Cancer Res* 46: 5618-23.

76. Drapier JC, Wietzerbin J, Hibbs JB, Jr. 1988. Interferon-gamma and tumor necrosis factor induce the L-arginine-dependent cytotoxic effector mechanism in murine macrophages. *Eur J Immunol* 18: 1587-92.

77. Amber IJ, Hibbs JB, Jr., Taintor RR, Vavrin Z. 1988. Cytokines induce an L-arginine-dependent effector system in nonmacrophage cells. *J Leukoc Biol* 44: 58-65.

78. Amber IJ, Hibbs JB, Jr., Taintor RR, Vavrin Z. 1988. The L-arginine dependent effector mechanism is induced in murine adenocarcinoma cells by culture supernatant from cytotoxic activated macrophages. *J Leukoc Biol* 43: 187-92.

79. Hibbs JB, Jr., Taintor RR, Vavrin Z. 1987. Macrophage cytotoxicity: role for L-arginine deiminase and imino nitrogen oxidation to nitrite. *Science* 235: 473-6.

80. Marletta MA, Yoon PS, Iyengar R, Leaf CD, Wishnok JS. 1988. Macrophage oxidation of L-arginine to nitrite and nitrate: nitric oxide is an intermediate. *Biochemistry* 27: 8706-11.

81. Hibbs JB, Jr., Westenfelder C, Taintor R, Vavrin Z, Kablitz C, Baranowski RL, Ward JH, Menlove RL, McMurry MP, Kushner JP, et al. 1992. Evidence for cytokine-inducible nitric oxide synthesis from L-arginine in patients receiving interleukin-2 therapy. *J Clin Invest* 89: 867-77.

82. Kondapaneni M, McGregor JR, Salvemini D, Laubach VE, Samlowski WE. 2008. Inducible nitric oxide synthase (iNOS) is not required for IL-2-induced hypotension and vascular leak syndrome in mice. *J Immunother* 31: 325-33.

83. Samlowski WE, Petersen R, Cuzzocrea S, Macarthur H, Burton D, McGregor JR, Salvemini D. 2003. A nonpeptidyl mimic of superoxide dismutase, M40403, inhibits dose-limiting hypotension associated with interleukin-2 and increases its antitumor effects. *Nat. Med.* 9: 750-5.

84. Furchgott RF, Zawadzki JV. 1980. The obligatory role of endothelial cells in the relaxation of arterial smooth muscle by acetylcholine. *Nature* 288: 373-6.

85. Ignarro LJ, Buga GM, Wood KS, Byrns RE, Chaudhuri G. 1987. Endothelium-derived relaxing factor produced and released from artery and vein is nitric oxide. *Proc Natl Acad Sci U S A* 84: 9265-9.

86. Palmer RM, Ferrige AG, Moncada S. 1987. Nitric oxide release accounts for the biological activity of endothelium-derived relaxing factor. *Nature* 327: 524-6.

87. Furchgott RF. 1988. Studies on relaxation of rabbit aorta by sodium nitrite: the basis for the proposal that the acid-activable inhibitory factor from bovine retractor penis is organic nitrite and the endothelium-derived relaxing factor is nitric oxide. In *Mechanisms of Vasodilation*, ed. PM Vanhoutte, pp. 401-18. New York: Raven Press.

88. Ignarro LJ. 1996. Physiology and pathophysiology of nitric oxide. *Kidney Int Suppl* 55: S2-5.

89. Lamontagne D, Pohl U, Busse R. 1992. Mechanical deformation of vessel wall and shear stress determine the basal release of endothelium-derived relaxing factor in the intact rabbit coronary vascular bed. *Circ Res* 70: 123-30.

90. Bevan JA, Kaley G, Rubanyi GM. 1995. *Flow-dependent Regulation of Vascular Function*. New York: Oxford University Press.

91. Bredt DS. 1999. Endogenous nitric oxide synthesis: biological functions and pathophysiology. *Free Radic Res* 31: 577-96.

92. Mashimo H, Goyal RK. 1999. Lessons from genetically engineered animal models. IV. Nitric oxide synthase gene knockout mice. *Am J Physiol* 277: G745-50.

93. Bogdan C. 2001. Nitric oxide and the regulation of gene expression. *Trends Cell Biol* 11: 66-75.

94. Rapoport RM, Murad F. 1983. Agonist-induced endothelium-dependent relaxation in rat thoracic aorta may be mediated through cGMP. *Circ Res* 52: 352-7.

95. Craven PA, DeRubertis FR. 1978. Restoration of the responsiveness of purified guanylate cyclase to nitrosoguanidine, nitric oxide, and related activators by heme and hemeproteins. Evidence for involvement of the paramagnetic nitrosyl-heme complex in enzyme activation. *J Biol Chem* 253: 8433-43.

96. Ignarro LJ, Degnan JN, Baricos WH, Kadowitz PJ, Wolin MS. 1982. Activation of purified guanylate cyclase by nitric oxide requires heme. Comparison of heme-deficient, heme-reconstituted and heme-containing forms of soluble enzyme from bovine lung. *Biochim Biophys Acta* 718: 49-59.

97. Ignarro LJ. 1994. Regulation of cytosolic guanylyl cyclase by porphyrins and metalloporphyrins. *Adv Pharmacol* 26: 35-65.

98. Drewett JG, Garbers DL. 1994. The family of guanylyl cyclase receptors and their ligands. *Endocr Rev* 15: 135-62.

99. Lincoln TM, Cornwell TL, Komalavilas P, Boerth N. 1996. Cyclic GMP-dependent protein kinase in nitric oxide signaling. *Methods Enzymol* 269: 149-66.

100. Francis SH, Corbin JD. 1994. Progress in understanding the mechanism and function of cyclic GMP-dependent protein kinase. *Adv Pharmacol* 26: 115-70.

101. Hirata M, Murad F. 1994. Interrelationships of cyclic GMP, inositol phosphates, and calcium. *Adv Pharmacol* 26: 195-216.

102. Hobbs AJ, Ignarro LJ. 1996. Nitric oxide-cyclic GMP signal transduction system. *Methods Enzymol* 269: 134-48.

103. Quignard JF, Frapier JM, Harricane MC, Albat B, Nargeot J, Richard S. 1997. Voltage-gated calcium channel currents in human coronary myocytes. Regulation by cyclic GMP and nitric oxide. *J Clin Invest* 99: 185-93.

104. Murad F. 1994. Regulation of cytosolic guanylyl cyclase by nitric oxide: the NO-cyclic GMP signal transduction system. *Adv Pharmacol* 26: 19-33.

105. Torfgard KE, Ahlner J. 1994. Mechanisms of action of nitrates. *Cardiovasc Drugs Ther* 8: 701-17.

106. Arnold WP, Mittal CK, Katsuki S, Murad F. 1977. Nitric oxide activates guanylate cyclase and increases guanosine 3':5'-cyclic monophosphate levels in various tissue preparations. *Proc Natl Acad Sci U S A* 74: 3203-7.

107. Ignarro LJ, Lippton H, Edwards JC, Baricos WH, Hyman AL, Kadowitz PJ, Gruetter CA. 1981. Mechanism of vascular smooth muscle relaxation by organic nitrates, nitrites, nitroprusside and nitric oxide: evidence for the involvement of S-nitrosothiols as active intermediates. *J Pharmacol Exp Ther* 218: 739-49.

108. Vallance P, Collier J, Moncada S. 1989. Effects of endothelium-derived nitric oxide on peripheral arteriolar tone in man. *Lancet* 2: 997-1000.

109. Vallance P, Collier J, Moncada S. 1989. Nitric oxide synthesised from L-arginine mediates endothelium dependent dilatation in human veins in vivo. *Cardiovasc Res* 23: 1053-7.

110. Aisaka K, Gross SS, Griffith OW, Levi R. 1989. NG-methylarginine, an inhibitor of endothelium-derived nitric oxide synthesis, is a potent pressor agent in the guinea pig: does nitric oxide regulate blood pressure in vivo? *Biochem Biophys Res Commun* 160: 881-6.

111. Whittle BJ, Lopez-Belmonte J, Rees DD. 1989. Modulation of the vasodepressor actions of acetylcholine, bradykinin, substance P and endothelin in the rat by a specific inhibitor of nitric oxide formation. *Br J Pharmacol* 98: 646-52.

112. Rees DD, Palmer RM, Moncada S. 1989. Role of endothelium-derived nitric oxide in the regulation of blood pressure. *Proc Natl Acad Sci U S A* 86: 3375-8.

113. Furlong B, Henderson AH, Lewis MJ, Smith JA. 1987. Endothelium-derived relaxing factor inhibits in vitro platelet aggregation. *Br J Pharmacol* 90: 687-92.

114. Radomski MW, Palmer RM, Moncada S. 1987. The anti-aggregating properties of vascular endothelium: interactions between prostacyclin and nitric oxide. *Br J Pharmacol* 92: 639-46.

115. Radomski MW, Palmer RM, Moncada S. 1990. An L-arginine/nitric oxide pathway present in human platelets regulates aggregation. *Proc Natl Acad Sci U S A* 87: 5193-7.

116. Radomski MW, Palmer RM, Moncada S. 1987. Endogenous nitric oxide inhibits human platelet adhesion to vascular endothelium. *Lancet* 2: 1057-8.

117. Sneddon JM, Vane JR. 1988. Endothelium-derived relaxing factor reduces platelet adhesion to bovine endothelial cells. *Proc Natl Acad Sci U S A* 85: 2800-4.

118. Rhoads JM, Chen W, Gookin J, Wu GY, Fu Q, Blikslager AT, Rippe RA, Argenzio RA, Cance WG, Weaver EM, Romer LH. 2004. Arginine stimulates intestinal cell migration through a focal adhesion kinase dependent mechanism. *Gut* 53: 514-22.

119. McMahon TJ, Moon RE, Luschinger BP, Carraway MS, Stone AE, Stolp BW, Gow AJ, Pawloski JR, Watke P, Singel DJ, Piantadosi CA, Stamler JS. 2002. Nitric oxide in the human respiratory cycle. *Nat Med* 8: 711-7.

120. Lane P, Gross S. 2002. Hemoglobin as a chariot for NO bioactivity. *Nat Med* 8: 657-8.

121. Mack AK, Kato GJ. 2006. Sickle cell disease and nitric oxide: a paradigm shift? *Int J Biochem Cell Biol* 38: 1237-43.

122. Nathan C. 1992. Nitric oxide as a secretory product of mammalian cells. *FASEB J* 6: 3051-64.

123. Burgner D, Rockett K, Kwiatkowski D. 1999. Nitric oxide and infectious diseases. *Arch Dis Child* 81: 185-8.

124. Laroux FS, Pavlick KP, Hines IN, Kawachi S, Harada H, Bharwani S, Hoffman JM, Grisham MB. 2001. Role of nitric oxide in inflammation. *Acta Physiol Scand* 173: 113-8.

125. Karupiah G, Xie QW, Buller RM, Nathan C, Duarte C, MacMicking JD. 1993. Inhibition of viral replication by interferon-gamma-induced nitric oxide synthase. *Science* 261: 1445-8.

126. Lowenstein CJ, Hill SL, Lafond-Walker A, Wu J, Allen G, Landavere M, Rose NR, Herskowitz A. 1996. Nitric oxide inhibits viral replication in murine myocarditis. *J Clin Invest* 97: 1837-43.

127. Garthwaite J, Charles SL, Chess-Williams R. 1988. Endothelium-derived relaxing factor release on activation of NMDA receptors suggests role as intercellular messenger in the brain. *Nature* 336: 385-8.

128. Garthwaite J. 1991. Glutamate, nitric oxide and cell-cell signalling in the nervous system. *Trends Neurosci* 14: 60-7.

129. Bredt DS, Snyder SH. 1989. Nitric oxide mediates glutamate-linked enhancement of cGMP levels in the cerebellum. *Proc Natl Acad Sci U S A* 86: 9030-3.

130. Bredt DS, Snyder SH. 1990. Isolation of nitric oxide synthetase, a calmodulin-requiring enzyme. *Proc Natl Acad Sci U S A* 87: 682-5.

131. Snyder SH. 1992. Nitric oxide and neurons. *Curr Opin Neurobiol* 2: 323-7.

132. Dawson TM, Dawson VL, Snyder SH. 1992. A novel neuronal messenger molecule in brain: the free radical, nitric oxide. *Ann Neurol* 32: 297-311.

133. Bohme GA, Bon C, Lemaire M, Reibaud M, Piot O, Stutzmann JM, Doble A, Blanchard JC. 1993. Altered synaptic plasticity and memory formation in nitric oxide synthase inhibitor-treated rats. *Proc Natl Acad Sci U S A* 90: 9191-4.

134. Williams JH, Li YG, Nayak A, Errington ML, Murphy KP, Bliss TV. 1993. The suppression of long-term potentiation in rat hippocampus by inhibitors of nitric oxide synthase is temperature and age dependent. *Neuron* 11: 877-84.

135. Jaffrey SR, Snyder SH. 1995. Nitric oxide: a neural messenger. *Annu Rev Cell Dev Biol* 11: 417-40.

136. Nelson RJ, Demas GE, Huang PL, Fishman MC, Dawson VL, Dawson TM, Snyder SH. 1995. Behavioural abnormalities in male mice lacking neuronal nitric oxide synthase. *Nature* 378: 383-6.

137. Murphy S, Minor RL, Jr., Welk G, Harrison DG. 1990. Evidence for an astrocyte-derived vasorelaxing factor with properties similar to nitric oxide. *J Neurochem* 55: 349-51.

138. Shibuki K, Okada D. 1991. Endogenous nitric oxide release required for long-term synaptic depression in the cerebellum. *Nature* 349: 326-8.

139. Malinski T, Bailey F, Zhang ZG, Chopp M. 1993. Nitric oxide measured by a porphyrinic microsensor in rat brain after transient middle cerebral artery occlusion. *J Cereb Blood Flow Metab* 13: 355-8.

140. Schuman EM, Madison DV. 1994. Nitric oxide and synaptic function. *Annu Rev Neurosci* 17: 153-83.

141. Dawson VL, Dawson TM. 1996. Nitric oxide in neuronal degeneration. *Proc Soc Exp Biol Med* 211: 33-40.

142. Mayer B, John M, Bohme E. 1990. Purification of a Ca2+/calmodulin-dependent nitric oxide synthase from porcine cerebellum. Cofactor-role of tetrahydrobiopterin. *FEBS Lett* 277: 215-9.

143. Schmidt HH, Pollock JS, Nakane M, Gorsky LD, Forstermann U, Murad F. 1991. Purification of a soluble isoform of guanylyl cyclase-activating-factor synthase. *Proc Natl Acad Sci U S A* 88: 365-9.

144. Hevel JM, White KA, Marletta MA. 1991. Purification of the inducible murine macrophage nitric oxide synthase. Identification as a flavoprotein. *J Biol Chem* 266: 22789-91.

145. Yui Y, Hattori R, Kosuga K, Eizawa H, Hiki K, Kawai C. 1991. Purification of nitric oxide synthase from rat macrophages. *J Biol Chem* 266: 12544-7.

146. Stuehr DJ, Cho HJ, Kwon NS, Weise MF, Nathan CF. 1991. Purification and characterization of the cytokine-induced macrophage nitric oxide synthase: an FAD- and FMN-containing flavoprotein. *Proc Natl Acad Sci U S A* 88: 7773-7.

147. Evans T, Carpenter A, Cohen J. 1992. Purification of a distinctive form of endotoxin-induced nitric oxide synthase from rat liver. *Proc Natl Acad Sci U S A* 89: 5361-5.

148. Pollock JS, Forstermann U, Mitchell JA, Warner TD, Schmidt HH, Nakane M, Murad F. 1991. Purification and characterization of particulate endothelium-derived relaxing factor synthase from cultured and native bovine aortic endothelial cells. *Proc Natl Acad Sci U S A* 88: 10480-4.

149. Bates TE, Loesch A, Burnstock G, Clark JB. 1995. Immunocytochemical evidence for a mitochondrially located nitric oxide synthase in brain and liver. *Biochem Biophys Res Commun* 213: 896-900.

150. Bates TE, Loesch A, Burnstock G, Clark JB. 1996. Mitochondrial nitric oxide synthase: a ubiquitous regulator of oxidative phosphorylation? *Biochem Biophys Res Commun* 218: 40-4.

151. Ghafourifar P, Richter C. 1997. Nitric oxide synthase activity in mitochondria. *FEBS Lett* 418: 291-6.

152. Giulivi C, Poderoso JJ, Boveris A. 1998. Production of nitric oxide by mitochondria. *J Biol Chem* 273: 11038-43.

153. Masters BS, McMillan K, Sheta EA, Nishimura JS, Roman LJ, Martasek P. 1996. Neuronal nitric oxide synthase, a modular enzyme formed by convergent evolution: structure studies of a cysteine thiolate-liganded heme protein that hydroxylates L-arginine to produce NO. as a cellular signal. *FASEB J* 10: 552-8.

154. Narhi LO, Fulco AJ. 1987. Identification and characterization of two functional domains in cytochrome P-450BM-3, a catalytically self-sufficient monooxygenase induced by barbiturates in Bacillus megaterium. *J Biol Chem* 262: 6683-90.

155. Siddhanta U, Presta A, Fan B, Wolan D, Rousseau DL, Stuehr DJ. 1998. Domain swapping in inducible nitric-oxide synthase. Electron transfer occurs between flavin and heme groups located on adjacent subunits in the dimer. *J Biol Chem* 273: 18950-8.

156. Moncada S, Palmer RM, Higgs EA. 1991. Nitric oxide: physiology, pathophysiology, and pharmacology. *Pharmacol Rev* 43: 109-42.

157. Stuehr DJ, Kwon NS, Nathan CF, Griffith OW, Feldman PL, Wiseman J. 1991. N omega-hydroxy-L-arginine is an intermediate in the biosynthesis of nitric oxide from L-arginine. *J Biol Chem* 266: 6259-63.

158. Stuehr DJ, Santolini J, Wang ZQ, Wei CC, Adak S. 2004. Update on mechanism and catalytic regulation in the NO synthases. *J Biol Chem* 279: 36167-70.

159. Griffith OW, Stuehr DJ. 1995. Nitric oxide synthases: properties and catalytic mechanism. *Annu Rev Physiol* 57: 707-36.

160. White KA, Marletta MA. 1992. Nitric oxide synthase is a cytochrome P-450 type hemoprotein. *Biochemistry* 31: 6627-31.

161. Klatt P, Schmidt K, Uray G, Mayer B. 1993. Multiple catalytic functions of brain nitric oxide synthase. Biochemical characterization, cofactor-requirement, and the role of N omega-hydroxy-L-arginine as an intermediate. *J Biol Chem* 268: 14781-7.

162. Abu-Soud HM, Feldman PL, Clark P, Stuehr DJ. 1994. Electron transfer in the nitric-oxide synthases. Characterization of L-arginine analogs that block heme iron reduction. *J Biol Chem* 269: 32318-26.

163. Abu-Soud HM, Presta A, Mayer B, Stuehr DJ. 1997. Analysis of neuronal NO synthase under single-turnover conditions: conversion of Nomega-hydroxyarginine to nitric oxide and citrulline. *Biochemistry* 36: 10811-6.

164. Dudzinski DM, Igarashi J, Greif D, Michel T. 2006. The regulation and pharmacology of endothelial nitric oxide synthase. *Annu Rev Pharmacol Toxicol* 46: 235-76.

165. Li H, Poulos TL. 2005. Structure-function studies on nitric oxide synthases. *J Inorg Biochem* 99: 293-305.

166. Elfering SL, Sarkela TM, Giulivi C. 2002. Biochemistry of mitochondrial nitric-oxide synthase. *J Biol Chem* 277: 38079-86.

167. Nathan C, Xie QW. 1994. Nitric oxide synthases: roles, tolls, and controls. *Cell* 78: 915-8.

168. Murad F. 2006. Shattuck Lecture. Nitric oxide and cyclic GMP in cell signaling and drug development. *N Engl J Med* 355: 2003-11.

169. Dawson TM, Dawson VL. 1996. Nitric oxide synthase: role as a transmitter/mediator in the brain and endocrine system. *Annu Rev Med* 47: 219-27.

170. Bredt DS, Snyder SH. 1994. Nitric oxide: a physiologic messenger molecule. *Annu Rev Biochem* 63: 175-95.

171. Riobo NA, Melani M, Sanjuan N, Fiszman ML, Gravielle MC, Carreras MC, Cadenas E, Poderoso JJ. 2002. The modulation of mitochondrial nitric-oxide synthase activity in rat brain development. *J Biol Chem* 277: 42447-55.

172. Lacza Z, Puskar M, Figueroa JP, Zhang J, Rajapakse N, Busija DW. 2001. Mitochondrial nitric oxide synthase is constitutively active and is functionally upregulated in hypoxia. *Free Radic Biol Med* 31: 1609-15.

173. Pollock JS, Klinghofer V, Forstermann U, Murad F. 1992. Endothelial nitric oxide synthase is myristylated. *FEBS Lett* 309: 402-4.

174. Shaul PW. 2002. Regulation of endothelial nitric oxide synthase: location, location, location. *Annu Rev Physiol* 64: 749-74.

175. Busconi L, Michel T. 1993. Endothelial nitric oxide synthase. N-terminal myristoylation determines subcellular localization. *J Biol Chem* 268: 8410-3.

176. Sessa WC, Barber CM, Lynch KR. 1993. Mutation of N-myristoylation site converts endothelial cell nitric oxide synthase from a membrane to a cytosolic protein. *Circ Res* 72: 921-4.

177. Liu J, Garcia-Cardena G, Sessa WC. 1995. Biosynthesis and palmitoylation of endothelial nitric oxide synthase: mutagenesis of palmitoylation sites, cysteines-15 and/or -26, argues against depalmitoylation-induced translocation of the enzyme. *Biochemistry* 34: 12333-40.

178. Robinson LJ, Busconi L, Michel T. 1995. Agonist-modulated palmitoylation of endothelial nitric oxide synthase. *J Biol Chem* 270: 995-8.

179. Sessa WC, Garcia-Cardena G, Liu J, Keh A, Pollock JS, Bradley J, Thiru S, Braverman IM, Desai KM. 1995. The Golgi association of endothelial nitric oxide synthase is necessary for the efficient synthesis of nitric oxide. *J Biol Chem* 270: 17641-4.

180. Garcia-Cardena G, Oh P, Liu J, Schnitzer JE, Sessa WC. 1996. Targeting of nitric oxide synthase to endothelial cell caveolae via palmitoylation: implications for nitric oxide signaling. *Proc Natl Acad Sci U S A* 93: 6448-53.

181. Shaul PW, Smart EJ, Robinson LJ, German Z, Yuhanna IS, Ying Y, Anderson RG, Michel T. 1996. Acylation targets emdothelial nitric-oxide synthase to plasmalemmal caveolae. *J Biol Chem* 271: 6518-22.

182. Liu J, Garcia-Cardena G, Sessa WC. 1996. Palmitoylation of endothelial nitric oxide synthase is necessary for optimal stimulated release of nitric oxide: implications for caveolae localization. *Biochemistry* 35: 13277-81.

183. Yeh DC, Duncan JA, Yamashita S, Michel T. 1999. Depalmitoylation of endothelial nitric-oxide synthase by acyl-protein thioesterase 1 is potentiated by Ca(2+)-calmodulin. *J Biol Chem* 274: 33148-54.

184. Nathan C, Xie QW. 1994. Regulation of biosynthesis of nitric oxide. *J Biol Chem* 269: 13725-8.

185. Bauer PM, Fulton D, Boo YC, Sorescu GP, Kemp BE, Jo H, Sessa WC. 2003. Compensatory phosphorylation and protein-protein interactions revealed by loss of function and gain of function mutants of multiple serine phosphorylation sites in endothelial nitric-oxide synthase. *J Biol Chem* 278: 14841-9.

186. Vanhaesebroeck B, Leevers SJ, Panayotou G, Waterfield MD. 1997. Phosphoinositide 3-kinases: a conserved family of signal transducers. *Trends Biochem Sci* 22: 267-72.

187. Boo YC, Hwang J, Sykes M, Michell BJ, Kemp BE, Lum H, Jo H. 2002. Shear stress stimulates phosphorylation of eNOS at Ser(635) by a protein kinase A-dependent mechanism. *Am J Physiol Heart Circ Physiol* 283: H1819-28.

188. Fleming I, Fisslthaler B, Dimmeler S, Kemp BE, Busse R. 2001. Phosphorylation of Thr(495) regulates Ca(2+)/calmodulin-dependent endothelial nitric oxide synthase activity. *Circ Res* 88: E68-75.

189. Hink U, Li H, Mollnau H, Oelze M, Matheis E, Hartmann M, Skatchkov M, Thaiss F, Stahl RA, Warnholtz A, Meinertz T, Griendling K, Harrison DG, Forstermann U, Munzel T. 2001. Mechanisms underlying endothelial dysfunction in diabetes mellitus. *Circ Res* 88: E14-22.

190. Munzel T, Sayegh H, Freeman BA, Tarpey MM, Harrison DG. 1995. Evidence for enhanced vascular superoxide anion production in nitrate tolerance. A novel mechanism underlying tolerance and cross-tolerance. *J Clin Invest* 95: 187-94.

191. Oelze M, Mollnau H, Hoffmann N, Warnholtz A, Bodenschatz M, Smolenski A, Walter U, Skatchkov M, Meinertz T, Munzel T. 2000. Vasodilator-stimulated phosphoprotein serine 239 phosphorylation as a sensitive monitor of defective nitric oxide/cGMP signaling and endothelial dysfunction. *Circ Res* 87: 999-1005.

192. Huie RE, Padmaja S. 1993. The reaction of no with superoxide. *Free Radic Res Commun* 18: 195-9.

193. Hogg N, Joseph J, Kalyanaraman B. 1994. The oxidation of alpha-tocopherol and trolox by peroxynitrite. *Arch Biochem Biophys* 314: 153-8.

194. Vasquez-Vivar J, Santos AM, Junqueira VB, Augusto O. 1996. Peroxynitrite-mediated formation of free radicals in human plasma: EPR detection of ascorbyl, albumin-thiyl and uric acid-derived free radicals. *Biochem J* 314 (Pt 3): 869-76.

195. Guzik TJ, Mussa S, Gastaldi D, Sadowski J, Ratnatunga C, Pillai R, Channon KM. 2002. Mechanisms of increased vascular superoxide production in human diabetes mellitus: role of NAD(P)H oxidase and endothelial nitric oxide synthase. *Circulation* 105: 1656-62.

196. Kossenjans W, Eis A, Sahay R, Brockman D, Myatt L. 2000. Role of peroxynitrite in altered fetal-placental vascular reactivity in diabetes or preeclampsia. *Am J Physiol Heart Circ Physiol* 278: H1311-9.

197. Zou MH, Shi C, Cohen RA. 2002. Oxidation of the zinc-thiolate complex and uncoupling of endothelial nitric oxide synthase by peroxynitrite. *J Clin Invest* 109: 817-26.

198. Saris SC, Patronas NJ, Rosenberg SA, Alexander JT, Frank J, Schwartzentruber DJ, Rubin JT, Barba D, Oldfield EH. 1989. The effect of intravenous interleukin-2 on brain water content. *J Neurosurg* 71: 169-74.

199. Ellison MD, Povlishock JT, Merchant RE. 1987. Blood-brain barrier dysfunction in cats following recombinant interleukin-2 infusion. *Cancer Res* 47: 5765-70.

200. Watts RG, Wright JL, Atkinson LL, Merchant RE. 1989. Histopathological and blood-brain barrier changes in rats induced by an intracerebral injection of human recombinant interleukin 2. *Neurosurgery* 25: 202-8.

201. Alexander JT, Saris SC, Oldfield EH. 1989. The effect of interleukin-2 on the blood-brain barrier in the 9L gliosarcoma rat model. *J Neurosurg* 70: 92-6.

202. Perazella MA. 2009. Current status of gadolinium toxicity in patients with kidney disease. *Clin. J. Am. Soc. Nephrol.* 4: 461-9.

203. Pietsch H, Lengsfeld P, Steger-Hartmann T, Lowe A, Frenzel T, Hutter J, Sieber MA. 2009. Impact of renal impairment on long-term retention of gadolinium in the rodent skin following the administration of gadolinium-based contrast agents. *Invest. Radiol.* 44: 226-33.

204. Kribben A, Witzke O, Hillen U, Barkhausen J, Daul AE, Erbel R. 2009. Nephrogenic systemic fibrosis: pathogenesis, diagnosis, and therapy. *J. Am. Coll. Cardiol.* 53: 1621-8.

205. Yim CY, McGregor JR, Kwon OD, Bastian NR, Rees M, Mori M, Hibbs JB, Jr., Samlowski WE. 1995. Nitric oxide synthesis contributes to IL-2-induced antitumor responses against intraperitoneal Meth A tumor. *J. Immunol.* 155: 4382-90.

206. Angus DC, Linde-Zwirble WT, Lidicker J, Clermont G, Carcillo J, Pinsky MR. 2001. Epidemiology of severe sepsis in the United States: analysis of incidence, outcome, and associated costs of care. *Crit Care Med* 29: 1303-10.

207. Martin GS, Mannino DM, Eaton S, Moss M. 2003. The epidemiology of sepsis in the United States from 1979 through 2000. *N Engl J Med* 348: 1546-54.

208. Pinner RW, Teutsch SM, Simonsen L, Klug LA, Graber JM, Clarke MJ, Berkelman RL. 1996. Trends in infectious diseases mortality in the United States. *Jama* 275: 189-93.

209. Riedemann NC, Guo RF, Ward PA. 2003. The enigma of sepsis. *J Clin Invest* 112: 460-7.

210. O'Brien JM, Jr., Ali NA, Aberegg SK, Abraham E. 2007. Sepsis. *Am. J. Med.* 120: 1012-22.

211. Martin S, Maruta K, Burkart V, Gillis S, Kolb H. 1988. IL-1 and IFN-gamma increase vascular permeability. *Immunology* 64: 301-5.

212. Maruo N, Morita I, Shirao M, Murota S. 1992. IL-6 increases endothelial permeability in vitro. *Endocrinology* 131: 710-4.

213. Nooteboom A, Van Der Linden CJ, Hendriks T. 2002. Tumor necrosis factor-alpha and interleukin-1beta mediate endothelial permeability induced by lipopolysaccharide-stimulated whole blood. *Crit. Care Med.* 30: 2063-8.

CHAPTER 2

QUANTITATIVE ANALYSIS OF CYTOKINE-INDUCED VASCULAR TOXICITY AND VASCULAR LEAK IN THE MOUSE BRAIN

Abstract

A storm of inflammatory cytokines is released during treatment with pro-inflammatory cytokines, such as interleukin-2 (IL-2), closely approximating changes initially observed during sepsis. These signals induce profound changes in neurologic function and cognition. Little is known about the mechanisms involved. We evaluated a number of experimental methods to quantify changes in brain blood vessel integrity in a well-characterized IL-2 treatment mouse model. Measurement of wet versus dry weight and direct measurement of small molecule accumulation (e.g. [^{3}H]-H_2O, sodium fluorescein) were not sensitive or reliable enough to detect small changes in mouse brain vascular permeability. Estimation of brain water content using proton density magnetic resonance imaging (MRI) measurements using a 7 T mouse MRI system was sensitive to 1-2% changes in brain water content, but was difficult to reproduce in replicate experiments. Successful techniques included use of immunohistochemistry using specific endothelial markers to identify vasodilation in carefully matched regions of brain parenchyma and dynamic contrast enhanced (DCE) MRI. Both techniques indicated that IL-2 treatment induced vasodilation of the brain blood vessels. DCE MRI further showed a 2-fold increase in the brain blood vessel permeability to gadolinium in IL-2 treated mice compared to controls. Both immunohistochemistry and DCE MRI data suggested that IL-2 induced toxicity in the brain results from vasodilation of the brain blood vessels and increased microvascular permeability, resulting in perivascular edema. These experimental techniques provide us with the tools to further characterize the mechanism responsible for cytokine-induced neuropsychiatric toxicity.

Introduction

Cytokines are important signaling proteins secreted by cells to regulate the immune system. Interleukin-2 (IL-2) is a 15 kDa cytokine which activates lymphocytes via its well-characterized heterotrimeric receptor (1-2). IL-2 plays an important role in the development of cell-mediated immunity (3). In the presence of properly processed and presented antigenic peptides, low concentrations (10-100 IU/ml) of IL-2 are essential for the activation of cytolytic lymphocytes and their clonal expansion (4). Additionally, when murine or human lymphocytes are exposed to high concentrations of IL-2 (> 600 IU/ml) over 3-4 days either *in vitro* or *in vivo*, IL-2 rapidly activates a population of cytotoxic lymphocytes called lymphokine-activated killer (LAK) cells (5). LAK cells are termed "non-specific" killer cells as their cytotoxicity does not require antigen presentation in the context of self-MHC on target cells nor is it tumor-specific. LAK cells demonstrate cytotoxicity against almost all freshly isolated and cultured malignant cells (6-7), including multidrug-resistant tumor cells (8).

Activation of lymphocyte cytotoxicity against tumor cells *in vitro* by IL-2 led to evaluation of this cytokine as an anti-cancer therapy. In preclinical studies, concomitant IL-2 and LAK cells administrations on tumor-bearing mice resulted in regression of lung and liver metastases (9-10). Tumor regression in experimental mice was associated with prolonged survival (11-12). In clinical studies, high-dose i.v bolus IL-2 treatment induced 5-7% complete and 10-15% partial responses in patients with malignant melanoma and metastatic renal cell carcinoma (13-14). Approximately 60% of complete responses to high-dose IL-2 proved durable, with up to 20 years of follow-up (15).

Currently, IL-2 therapy is FDA approved for treatment of metastatic renal cell (RC) carcinoma and melanoma. IL-2 remains the only agent that can induce durable complete remissions of metastatic RC in approximately 5% of patients. Despite the dramatic increase in treatment options for metastatic RC in the past 4 years, including agents that inhibit vascular endothelial growth factor (VEGF) and mammalian target of rapamycin (mTOR) pathways (16), these agents predominantly induce disease arrest, requiring ongoing administration of expensive drugs to maintain a response. At the present time, IL-2 also remains the only clinically available remission-inducing agent for treatment of metastatic melanoma.

IL-2 therapy strongly induces synthesis of inflammatory cytokines termed a "cytokine storm" (17). These secondarily released cytokines, which include IFN-γ, tumor necrosis factor (TNFα, TNFβ), IL-1α, IL-1β, IL-5, and IL-6 (18-21) reach high levels in patient serum and are believed to trigger severe toxicities during IL-2 treatment. This pattern of cytokine secretion has strong similarities to the "cytokine storm" elicited by bacterial endotoxin (22-24). These secondarily released cytokines may also contribute to the therapeutic response to IL-2, as high dose steroids block IL-2 toxicity but also abrogate the therapeutic effectiveness of this agent (25).

The major dose-limiting toxicities of IL-2 are vascular leak syndrome (VLS) and hypotension. IL-2 induced VLS is generalized and dose dependent, characterized by loss of intravascular fluid into interstitial tissues. VLS is associated with marked fluid retention (weight gain), reversible renal dysfunction, and noncardiac pulmonary edema (26). IL-2 induced hypotension is due to a marked decrease in systemic vascular resistance, resulting in hypoperfusion of vital organs, such as heart and kidneys (27), in

conjunction with VLS and intravascular volume depletion. It has also been recognized that reversible neuropsychiatric toxicity represents the third IL-2 dose-limiting toxicity. Denicoff et al. showed that there were striking neuropsychiatric changes in the majority of patients after the onset of IL-2 treatment, with 30-50% of patients experienced severe behavioral and cognitive changes (28). All patients returned to their baseline cognitive scores at follow-up (28). It should be noted that the pattern of hypotension, VLS, and delirium following IL-2 therapy in patients appears very similar to the clinical presentation of patients who have severe bacterial infection and septic shock (27). The major apparent difference is the complete resolution of renal function changes following completion of IL-2 therapy, unlike the high incidence of acute tubular necrosis during septic shock. It has become increasingly clear that even if hypotension and VLS can be attenuated, dose limitations related neuropsychiatric toxicity prevent effective IL-2 dose escalation.

To date, the effects of inflammatory cytokines that trigger neuropsychiatric toxicity in the brain are not well understood. Moreover, technical challenges exist to study these effects after 4-5 days of IL-2 treatment (similar to treatment sequence used in human patients). Studies in patients and animal models have suggested that brain edema could play a role (29-32). However, Alexander et al. suggested that IL-2 induced brain edema occurred predominantly in tumor-bearing rat brain but not in normal brain (30). Since tumors are known to have abnormal blood vessel permeability, it is strongly believed that this could result in increased brain edema following IL-2 treatment. We therefore evaluated a number of potential approaches to more directly evaluate cytokine

effects on the non-tumor bearing central nervous system (CNS) using IL-2 treatment as a model in a well-characterized murine system (33-34).

Materials and Methods

Mice. Pathogen-free C3H/HeN mice were obtained from Charles River Laboratories. Mice were maintained under guidelines established by the Institutional Animal Care and Use Committee (IACUC). The IACUC also approved all the animal experimental protocols. Mice were age- and sex-matched in each experiment.

IL-2 treatment. IL-2 treated mice received 150,000 IU of IL-2 (Aldesleukin Proleukin®; Novartis, Emeryville, CA) in 0.2 ml PBS (phosphate buffered saline) intraperitoneally (i.p.), b.i.d. (twice a day) for 5 days (10 doses total) in all experiments, except in experiments using MRI. For MRI studies, mice received 8 doses of 150,000 IU of IL-2 in 0.2 ml PBS i.p., b.i.d. (4 days). Control mice received no treatment, except in wet versus dry brain weight experiments, where control mice were treated with an equivalent volume of PBS (without IL-2).

Comparison of wet versus dry brain weight. Brains were harvested from each IL-2 treated and control mouse after 5 days of IL-2 and PBS treatment, respectively. Each brain was weighed before and after drying by Heto vacuum centrifuge (ATR, Laurel, Maryland) overnight in 60°C. The water content of the brain was calculated as:

$$\%\ \text{tissue water} = \frac{\text{wet weight} - \text{dry weight}}{\text{wet weight}} \text{x}\, 100.$$

[^{125}I]-labeled albumin extravasation in the mouse brain. Approximately 100,000 counts per minute (cpm) of [^{125}I]-labeled albumin (specific activity 1-5 μCi/μg) in 100 μl PBS was injected intravenously (i.v.) into the tail veins of mice 2 h after the last

dose of IL-2. Mice were sacrificed 6 h after the last dose of IL-2 and the brains excised. Each brain was analyzed for albumin accumulation. Data was calculated as follow:

$$\%\ \text{cpm} = \frac{\text{brain cpm x } 100\%}{\text{total cpm recovered from the mouse}}.$$

Tritiated water ([^{3}H]-H_2O) extravasation as a potential marker of IL-2 induced VLS. IL-2 treated or control mice were injected with approximately 300,000 cpm of [^{3}H]-H_2O in 100 µl PBS i.v. into the tail vein 2 h after the last dose of IL-2 or no treatment (control). Mice were then sacrificed at 4, 12, or 18 h after [^{3}H]-H_2O injection. The brain was harvested from each mouse, weighed, and homogenized in 1 ml PBS using Tissumizer (Tekmar, Cincinnati, OH). The homogenate (100 µl) was added into 2 ml scintillation fluid and quantified in a scintillation counter. To correct for tissue quenching, 100 µl brain homogenate from a normal mouse was directly mixed with 300,000 cpm [^{3}H]-H_2O in 100 µl PBS and 2 ml scintillation fluid, and quantified in a scintillation counter. The cpm recovered was expressed as percentage of 300,000 cpm and was used to correct the apparent cpm from the IL-2 treated and control mouse brain homogenates. The [^{3}H]-H_2O extravasation in each brain homogenate of IL-2 and control mice was expressed as cpm per gram tissue as follow:

$$\text{cpm/gram tissue} = \frac{\text{homogenate cpm x } 100\%}{\%\ \text{cpm recovered (quenching) x tissue weight (g)}}.$$

Sodium fluorescein extravasation in mouse pleural fluid, lungs, and brain as an indicator of VLS. IL-2 treated or control mice were injected with 1.5 mg fluorescein sodium salt (NaFl; Sigma-Aldrich, St. Louis, MO) in 100 µl PBS i.v. via tail vein, 4 h after the last dose of IL-2. The mice were sacrificed 10 min after NaFl injection. The pleural fluid from IL-2 treated mice was collected and the volume was measured. Since

control mice did not have detectable pleural fluid, the thoracic cavity was irrigated with 500 µl PBS, which was collected. The lungs and brain were also harvested and were homogenized in 1 ml PBS each, using Tissumizer (Tekmar, Cincinnati, OH). After centrifugation for 5 min, 100 µl of each homogenate was added in triplicate into a 96-well plate. Also in triplicate, 100 µl of the pleural fluid from each mouse was transferred into another 96-well plate. Plates were read using a Synergy 2 microplate reader (BioTek Instruments, Winooski, Vermont) at 519 nm emission and 495 nm excitation wavelengths. For the pleural fluid, the fluorescence was quantified using a standard curve and multiplied by the total volume recovered to calculate the total amount of NaFl (in µg) that leaked into the pleural fluid. In lung or brain homogenates, the fluorescence was corrected for tissue quenching and quantified using a standard curve. Data were expressed as µg NaFl/organ based on the total volume of homogenate.

Evaluation of brain blood vessel morphology using immunohistochemistry. Brains were excised from IL-2 treated or control mice. Each brain was embedded in Tissue-Tek O.C.T. Compound (Ted Pella, Redding, CA) and frozen at -20 °C overnight before sectioning. Matched sections (6 µm) of the mid-brain (Fig. 2.1) were dual-stained with Isolectin GS-IB_4 (Iso-B4) from *Griffonia simplicifolia*, conjugated to Alexa Fluor® 568 (Molecular Probes, Eugene, OR) and rabbit anti-human von Willebrand Factor (vWF; Sigma-Aldrich, St. Louis, MO), followed by a secondary Dichlorotriazinyl-aminofluorescein (DTAF)-conjugated donkey anti-rabbit IgG (Jackson ImmunoResearch Laboratories, West Grove, PA). Digital images of 20 specific regions of interest (4 different areas in the left cortex, right cortex, left striatum, right striatum, and the cerebral fissure; Fig. 2.1) in the stained brain sections were acquired using Olympus BX51

Figure 2.1

Cross section drawing of the mouse mid-brain section, which includes the cortex and striatum anatomic regions, derived from Dorr et al. (35). Inset figure represents the position at which the tissue slice was taken (Bregma 0.62-0.38 mm). The drawing shows the name of major cerebral vasculature structures found in the specific section. azPA = azygos pericallosal artery. Boxes show the locations of 19-20 digital images obtained from each section for vessel analysis. On the right are representative sections from the control and IL-2 treated mice, which were matched as closely as possible to the drawing on the left, stained with hematoxylin and eosin. These representative sections are located right by the sections used in the immunohistochemistry experiment.

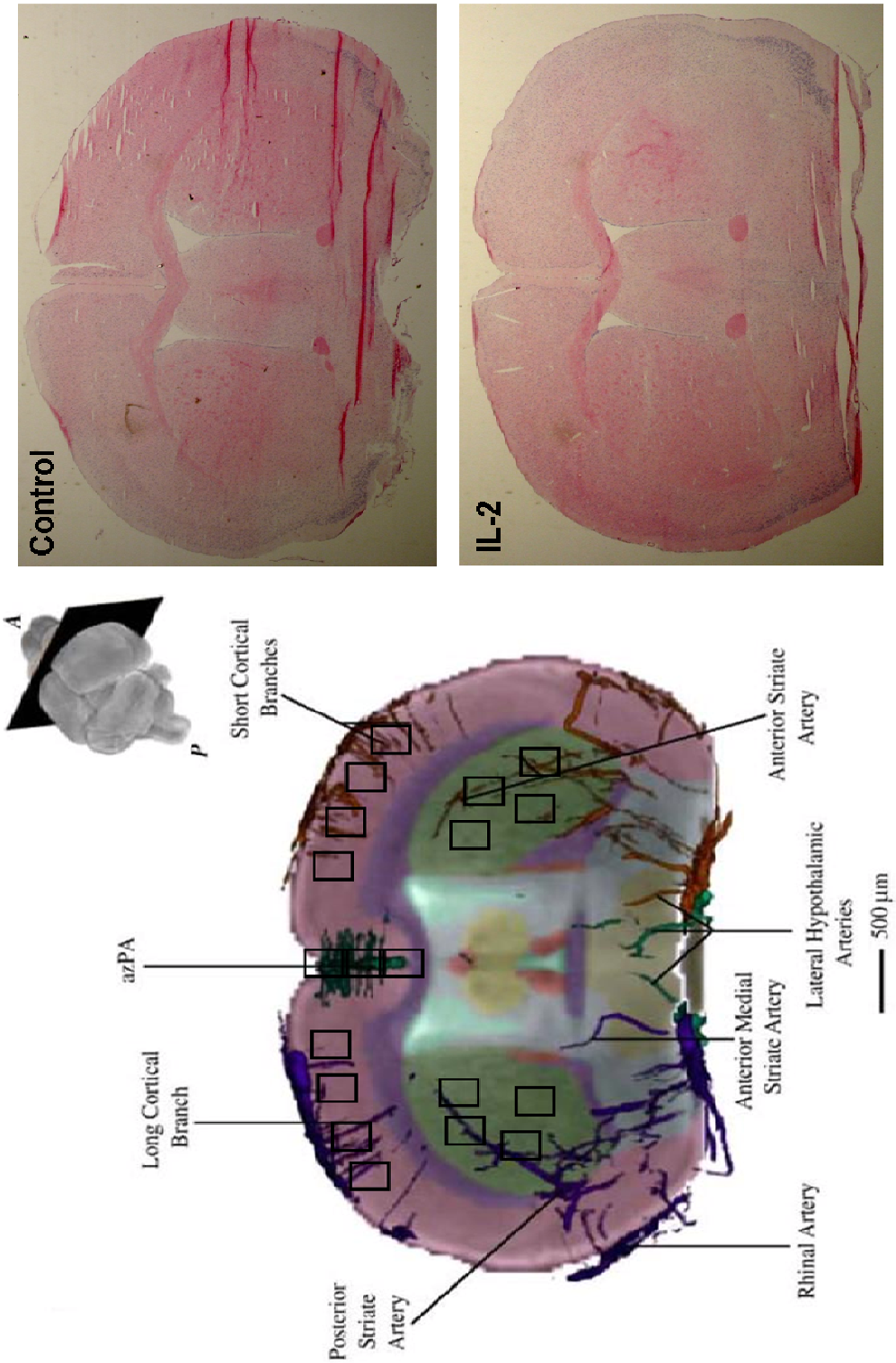
Control
IL-2
A
P
Short Cortical Branches
azPA
Long Cortical Branch
Posterior Striate Artery
Anterior Striate Artery
Lateral Hypothalamic Arteries
Anterior Medial Striate Artery
Rhinal Artery
500 µm

fluorescent microscope mounted with Olympus DP70 camera. Using ImageJ software (National Institutes of Health, NIH), the blood vessels (dual stained tubular structures) in each digital image were manually outlined and analyzed for the total number and average size of vessels.

Evaluation of brain water content using MRI proton density measurements. MRI was performed using a Bruker 7T/20 scanner, a 3.5 cm ID (inner diameter) quadrature transceiver coil, and a 7 cm ID unshielded gradient. Mice were anesthetized by i.p. injection of 80 mg/kg ketamine (Vetalar®; Aveco, Fort Dodge, IA) and maintained inside the magnet using isoflurane (Attane™; Minrad, Bethlehem, PA) inhalational anesthesia as required. Mouse temperature inside the magnet was maintained using a circulating warm water system. Each mouse was scanned both before and after IL-2 treatment. Proton density MRI was sequenced using a Fast Spin Echo sequence with a repetition time (TR) of 24 s, an echo time (TE) of 7.5 ms, and an echo train length of 4. Slice thickness was 1 mm, field of view was 2x2 cm^2, and matrix size was 256x192 pixels. The slice thickness and matrix size were optimized to detect proton density changes in the mouse brain of > 1%. The total scan time was 14 min and 24 s. Regions of interest (ROIs) were drawn manually on matched pre- and post-IL-2 mouse's brain DICOM (Digital Imaging and Communications in Medicine) images using OsiriX imaging software (http://www.osirix-viewer.com/). The signal intensity (SI) of each brain slice was normalized using a set of phantoms (60-100% H_2O/D_2O in 10% increment) and expressed as the percentage of proton density (%PD). We averaged the %PD over 8 MRI brain image slices for each mouse and compared the average %PD before and after IL-2 treatment.

Dynamic contrast enhanced (DCE) MRI. The MRI system and anesthesia were described above. Each mouse was scanned before and after IL-2 treatment, serving as its own control. Prior to imaging, the tail vein of each mouse was catheterized using a 30-gauge needle connected to an approximately 1 m long, 0.28 mm ID tube pre-filled with heparinized PBS (approximately 100 µl). DCE-MRI was performed using 2D-FLASH (Fast Low-Angle Shot): TR = 93.5 ms, TE = 3.1 ms, flip angel = 30 º, FOV = 2 x 2 cm, matrix = 128 x 128, slice thickness = 1 mm, number of slices = 11, single scan time = 9 s, number of repetitions = 54. After the first 5 repetitions, 0.1 mmol/kg contrast agent (gadobenate dimeglumine; MultiHance®, Bracco) was administered by bolus injection via the catheter. Customized MATLAB programs (The MathWorks, Natick, MA) were used to calculate the SI of the whole brain ROI in matched mid-brain sections of pre- and post-IL-2 DICOM images. The signal intensities of the left and right maxillary veins were averaged to derive the contrast agent concentrations in the blood pool. The average SI of ROI before contrast agent injection was used as the baseline and subtracted from all SI after contrast agent injection to calculate the increase in SI (ΔSI). ΔSI was assumed to be proportional to the change in contrast agent concentration when a low concentration of contrast agent was used (36). A two-compartment model was originally developed by Shames et al. (36) to characterize tumor vasculature and adapted by Feng et al. (37) to calculate the tumor fractional plasma volume (f^{PV}), endothelium transfer coefficient (K^{PS}), and permeability surface area product (PS). This method was similarly used to characterize the brain microvasculature.

Statistical analysis. All data are expressed as mean ± standard error of the mean (SEM). Statistical analyses on MRI data were performed by paired Student's 2-tailed t-

test using GraphPad PRISM software (GraphPad Software, La Jolla, CA). The immunohistochemistry data were analyzed using 2-factor analysis of variance (ANOVA) with a blocking factor for region of the brain. All the other data were analyzed using 2-sample Student's 2-tailed t-test. A p-value ≤ 0.05 was considered significant.

Results

Comparison of wet versus dry brain weight in IL-2 treated mice. Difference in wet versus dry tissue weight is assumed to be approximately the volume of interstitial fluid in the tissue. It was not certain whether this technique was sensitive enough to detect the small fluid shifts that were likely in the mouse brain related to cytokine treatment. We excised brains from IL-2 treated or control mice (treated with an equivalent volume of PBS) after 5 days of treatment and weighed each brain before and after drying by speed vacuum. The average brain water content of IL-2 treated mice was 43.05±1.84% of the wet weight while the control mice had a mean brain water content of 42.6±1.524% ($p = 0.85$; Fig. 2.2). It became clear from these results that this method lacked sensitivity to identify relatively small changes in the brain water content of mice related to IL-2 treatment.

[^{125}I]-labeled albumin extravasation in the mouse brain. Radioactive labeled [^{125}I]-bovine serum albumin has often been used to study IL-2 induced VLS in mice tissues (38). However, it had not been quantified as a VLS marker in the mouse brain. To test this, we injected IL-2 treated or control mice with [^{125}I]-labeled albumin bolus via tail vein. After 4 h, mice were sacrificed and the brains excised. The amount of [^{125}I]-labeled albumin recovered in the brain was quantified and expressed as a percentage of the total

Figure 2.2

Direct comparison of wet versus dry brain weight from IL-2 treated mice. Brains were excised from IL-2 treated and control mice (n = 9). Each mouse brain was weighed before and after drying in a vacuum centrifuge overnight in 60 °C. The wet and dry weight difference was expressed as a percentage of wet weight. Error bars represent SEM. The result was not significant (NS), $p > 0.05$.

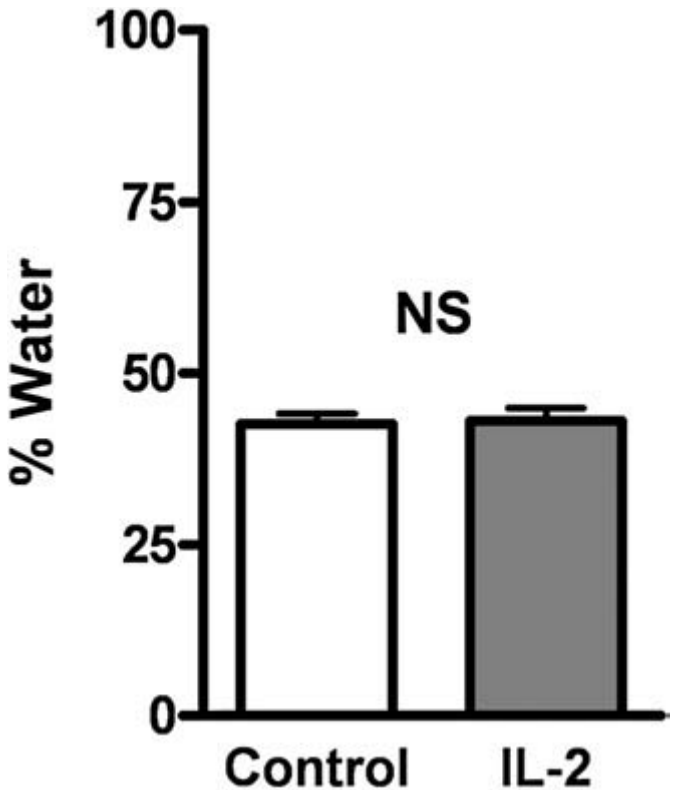
100
75
50
25
0
% Water
NS
Control
IL-2

amount of [^{125}I]-labeled albumin recovered from the mouse. Analysis of [^{125}I]-labeled albumin accumulation in the brain showed no significant increase following IL-2 treatment ($p = 0.17$; Fig. 2.3). The amount of [^{125}I]-labeled albumin recovered from the brain of IL-2 treated mice was 0.2172±0.04% while the control mice had 0.1364±0.04%. The small percentage of [^{125}I]-labeled albumin recovered from the mouse brain demonstrated that this method also lacked the sensitivity to measure a small increase in [^{125}I]-labeled albumin extravasation in the mouse brain induced by IL-2.

Tritiated water ([^{3}H]-H_2O) extravasation as a potential marker of IL-2 induced VLS. We hypothesized that vascular leak in the brain should correlate with the ability of water molecules (H_2O) to cross the BBB. To test [^{3}H]-H_2O as a potential marker of IL-2 induced fluid shifts in the mouse brain, IL-2 treated or control mice were injected with [^{3}H]-H_2O bolus via tail vein. At specified times, mice were sacrificed and the brain excised. Each brain was weighed and homogenized. The homogenate was quantified in a scintillation counter, and corrected for quenching of counts by tissue homogenate. At 4 and 12 h after the last IL-2 dose, significant [^{3}H]-H_2O retention in the brain of IL-2 treated mice could not be detected compared to the control mice (Fig. 2.4). At 4 h after the last IL-2 dose, there were 787.3±36.48 cpm [^{3}H]-H_2O/g brain in the IL-2 treated mice compared to 742.7±17.39 cpm [^{3}H]-H_2O/g brain in the control mice ($p = 0.332$). By 12 h, there were 713±37.29 cpm [^{3}H]-H_2O/g brain in the IL-2 treated mice and 653.5±24.28 cpm [^{3}H]-H_2O/g brain in the control mice ($p = 0.2024$). There was a trend toward increased [^{3}H]-H_2O retention in the brain of IL-2 treated mice at 18 h (810.8±70.82 cpm [^{3}H]-H_2O/g brain) compared to the control mice (552±24.03 cpm [^{3}H]-H_2O/g brain), $p = 0.003$ (Fig. 2.4). Despite use of syngeneic mice and a precisely timed

Figure 2.3

Evaluation of IL-2 induced vascular leak in the brain using [^{125}I]-labeled albumin. Mice (n = 6) were injected with approximately 100,000 cpm of [^{125}I]-labeled albumin in 100 µl PBS via tail vein 2 h after the last dose of IL-2 or no treatment (control). After 4 h, mice were sacrificed, the brains excised and analyzed for [^{125}I]-labeled albumin accumulation. The results were expressed as percentage of radiolabeled albumin recovered from the brain with the total amount recovered from the animal.

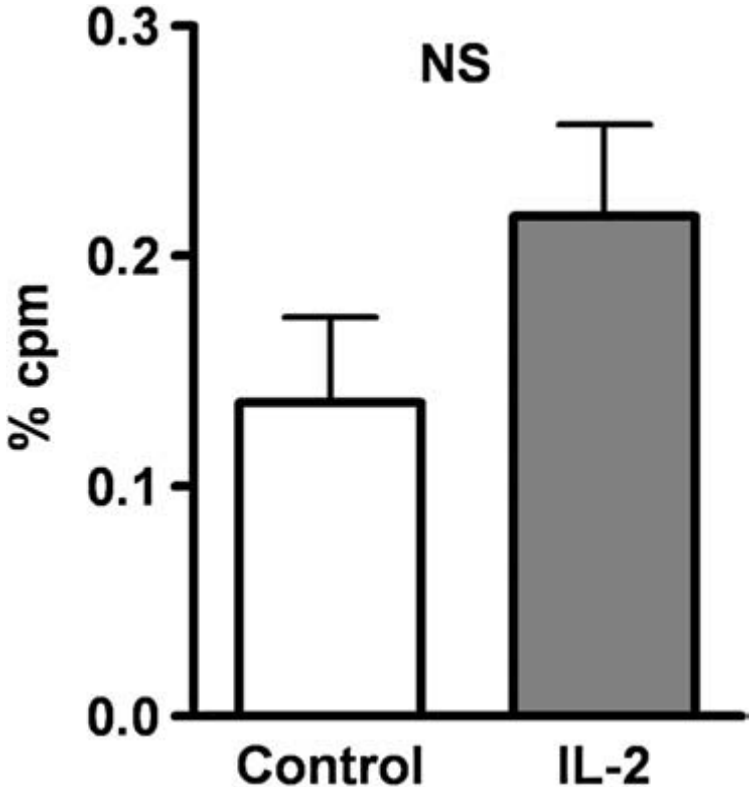
0.3
0.2
0.1
0.0
% cpm
NS
Control
IL-2

Figure 2.4

Evaluation of changes in brain water content using tritiated water ([^{3}H]-H_2O). Two hours after the last IL-2 dose or no treatment (control), mice (n = 3 at 4 h, n = 8 at 12 and 18 h) were injected with ~300,000 cpm [^{3}H]-H_2O in 100 µl PBS via tail vein. The brain was harvested from each cohort of control and IL-2-treated mice at the specified time (4 h, 12 h, or 18 h) after [^{3}H]-H_2O injection. Brains were homogenized and 100 µl was counted in 2 ml scintillation fluid on a scintillation counter. The results were corrected for tissue quenching and expressed as cpm/gram tissue. * indicates p = 0.003.

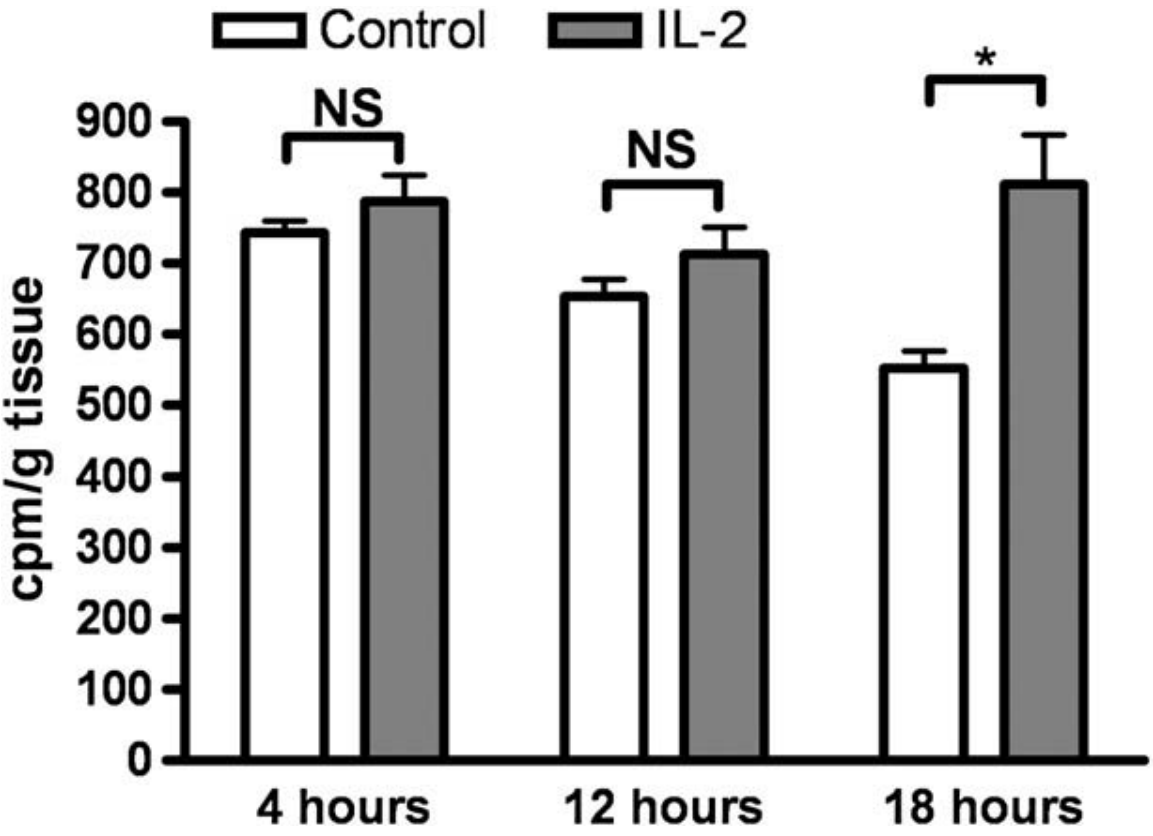
Control
IL-2
NS
NS
*
900
800
700
600
500
400
300
200
100
0
cpm/g tissue
4 hours
12 hours
18 hours

treatment schedule, this technique exhibited quite a bit of variability between experiments. This led us to conclude that measurement of [^{3}H]-H_2O retention was not a reliable means of measuring IL-2 induced fluid shifts in the mouse brain.

Measurement of Sodium Fluorescein (NaFl) extravasation in the mouse pleural fluid, lungs, and brain. NaFl is a small fluorescent molecule (MW = 376.27). This probe may provide increased sensitivity for detection of BBB disruption induced by IL-2 and decrease tissue quenching and volume of distribution problems related to the use of [^{3}H]-H_2O. We evaluated NaFl as an indicator for IL-2 induced VLS, based on its prior use as a marker for fluorescence imaging of BBB disruption in rats (39-40). Control and IL-2 treated mice were injected with 1.5 mg NaFl in 100 µl PBS via tail vein and sacrificed after 10 min. Pleural fluid was collected directly from the thoracic cavity of IL-2 treated mice whereas the thoracic cavity of the control mice was irrigated with 500 µl PBS, which was then collected. The entire recovered volume was quantified. Fluorescence was measured by spectrofluorometer. Using a standard curve, the concentration of NaFl recovered from each mouse was quantified. By multiplying the concentration of NaFl by the total volume of the fluid recovered, we calculated the total amount of NaFl leak. IL-2 treatment increased NaFl extravasation into the pleural space by 9-fold (9.59±0.82 µg total NaFl) compared to the control mice (1.09±0.13 µg total NaFl), $p < 0.0001$ (Fig. 2.5A).

In order to evaluate the usefulness of this technique for solid organs, the lungs and brain from these mice were excised. Each tissue was homogenized in 1 ml PBS, and the amount of NaFl in the homogenate quantified. Following correction of tissue-specific fluorescence quenching, we found 10.34±0.82 µg total NaFl in the lungs of IL-2 treated

mice. There was no detectable difference compared to NaFl content in lungs of the control mice (8.88±1.21 µg total NaFl, $p = 0.35$; Fig. 2.5B). There was also no detectable difference in the amount of total NaFl in the brains of IL-2 treated mice (1.06±0.05 µg total NaFl) compared to the control (1.14±0.06 µg total NaFl), $p = 0.34$ (Fig. 2.5C). This method proved useful in demonstrating small molecule leak resulting in pleural effusions, but not into solid organs of IL-2 treated mice. Perfusion of mice with saline to decrease intravascular NaFl retention did not seem to influence results in the brain (data not shown).

Evaluation of brain blood vessel morphology using immunohistochemistry. It is well known that nitric oxide (NO) produced by endothelial cells or from pharmacologic donors induces vasodilation (41-43). We therefore evaluated whether vasodilation could be identified in brain blood vessels via immunohistochemistry. We prepared 6 µm sections from carefully defined anatomic region of the mouse mid-brain (Fig. 2.1) chosen to reflect highly vascular areas based on a study by Dorr et al. (35). Areas selected included the cerebral fissure, the striatum and the cortex in the highly vascularized anatomic region shown (Fig. 2.1). We tested a number of putative endothelial cell-specific antibodies, CD34, CD144 (VE-cadherin), and anti-von Willebrand Factor (vWF). All of them showed speckled endothelial cell staining (data not shown). As vWF is specifically produced in blood vessels, this marker was selected. However, the granular nature of the stain made it difficult to outline vessels to measure the area. Isolectin GS-IB_4 (Iso-B4) demonstrates strong staining of perivascular cells. Unfortunately, Iso-B4 is also known to stain brain microglial cells. By using dual staining of vWF and Iso-B4, we were able to identify the circumference of blood vessels in the

Figure 2.5

Evaluation of blood vessel permeability using sodium fluorescein (NaFl) in the mouse A) pleural fluid, B) lungs, and C) brain. Mice (n = 5) were injected with 1.5 mg NaFl in 100 µl PBS via tail vein 4 h after the last IL-2 dose or no treatment (control). After 10 min, mice were sacrificed. The pleural fluid was collected and the brains and lungs were excised from each mouse. The lungs and brain were homogenized in 1 ml PBS and 100 µl of each homogenate or 100 µl of the collected pleural fluid was quantified by spectrofluorometer. The total amount (µg) of NaFl in each sample was calculated by using a standard curve, corrected for tissue quenching, and then multiplied by the total volume of organ homogenate (1 ml) or the measured volume of the collected pleural fluid.

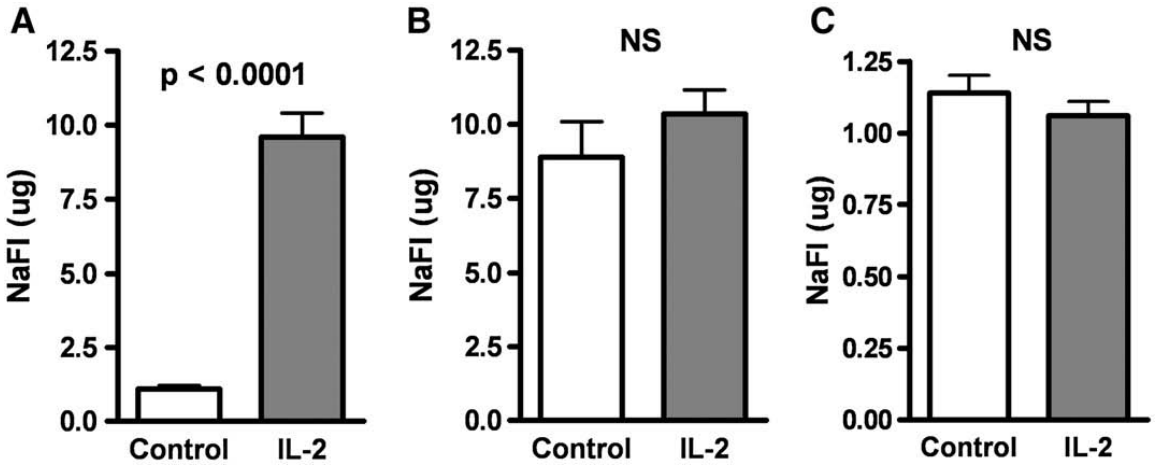
A
p < 0.0001
NaFl (ug)
12.5
10.0
7.5
5.0
2.5
0.0
Control
IL-2
B
NS
NaFl (ug)
12.5
10.0
7.5
5.0
2.5
0.0
Control
IL-2
C
NS
NaFl (ug)
1.25
1.00
0.75
0.50
0.25
0.00
Control
IL-2

mouse brain section. We obtained twenty 20x magnification digital images from precise anatomic locations of the brain section (4 of each left cortex area, right cortex, left striatum, right striatum, and the cerebral fissure) using fluorescence microscopy and analyzed each image for the numbers and size of blood vessels. The analysis showed that the average size of vessels in the brain was almost 2-fold larger in the IL-2 treated mice (37750.53±5598 pixel^2) compared to the control mice (20652.85±5598 pixel^2), $p = 0.0389$ (Fig. 2.6A), while the number of vessels in the brain of IL-2 treated mice (8.082±1.83) were not significantly different compared to the control mice (7.343±1.83), $p = 0.7765$ (Fig. 2.6B). The number of blood vessels was not expected to change during 5 days of IL-2 treatment. These results suggest that IL-2 strongly induced vasodilation of the brain blood vessels.

Evaluation of brain water content using MRI proton density. Intrinsic MR parameters, such as longitudinal (T_1) and transverse (T_2) relaxation times, are sensitive to changes in the proton density and therefore the water content of tissues. Therefore, MRI proton density (PD) provides a potential noninvasive technique to quantify changes in the brain water content induced by cytokine treatment. A prior study in IL-2 treated patients using a T_2-weighted MRI had suggested that particularly large changes in brain MR signal intensity were induced by IL-2 treatment (29). However, this study showed an extremely wide percentage range (3-48%) of the changes in the cerebral water content, raising questions as to the accuracy and reproducibility of this determination. We developed a high resolution murine imaging technique to critically assess MRI quantified PD changes in the brains of IL-2 treated mice. Imaging phantoms were prepared employing various ratios of H_2O/D_2O (60-100% in 10% increment), serving as

Figure 2.6

Immunostaining of brain sections to evaluate endothelial cell morphology. Brains were excised from IL-2 treated and control mice (n = 3). Sections (6 µm-thick) were carefully prepared to identify specific anatomic regions of the mid-brain. Each frozen section was dual-stained with Iso-B4 and anti-vWF to identify blood vessels and exclude microglial cells. The blood vessels were manually outlined on 20 digitized fluorescence images of each stained section and analyzed for A) the average size of vessels and B) total number of vessels using ImageJ software. The values were compared between pre- and post-IL2.

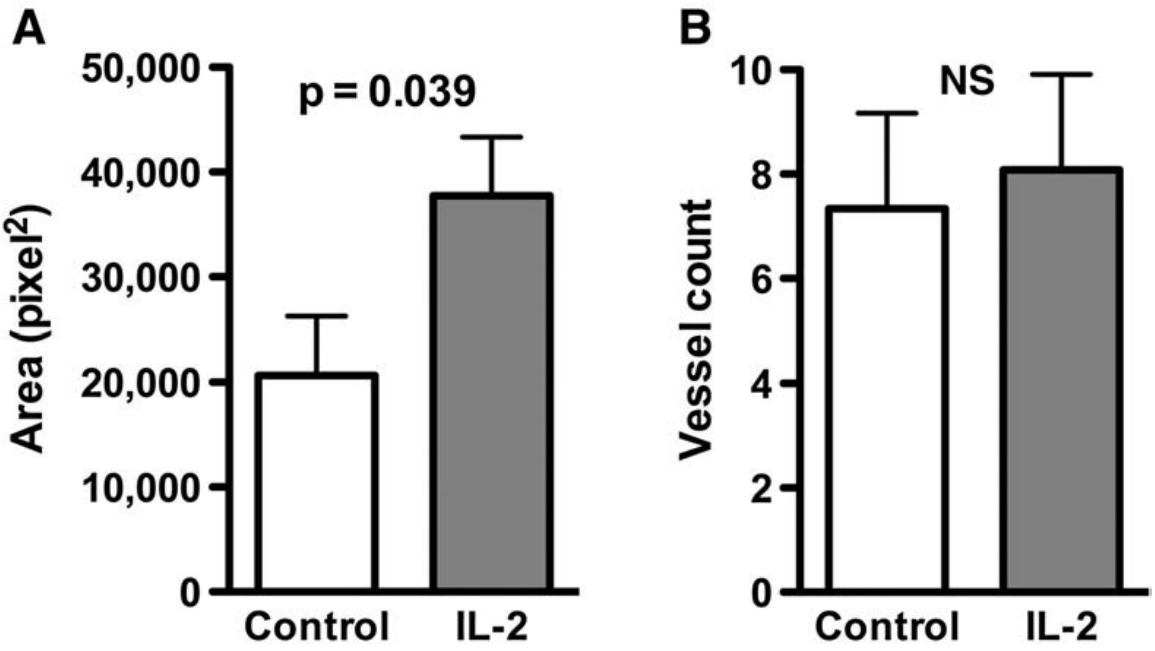
A
50,000
40,000
30,000
20,000
10,000
0
Area (pixel²)
p = 0.039
Control
IL-2
B
10
8
6
4
2
0
Vessel count
NS
Control
IL-2

references. We scanned anesthetized mice both before and after IL-2 treatment using MRI PD sequence using a 7T Bruker MRI system with a mouse-specific coil. We established that this sequence was sensitive enough to detect an approximate 1% change in PD in the mouse brain. PD was calculated using a ratio of the signal intensity (SI) from the manually drawn ROI (region of interest) around the whole mouse brain with that of the phantom SI. We averaged PD over 8 matched brain slices of pre- and post-IL-2 DICOM images for each mouse. The results of this experiment (Fig. 2.7) established that there was no significant difference ($p = 0.7892$) in MRI proton density of IL-2 treated mice (73.31 ± 0.7) compared to before receiving IL-2 treatment (73.65 ± 0.7). We also found that results obtained with this technique varied markedly between experiments. We concluded that the MRI PD sequence was too inconsistent to provide useful information concerning the small, most likely perivascular changes in mouse brain water content related to IL-2 administration.

Dynamic contrast-enhanced (DCE) MRI. DCE MRI is a quantitative, noninvasive technique to measure vascular permeability using a gadolinium-based contrast agent. DCE MRI has often been used clinically to assess tumor angiogenesis based on tumor vascular permeability. This technique provides physiologically meaningful quantitative assessment of vascular parameters, such as fractional plasma volume (f^{PV}), endothelial transfer coefficient (K^{PS}), and permeability surface area product (PS) (44). f^{PV} describes the plasma volume of the blood vessels in that tissue. K^{PS} reflects the permeability of the contrast agent from the blood vessels to the extravascular and extracellular space (EES) of the tissue. PS describes the surface area of the vasculature that is permeable to the contrast agent. We developed a protocol for DCE

Figure 2.7

Evaluation of proton density in the brains of IL-2 treated mice using a 7T MRI system. Mice (n = 5) were scanned both before and after 4 days of IL-2 treatment (150,000 U i.p, b.i.d.) using a MRI PD sequence as described in the *Materials and Methods*. Regions of interest were manually drawn on matched sections of mouse brain using OsiriX software and expressed as % proton density (PD) based on the phantoms (created using 60-100% H_2O/D_2O in 10% increment). The %PD was averaged over 8 slices for each mouse and compared between pre- and post-IL-2 treatment scans derived from the same mouse.

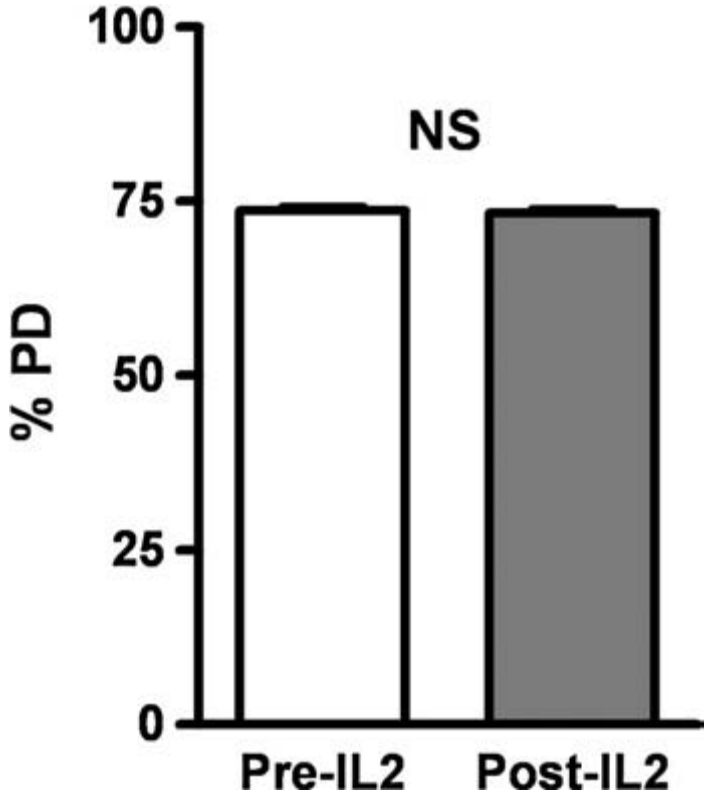
100
75
50
25
0
% PD
NS
Pre-IL2
Post-IL2

MRI to evaluate the brain microvasculature of IL-2 treated mice. Anesthetized mice were scanned before and after IL-2 treatment using 2D-FLASH MRI sequence. This MRI sequence provides good spatial resolution and has the advantage of allowing rapid scanning. We calculated SI from a manually drawn ROI on a selected mid-brain section of each mouse, matched between pre- and post-IL-2 images, using customized MATLAB programs. The contrast agent concentration in the blood pool was established by averaging the SI from the left and right maxillary veins. We used a two-compartment model consisting of the brain plasma compartment and the EES to calculate f^{PV}, K^{PS}, and PS as described previously by Feng et al. (37). DCE MRI data established a 2-fold increase of f^{PV} in the mice brain after receiving IL-2 treatment ($p = 0.0285$; Fig. 2.8A). The f^{PV} in the post-IL-2 mice brain was 3.048±0.56 whereas in the pre-IL-2 mice brain was 1.554±0.21. This result suggested vasodilation of the brain blood vessels following IL-2 treatment, independently verifying the results of brain immunohistochemical staining. DCE MRI also showed that IL-2 significantly increased brain microvascular permeability to the contrast agent by 2-fold ($p = 0.0079$; Fig. 2.8B). K^{PS} value in the mice brain after receiving IL-2 treatment was 0.4305±0.05 ml/min/100 cm^3 whereas prior to IL-2 treatment was 0.2039±0.04 ml/min/100 cm^3. Finally, the PS was 1.275±0.22 ml/min/100 cm^3 in the mice after receiving IL-2 while in the mice prior to the IL-2 treatment was 0.2953±0.05 ml/min/100 cm^3 (Fig. 2.8C). These data suggested a significant ($p = 0.0083$) 4-fold increase in the blood vessel surface area that was “leaky” to the contrast agent after IL-2 treatment. These changes in brain vascular parameters identified using DCE MRI established that IL-2 induces vasodilation of the brain blood vessels and increases perivascular permeability of these vessels.

Figure 2.8

Evaluation of IL-2 induced changes in the brain blood vessel permeability by dynamic contrast enhanced (DCE) MRI. Mice (n = 5) were scanned both before and after 4 days of IL-2 treatment (150,000 U i.p, b.i.d.) using 2D-FLASH MRI sequence as described in the *Materials and Methods*. After baseline imaging, 0.1 mmol/kg contrast agent was administered by bolus injection via tail vein catheterization. Customized MATLAB programs were used to calculate signal intensities from manually drawn ROI on a selected 1-mm mid-brain section of each mouse. We averaged the left and right maxillary veins to derive the contrast agent concentration in the blood pool and a two-compartment model was used to calculate A) fractional plasma volume (f^{PV}), B) endothelium transfer coefficient (K^{PS}), and C) permeability surface area product (PS). IL-2 treatment significantly increased f^{PV} and K^{PS} by 2-fold, and PS by 4-fold.

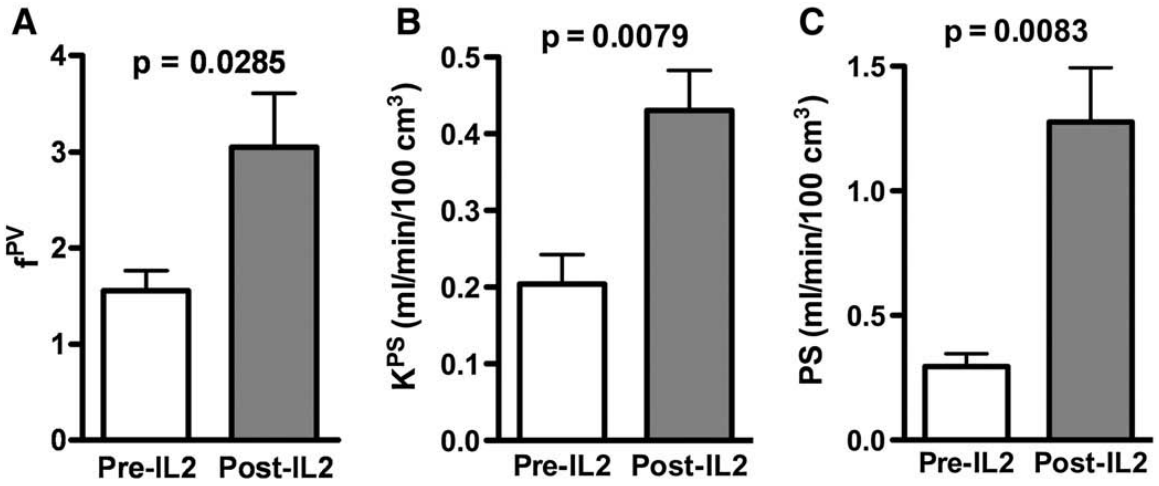
A
p = 0.0285
f^{PV}
4
3
2
1
0
Pre-IL2
Post-IL2
B
p = 0.0079
K^{PS} (ml/min/100 cm^3)
0.5
0.4
0.3
0.2
0.1
0.0
Pre-IL2
Post-IL2
C
p = 0.0083
PS (ml/min/100 cm^3)
1.5
1.0
0.5
0.0
Pre-IL2
Post-IL2

Discussion

Sepsis causes an estimated 215,000 deaths (9.3% of all deaths) in the US and considerable morbidity, mortality, health care utilization, and cost (45). Patients of early stages of sepsis develop similar symptoms to the side effects of IL-2 therapy, particularly hypotension, vascular leak, and neuropsychiatric toxicity (i.e., delirium). However, as sepsis progresses, patients experience irreversible organ failure, and eventually death. IL-2 dose limiting toxicities are reversible and therefore may provide useful to model the early cardiovascular and neuropsychiatric effects of sepsis.

A poorly characterized percentage of patients receiving IL-2 therapy become mentally slowed or confused (perhaps as high as 40% in our experience) and approximately 10-20% of patients become agitated, sometimes with hallucinations or delusions. The pathophysiology of IL-2 induced neuropsychiatric toxicity remains poorly understood. It is likely that the “cytokine storm” released during IL-2 treatment and sepsis induces changes in brain microvasculature, such as vascular leak and brain edema, which relate to changes in the CNS function and thus cause neuropsychiatric toxicity. We therefore evaluated a number of potential experimental methods to quantify the effect of cytokine-induced changes on brain blood vessels, utilizing a well-characterized IL-2 treatment murine model.

We have performed extensive studies of different doses of IL-2 in mice. The dose of IL-2 chosen for the current experiments (150-180,000 IU twice daily) is based on dose and time response studies previously performed in our lab to evaluate changes in systemic vascular permeability and hypotension in our murine model, and is approximately the LD10 (lethal dose for ~10% of mice) in C3H/HeN mouse strain. It was

designed to mirror the effect of massive doses of IL-2 administered to human patients (600,000 IU/kg q8h for 14 doses).

Previous studies have been attempted to delineate the mechanisms of IL-2 dose-limiting toxicities with the eventual goal of blocking these toxicities without affecting the therapeutic effectiveness of IL-2. Nitric oxide (NO) and superoxide have been identified as key players in systemic IL-2 induced VLS and hypotension, respectively (33, 46). The role of these mediators in the brain is currently unknown. Saris et al. have looked at the effects of IL-2 in the brain of patients with extracranial cancer without evidence of intracranial metastases (29). This study used T_2-weighted MRI to look at changes in signal intensities in the brain, which correlated with changes in cerebral water content, before and after IL-2 therapy. Even though their results suggested a massive increase of cerebral water content in both the white matter (17±6.2%) and gray matter (12.6±7.3%) after IL-2 therapy, only 3 out of these 7 patients were mildly lethargic (29). Moreover, the range of these measurements varied from 3% to 48%, raising questions concerning the accuracy of these determinations in critically ill patients. The magnitude of these apparent proton density increases are difficult to believe, since they are far greater magnitude than vascular leak measured in any other organ or even overall weight changes in the intact IL-2 treated animals or patients.

In cats and rats, a single bolus intravenous injection of recombinant IL-2 increased permeability of horseradish peroxidase into the brain, suggesting that IL-2 disrupted the blood-brain barrier (BBB) and cerebrovascular morphological integrity (31-32). A study on the effect of IL-2 on the BBB in gliosarcoma rat model suggested that IL-2 increased the transfer constant of carbon-14-labeled aminoisobutyric acid from BBB

into the brain in tumor-bearing rat brain but not in normal brain (30). However, tumors are known to have abnormal blood vessel permeability and are suspected of contributing to increased brain edema following IL-2 treatment, raising uncertainty concerning the significance of this finding.

Our results showed no detectable differences in the mouse brain interstitial fluid between IL-2 treated and controls measured using wet versus dry brain weight (Fig. 2.2), quantification of radioactive labeled [^{125}I]-bovine serum albumin (Fig. 2.3), tritiated water retention (Fig. 2.4) or fluorescence marker (Fig. 2.5C), and MRI proton density measurements (Fig. 2.7). This is likely due to the small magnitude of changes in brain water content or edema (<5%) that produces symptoms. In addition, quenching of the signal related to tritiated water, and to some degree tissue fluorescence (for NaFl) required compensation, further decreasing sensitivity. Another problem was that even in syngeneic mice treated on a very precise schedule, there was substantial inter-experiment variability. This further limited the usefulness of these techniques.

However, our mouse brain immunohistochemical staining (Fig. 2.6A) and DCE MRI f^{PV} values (Fig. 2.8A) independently demonstrated a 2-fold increase in the area and volume of the brain blood vessels, respectively, in IL-2 treated mice. These data indicated vasodilation of the brain blood vessels. Further characterization of the brain blood vessels by DCE MRI also showed a 2-fold increase of the mouse brain blood vessel permeability (K^{PS}) to the contrast agent after IL-2 treatment (Fig. 2.8B). These increases in DCE MRI f^{PV} and K^{PS} values induced by IL-2 resulted in a 4-fold increase in the surface area of the mouse brain blood vessels that become “leaky” to the contrast agent (Fig. 2.8C).

We established that additional methods quantifying changes in brain interstitial fluid induced by cytokines in mice were not informative. We used microscopy to evaluate changes in fixable Alexa Fluor® 594-conjugated dextran (10,000 MW; Molecular Probes, Oregon) or Hoechst 33342 (616 MW; Aldrich Chem., Milwaukee) staining in the mouse brain (47) following IL-2 treatment (data not shown). None of these dyes were able to accurately quantify the small changes in brain interstitial fluid in mice related to IL-2 therapy. A normal mouse brain weighs about 0.5 g. Approximately 5% of the mouse brain weight (25 mg) represents interstitial/or extracellular fluid. Assuming that IL-2 changes the mouse brain fluid content by 5-7%, a magnitude similar to the maximum increase in the mouse body weight during IL-2 treatment (data not shown), only about 1-2 mg changes in weight or 1-2 µl changes in water volume are predicted to occur within the brain parenchyma. This miniscule amount could not be measured accurately using small molecule probes in homogenates of brain tissue or by microscopy.

Despite failure to measure changes in the brain interstitial fluid after IL-2 therapy using NaFl, a significant 9-fold increase of NaFl was detected in pleural fluid of IL-2 treated mice, $p = 0.0003$ (Fig. 2.5A), consistent with the noncardiac pulmonary edema and vascular leak experienced by patients receiving IL-2 therapy (26). However, we did not detect a significant difference of NaFl in the lung parenchyma after IL-2 treatment, $p = 0.47$ (Fig. 2.5B). Our studies indicate that NaFl quantification in pleural fluid appears to be a sensitive marker for systemic VLS in mice. This result appears to contradict prior studies of IL-2 induced VLS in the mouse lungs, which have been described using [^{125}I]-albumin and Evans Blue dye (38, 48). It became apparent to us that even minimal carry-

over of pleural fluid during excision of lungs in these experiments could induce a significant error.

Dual staining using anti-von Willebrand Factor (vWF) and isolectin GS-IB_4 (Iso-B4) specifically identifies the blood vessels in the mouse brain sections and was able to show brain blood vessel vasodilation induced by IL-2. One difficulty using this technique was to closely match all the brain cross-sections. We chose to analyze a section through the mid-brain including the cerebral cortex and striatum as both of these regions are gray matter, which consists of neuronal cell bodies, glial cells (oligodendrocytes and astroglia), neuropil (axons and dendrites), and capillary blood vessels. The striatum is best known for its role in cognitive processes while the cerebral cortex plays an essential role in attention, thought, memory, perceptual awareness, and consciousness. Previous studies in humans receiving IL-2 have suggested that these processes are significantly affected during IL-2 induced neuropsychiatric toxicity (28). Vasodilation in these specific anatomic regions therefore appears to strongly correlate with the IL-2 induced behavior and cognitive changes in treated patients.

Although we established a MRI sequence that was sensitive enough to detect approximately 1% change in phantoms using a 7T Bruker MRI system with a mouse-specific coil, the PD changes in the mouse brain obtained with this technique were markedly different between replicate experiments. There are four potential issues why the MRI PD data exhibited such variation. First, it was difficult to completely align matched MRI coronal sections between pre- and post-IL-2 scans of each individual mouse. Second, we obtained 1-mm thick axial slices throughout the mouse brain. This thickness was needed to increase the signal to noise ratio of the MRI images. However, it decreased

the sensitivity to measure small or localized changes of PD in the mouse brain. This is particularly relevant, since the permeability surface coefficient derived from DCE-MRI studies suggests that IL-2 induced changes in brain water content may be perivascular rather than evenly distributed throughout the brain parenchyma. The third potential problem using a 7T MRI may relate to inhomogeneity of the static and rotating magnetic fields (B_0 and B_1). We attempted to minimize these effects by standardized placement of the mouse and phantoms within the coil. The final caveat was that manual segmentation of the mouse brain on the images proved somewhat error prone. It is not possible to perfectly outline the brain, resulting in some variability due to inadvertent inclusions of CSF water density pixels. With a relatively large standard deviation of the SI, the accuracy of measuring proton density changes is further decreased. It is possible that an automated MATLAB data extraction algorithm could be written to better exclude this potential artifact and improve reproducibility.

As measurement of IL-2 induced changes in average mouse brain water content proved problematic, a quantitative assessment of the vascular permeability to a small molecule contrast agent over a period of time using DCE MRI seemed more effective. DCE MRI is noninvasive, which allows for the same mice being scanned before and after IL-2 treatment, eliminating brain variability between individual mice. The 2D-FLASH MRI sequence provided a good spatial resolution and was fast. One major advantage using this technique is simultaneous characterization of the mouse brain blood vessel area and permeability to a small molecular probe. This method can be used to show increased vascular permeability changes in other tissues, such as liver and lungs. For example, changes in tumor blood vessel permeability are commonly studied using DCE MRI (49-

51). However, this adds additional technical challenges, such as compensation for organ movement due to breathing and heartbeat. Gating will be required and this prolongs scanning time, which may be detrimental in critically ill and unstable mice or patients.

To our knowledge, there are currently no published data of DCE MRI technique in patients with sepsis or receiving inflammatory cytokine administration. These processes are virtually impossible to study in critically ill human patients, who generally are hospitalized in intensive care units. Once these patients exhibit neuropsychiatric toxicity (delirium), it would be quite difficult to perform DCE MRI studies, as they are frequently intubated and receiving intravenous pressor agents and would not be stable enough to undergo MRI studies. Another concern is that gadolinium-based contrast agent, which is mainly used for DCE MRI, has been shown to be associated with the development of nephrogenic fibrosing dermopathy (NFD) and nephrogenic systemic fibrosis (NSF) in patients with kidney dysfunction (52-54). Therefore, this contrast agent may have an adverse effect in IL-2 treated or sepsis patients, who usually have at least some element of acute renal dysfunction.

In conclusion, we were able to show that IL-2 induced vasodilation of the brain blood vessels and increased permeability of these vessels in mice, suggesting that IL-2 induced neuropsychiatric toxicity may correlate with small blood vessel vasodilation in the brain as well as small increases in brain water content (edema). We are currently using these methods to evaluate the neuropsychiatric toxicity of IL-2 induced vascular leak in the brain. The long term goal is to identify pharmacologic inhibitors that block hypotension, vascular leak, and neuropsychiatric toxicity for testing in patients following inflammatory cytokine administration or with sepsis.

Acknowledgments

We thank Chiron (Novartis) for providing IL-2 used in these studies.

References

1. Nakarai T, Robertson MJ, Streuli M, Wu Z, Ciardelli TL, Smith KA, Ritz J. 1994. Interleukin 2 receptor gamma chain expression on resting and activated lymphoid cells. *J. Exp. Med.* 180: 241-51.

2. Sana TR, Wu Z, Smith KA, Ciardelli TL. 1994. Expression and ligand binding characterization of the beta-subunit (p75) ectodomain of the interleukin-2 receptor. *Biochemistry* 33: 5838-45.

3. Mertelsmann R, Welte K. 1986. Human interleukin 2: molecular biology, physiology and clinical possibilities. *Immunobiology* 172: 400-19.

4. Weiss A. 1993. T lymphocyte activation. In *Fundamental Immunology.*, ed. W Paul, pp. 467-504. New York: Raven Press.

5. Lotze MT, Grimm EA, Mazumder A, Strausser JL, Rosenberg SA. 1981. Lysis of fresh and cultured autologous tumor by human lymphocytes cultured in T-cell growth factor. *Cancer Res.* 41: 4420-5.

6. Hank JA, Kohler PC, Weil-Hillman G, Rosenthal N, Moore KH, Storer B, Minkoff D, Bradshaw J, Bechhofer R, Sondel PM. 1988. In vivo induction of the lymphokine-activated killer phenomenon: interleukin 2-dependent human non-major histocompatibility complex-restricted cytotoxicity generated in vivo during administration of human recombinant interleukin 2. *Cancer Res.* 48: 1965-71.

7. Rayner AA, Grimm EA, Lotze MT, Wilson DJ, Rosenberg SA. 1985. Lymphokine-activated killer (LAK) cell phenomenon. IV. Lysis by LAK cell clones of fresh human tumor cells from autologous and multiple allogeneic tumors. *J. Natl. Cancer Inst.* 75: 67-75.

8. Harker WG, Tom C, McGregor JR, Slade L, Samlowski WE. 1990. Human tumor cell line resistance to chemotherapeutic agents does not predict resistance to natural killer or lymphokine-activated killer cell-mediated cytolysis. *Cancer Res.* 50: 5931-6.

9. Papa MZ, Mule JJ, Rosenberg SA. 1986. Antitumor efficacy of lymphokine-activated killer cells and recombinant interleukin 2 in vivo: successful immunotherapy of established pulmonary metastases from weakly immunogenic and nonimmunogenic murine tumors of three district histological types. *Cancer Res.* 46: 4973-8.

10. Lafreniere R, Rosenberg SA. 1985. Successful immunotherapy of murine experimental hepatic metastases with lymphokine-activated killer cells and recombinant interleukin 2. *Cancer Res.* 45: 3735-41.

11. Mule JJ, Shu S, Rosenberg SA. 1985. The anti-tumor efficacy of lymphokine-activated killer cells and recombinant interleukin 2 in vivo. *J. Immunol.* 135: 646-52.

12. Eberlein TJ, Rosenstein M, Rosenberg SA. 1982. Regression of a disseminated syngeneic solid tumor by systemic transfer of lymphoid cells expanded in interleukin 2. *J. Exp. Med.* 156: 385-97.

13. Rosenberg SA, Yang JC, Topalian SL, Schwartzentruber DJ, Weber JS, Parkinson DR, Seipp CA, Einhorn JH, White DE. 1994. Treatment of 283 consecutive patients with metastatic melanoma or renal cell cancer using high-dose bolus interleukin 2. *JAMA* 271: 907-13.

14. Atkins MB, Lotze MT, Dutcher JP, Fisher RI, Weiss G, Margolin K, Abrams J, Sznol M, Parkinson D, Hawkins M, Paradise C, Kunkel L, Rosenberg SA. 1999. High-dose recombinant interleukin 2 therapy for patients with metastatic melanoma: analysis of 270 patients treated between 1985 and 1993. *J Clin Oncol* 17: 2105-16.

15. Atkins MB, Kunkel L, Sznol M, Rosenberg SA. 2000. High-dose recombinant interleukin-2 therapy in patients with metastatic melanoma: long-term survival update. *Cancer J. Sci. Am.* 6 Suppl 1: S11-4.

16. Samlowski WE, Wong B, Vogelzang NJ. 2008. Management of renal cancer in the tyrosine kinase inhibitor era: a view from 3 years on. *BJU Int.* 102: 162-5.

17. Panelli MC, White R, Foster M, Martin B, Wang E, Smith K, Marincola FM. 2004. Forecasting the cytokine storm following systemic interleukin (IL)-2 administration. *J. Transl. Med.* 2: 17.

18. Jablons DM, Mule JJ, McIntosh JK, Sehgal PB, May LT, Huang CM, Rosenberg SA, Lotze MT. 1989. IL-6/IFN-beta-2 as a circulating hormone. Induction by cytokine administration in humans. *J. Immunol.* 142: 1542-7.

19. Schaafsma MR, Falkenburg JH, Landegent JE, Duinkerken N, Osanto S, Ralph P, Kaushansky K, Wagemaker G, Van Damme J, Willemze R, et al. 1991. In vivo production of interleukin-5, granulocyte-macrophage colony-stimulating factor, macrophages colony-stimulating factor, and interleukin-6 during intravenous administration of high-dose interleukin-2 in cancer patients. *Blood* 78: 1981-7.

20. Mier JW, Vachino G, van der Meer JW, Numerof RP, Adams S, Cannon JG, Bernheim HA, Atkins MB, Parkinson DR, Dinarello CA. 1988. Induction of circulating tumor necrosis factor (TNF alpha) as the mechanism for the febrile response to interleukin-2 (IL-2) in cancer patients. *J. Clin. Immunol.* 8: 426-36.

21. Gemlo BT, Palladino MA, Jr., Jaffe HS, Espevik TP, Rayner AA. 1988. Circulating cytokines in patients with metastatic cancer treated with recombinant interleukin 2 and lymphokine-activated killer cells. *Cancer Res.* 48: 5864-7.

22. Nooteboom A, Van Der Linden CJ, Hendriks T. 2002. Tumor necrosis factor-alpha and interleukin-1beta mediate endothelial permeability induced by lipopolysaccharide-stimulated whole blood. *Crit. Care Med.* 30: 2063-8.

23. Maruo N, Morita I, Shirao M, Murota S. 1992. IL-6 increases endothelial permeability in vitro. *Endocrinology* 131: 710-4.

24. Martin S, Maruta K, Burkart V, Gillis S, Kolb H. 1988. IL-1 and IFN-gamma increase vascular permeability. *Immunology* 64: 301-5.

25. Papa MZ, Vetto JT, Ettinghausen SE, Mule JJ, Rosenberg SA. 1986. Effect of corticosteroid on the antitumor activity of lymphokine-activated killer cells and interleukin 2 in mice. *Cancer Res.* 46: 5618-23.

26. Mann H, Ward JH, Samlowski WE. 1990. Vascular leak syndrome associated with interleukin-2: chest radiographic manifestations. *Radiology* 176: 191-4.

27. Ognibene FP, Rosenberg SA, Lotze M, Skibber J, Parker MM, Shelhamer JH, Parrillo JE. 1988. Interleukin-2 administration causes reversible hemodynamic changes and left ventricular dysfunction similar to those seen in septic shock. *Chest* 94: 750-4.

28. Denicoff KD, Rubinow DR, Papa MZ, Simpson C, Seipp CA, Lotze MT, Chang AE, Rosenstein D, Rosenberg SA. 1987. The neuropsychiatric effects of treatment with interleukin-2 and lymphokine-activated killer cells. *Ann. Intern Med.* 107: 293-300.

29. Saris SC, Patronas NJ, Rosenberg SA, Alexander JT, Frank J, Schwartzentruber DJ, Rubin JT, Barba D, Oldfield EH. 1989. The effect of intravenous interleukin-2 on brain water content. *J. Neurosurg.* 71: 169-74.

30. Alexander JT, Saris SC, Oldfield EH. 1989. The effect of interleukin-2 on the blood-brain barrier in the 9L gliosarcoma rat model. *J. Neurosurg.* 70: 92-6.

31. Ellison MD, Povlishock JT, Merchant RE. 1987. Blood-brain barrier dysfunction in cats following recombinant interleukin-2 infusion. *Cancer Res.* 47: 5765-70.

32. Watts RG, Wright JL, Atkinson LL, Merchant RE. 1989. Histopathological and blood-brain barrier changes in rats induced by an intracerebral injection of human recombinant interleukin 2. *Neurosurgery* 25: 202-8.

33. Samlowski WE, Petersen R, Cuzzocrea S, Macarthur H, Burton D, McGregor JR, Salvemini D. 2003. A nonpeptidyl mimic of superoxide dismutase, M40403,

inhibits dose-limiting hypotension associated with interleukin-2 and increases its antitumor effects. *Nat. Med.* 9: 750-5.

34. Yim CY, McGregor JR, Kwon OD, Bastian NR, Rees M, Mori M, Hibbs JB, Jr., Samlowski WE. 1995. Nitric oxide synthesis contributes to IL-2-induced antitumor responses against intraperitoneal Meth A tumor. *J. Immunol.* 155: 4382-90.

35. Dorr A, Sled JG, Kabani N. 2007. Three-dimensional cerebral vasculature of the CBA mouse brain: a magnetic resonance imaging and micro computed tomography study. *Neuroimage* 35: 1409-23.

36. Shames DM, Kuwatsuru R, Vexler V, Muhler A, Brasch RC. 1993. Measurement of capillary permeability to macromolecules by dynamic magnetic resonance imaging: a quantitative noninvasive technique. *Magn. Reson. Med.* 29: 616-22.

37. Feng Y, Jeong EK, Mohs AM, Emerson L, Lu ZR. 2008. Characterization of tumor angiogenesis with dynamic contrast-enhanced MRI and biodegradable macromolecular contrast agents in mice. *Magn. Reson. Med.* 60: 1347-52.

38. Ettinghausen SE, Puri RK, Rosenberg SA. 1988. Increased vascular permeability in organs mediated by the systemic administration of lymphokine-activated killer cells and recombinant interleukin-2 in mice. *J. Natl. Cancer Inst.* 80: 177-88.

39. Kawamura S, Yasui N. 1994. In vivo effects of the Ca2+ entry blocker nilvadipine on brain surface microvessels in rats. *Neurol. Med. Chir. (Tokyo)* 34: 663-7.

40. Hawkins BT, Egleton RD. 2006. Fluorescence imaging of blood-brain barrier disruption. *J. Neurosci. Methods* 151: 262-7.

41. Torfgard KE, Ahlner J. 1994. Mechanisms of action of nitrates. *Cardiovasc. Drugs Ther.* 8: 701-17.

42. Vallance P, Collier J, Moncada S. 1989. Effects of endothelium-derived nitric oxide on peripheral arteriolar tone in man. *Lancet* 2: 997-1000.

43. Brenner BM, Troy JL, Ballermann BJ. 1989. Endothelium-dependent vascular responses. Mediators and mechanisms. *J. Clin. Invest.* 84: 1373-8.

44. Daldrup H, Shames DM, Wendland M, Okuhata Y, Link TM, Rosenau W, Lu Y, Brasch RC. 1998. Correlation of dynamic contrast-enhanced MR imaging with histologic tumor grade: comparison of macromolecular and small-molecular contrast media. *AJR Am. J. Roentgenol.* 171: 941-9.

45. O'Brien JM, Jr., Ali NA, Aberegg SK, Abraham E. 2007. Sepsis. *Am. J. Med.* 120: 1012-22.

46. Samlowski WE. 2001. Nitric oxide as a mediator of interleukin-2 induced cardiovascular toxicity and antitumor activity. In *Nitric Oxide and Inflammation*, ed. TTBaYV D. Salvemini, pp. 249. Basel: Birkhäuser Verlag.

47. Nitta T, Hata M, Gotoh S, Seo Y, Sasaki H, Hashimoto N, Furuse M, Tsukita S. 2003. Size-selective loosening of the blood-brain barrier in claudin-5-deficient mice. *J. Cell Biol.* 161: 653-60.

48. Hornyak SC, Orentas DM, Karavodin LM, Gehlsen KR. 2005. Histamine improves survival and protects against interleukin-2-induced pulmonary vascular leak syndrome in mice. *Vascul. Pharmacol.* 42: 187-93.

49. Dafni H, Kim SJ, Bankson JA, Sankaranarayanapillai M, Ronen SM. 2008. Macromolecular dynamic contrast-enhanced (DCE)-MRI detects reduced vascular permeability in a prostate cancer bone metastasis model following anti-platelet-derived growth factor receptor (PDGFR) therapy, indicating a drop in vascular endothelial growth factor receptor (VEGFR) activation. *Magn. Reson. Med.* 60: 822-33.

50. Mross K, Drevs J, Muller M, Medinger M, Marme D, Hennig J, Morgan B, Lebwohl D, Masson E, Ho YY, Gunther C, Laurent D, Unger C. 2005. Phase I clinical and pharmacokinetic study of PTK/ZK, a multiple VEGF receptor inhibitor, in patients with liver metastases from solid tumours. *Eur. J. Cancer* 41: 1291-9.

51. Rosen MA, Schnall MD. 2007. Dynamic contrast-enhanced magnetic resonance imaging for assessing tumor vascularity and vascular effects of targeted therapies in renal cell carcinoma. *Clin. Cancer Res.* 13: 770s-6s.

52. Perazella MA. 2009. Current status of gadolinium toxicity in patients with kidney disease. *Clin. J. Am. Soc. Nephrol.* 4: 461-9.

53. Pietsch H, Lengsfeld P, Steger-Hartmann T, Lowe A, Frenzel T, Hutter J, Sieber MA. 2009. Impact of renal impairment on long-term retention of gadolinium in the rodent skin following the administration of gadolinium-based contrast agents. *Invest. Radiol.* 44: 226-33.

54. Kribben A, Witzke O, Hillen U, Barkhausen J, Daul AE, Erbel R. 2009. Nephrogenic systemic fibrosis: pathogenesis, diagnosis, and therapy. *J. Am. Coll. Cardiol.* 53: 1621-8.

CHAPTER 3

NEUROLOGIC TOXICITY CORRELATES WITH ENDOTHELIAL NITRIC OXIDE SYNTHASE INDUCED CEREBRAL VASODILATION AND MICROVASCULAR PERMEABILITY FOLLOWING MURINE INTERLEUKIN-2 TREATMENT

Abstract

Interleukin-2 (IL-2) is the only agent that produces durable remissions in 5–10% of metastatic melanoma and renal cancer patients. Neuropsychiatric toxicity is frequent and dose-limiting. The pathophysiology is not currently understood. Behavioral changes following IL-2 therapy were quantified in a murine model, demonstrating that spontaneous movement, rearing, and grooming were decreased by day 2 of IL-2. Motor strength was affected by day 4. Immunohistochemical and DCE MRI evaluation of the brain vasculature demonstrated that IL-2 induced vasodilation and increased permeability by 2- to 4-fold on day 4. We hypothesized that nitric oxide (NO) synthesis was responsible. IL-2 induced behavioral changes and vasodilation were attenuated in eNOS knockout mice, while permeability was abrogated in both eNOS and iNOS knockout mice. These results establish that activation of eNOS-mediated vasodilation and vascular permeability changes correlate with motor function changes induced by IL-2. NO does not appear to mediate early changes in spontaneous behavior.

Introduction

At low concentrations (10–100 IU/ml), IL-2 is a cytokine that is essential for activation and clonal expansion of cytotoxic lymphocytes (1). Higher concentrations of IL-2 (> 600 IU/ml) result in activation of natural killer cell-derived cytotoxic lymphocytes called lymphokine-activated killer (LAK) cells (2). These cells kill tumor cells with antigen-independent mechanisms (3), and therefore demonstrate cytotoxicity against almost all freshly isolated (4) and cultured malignant cells (5), including multidrug-resistant cancer cells (6). Extensive preclinical and clinical studies have

established the anticancer activity of IL-2 (7-8). There has been a dramatic increase in treatment options for metastatic renal cancer and melanoma in the past 4 years, including development of “targeted” therapy such as mTOR (mammalian target of rapamycin) and VEGF (vascular endothelial growth factor) pathway inhibitors (9), as well as V600E B-raf specific inhibitors (10). However, IL-2 remains the only therapy that can induce durable complete remissions in approximately 5–10% of patients with these cancers (11-12). Clinical follow-up of these remissions in some cases now extends to over 20 years. Other currently available agents require lengthy administration of expensive drugs to maintain clinical responses, with eventual, but inevitable tumor progression and death.

Broader applications of IL-2 in cancer therapy are restricted by severe dose-limiting toxicities (13-14). Two major cardiovascular toxicities of IL-2 administration are vascular leak syndrome (VLS) and hypotension. VLS is characterized by generalized extravasations of intravascular fluid into interstitial tissues, fluid retention (weight gain), noncardiac pulmonary edema, and reversible renal dysfunction (15). In conjunction with VLS and intravascular volume depletion, IL-2 also results in hypotension, due to decreased systemic vascular resistance. These toxicities result in hypoperfusion of vital organs, such as kidneys and heart (16).

IL-2 induced cardiovascular toxicities are thought to be indirectly mediated via a large number of secondarily released inflammatory cytokines, termed a “cytokine storm” (17). These cytokines include tumor necrosis factor (TNFα and TNFβ), IFN-γ, IL-1, IL-5, and IL-6 (18-21). High doses of steroids can block IL-2 induced toxicity, but also completely abrogate therapeutic responses (22). These inflammatory mediators induce secretion of nitric oxide (NO) via activation of the inducible L-arginine:NO synthesis

pathway (23-27). Hibbs et al. showed that serum and urine nitrate levels (metabolites of NO) are elevated 6- to 10-fold in patients on days 5–7 after a 5-day treatment course of IL-2 (28). Previous studies in our lab suggested that the mechanism of IL-2 induced VLS results from induction of NO synthesis (29), while hypotension appears to be due to catecholamine oxidation (30).

Our clinical experience with pharmacological inhibitors of hypotension and VLS suggests that dose escalation of IL-2 therapy is further limited by the onset of neuropsychiatric toxicity, even if other cardiovascular toxicity is controlled. A large percentage of patients develop some manifestations of neuropsychiatric toxicity while receiving IL-2 treatment, with 30–50% of patients experiencing cognitive and behavioral changes (31). Perhaps 10–20% of patients develop more severe manifestations, such as agitation, hallucinations, or delusions. To date, the pathophysiology of IL-2 induced neuropsychiatric toxicity is not well understood. We have therefore utilized IL-2 treatment murine model to characterize cytokine-induced changes in the central nervous system (CNS) that lead to neuropsychiatric toxicity.

Materials and Methods

Mice. Pathogen-free C3H/HeN and C57/Bl6 mice were purchased from Charles River Laboratories. Breeding pairs of $eNOS^{-/-}$ mice (B6.129P2-$Nos3^{tm1Unc}$/J) were purchased from Jackson Laboratories and bred by heterozygous male to homozygous $eNOS^{-/-}$ female mating. $iNOS^{-/-}$ mice backcrossed onto a C57/Bl6 background were generously donated by Dr. Victor Laubach (University of Virginia, Charlottesville, VA) and bred by homozygous sibling mating. Derivation of these knockout mice has been

previously described (32-33). WT C57/Bl6 served as controls for experiments with the knockout mice. Mice were maintained under guidelines established by the Institutional Animal Care and Use Committee (IACUC), which also approved all experimental protocols. Mice were age- and sex-matched in each experiment. Knockout mice were genotyped before being used in experiments.

Verification of genotype of knockout mice. iNOS$^{-/-}$ mice were genotyped using previously published methods (29). eNOS$^{-/-}$ mice were genotyped using similar methods with the following primers: oIMR1823 – 5' ATT TCC TGT CCC CTG CCT TC 3' (common upstream primer), oIMR1824 – 5' GGC CAG TCT CAG AGC CAT AC 3' (lies in exon 12, which is deleted in mutant), and oIMR0094 – 5' TGG CTA CCC GTG ATA TTG CT 3' (neo cassette specific primer), and these changes in PCR parameters: annealing at 65^{o}C and 35 cycles. eNOS$^{-/-}$ produced a 500 bp PCR product whereas WT yielded a 442 bp product and heterozygotes yielded both.

IL-2 treatment. C3H/HeN mice were treated with 150,000 IU of IL-2 (Proleukin®; Novartis, Emeryville, CA) intraperitoneally (i.p.), b.i.d. (twice a day) for 5 days (a total of 10 doses) or 8 doses (4 days) for mice used in MRI studies to decrease anesthetic-induced mortality during scanning. C57/Bl6, eNOS$^{-/-}$, and iNOS$^{-/-}$ mice were treated with 800,000 IU of IL-2 i.p., b.i.d. for 5 days (10 doses), as we have previously established this to be the equipotent dose to induce hypotension and VLS in this mouse strain (29). Initial dilutions of IL-2 were made in sterile water and further diluted in PBS (phosphate buffered saline) immediately prior to administration. Control mice received no treatment, unless otherwise noted.

Measurement of spontaneous motor activity. Mouse spontaneous motor activity was measured using an Opto-Varimex apparatus (Columbus Instruments, Columbus, OH) as previously described (34). In a single experiment, 2 Opto-Varimex activity monitors (42.2 x 42.5 x 20.5 cm) were used. After the mice were acclimated to the environment of the activity monitors for 10 min, spontaneous activity was recorded for 60 min in an isolated room (dark and no noise) in the evening. The following parameters were analyzed using an Auto-Track software (Columbus Instruments, Columbus, OH): 1) total distance traveled by the animal in 1 hour (centimeters), 2) stereotypic activity count (grooming), and 3) vertical activity (rearing). Each mouse was acclimated to the apparatus prior to IL-2 treatment, serving as its own control. The post-IL-2 data were then expressed as percentages of baseline (pre-IL-2) for each mouse and averaged for each day.

Motor coordination. Mouse motor coordination and balance were assessed using a 3-cm diameter rod rotating at a fixed speed of 20 revolutions per minute (rpm) (35). Normal mice can walk on the rotor rod without falling for 180 seconds (36-37). All mice were trained on the rotor rod daily for 7 days prior to the onset of IL-2 treatment. Each animal acted as its own control. Measurements were obtained every day during IL-2 treatment.

Immunohistochemistry. Mice brains were processed and analyzed as previously described (38). Digital image size in pixel was converted to mm (17 pixels = 1 mm).

DCE MRI. DCE MRI of C3H/HeN mice was performed as previously described (38). C57/Bl6 WT, $eNOS^{-/-}$, and $iNOS^{-/-}$ mice were scanned using the following T_1-weighted 2D-FLASH (Fast Low-Angle Shot) parameters: repetition time (TR) of 84.992

ms, echo time (TE) of 3.06 ms, 40º flip angle, 1 mm slice thickness, number of slices = 10, field of view = 2 x 2 cm, matrix = 128 x 128 pixels, a single scan time of 8.159 s, and 60 total repetitions. Each mouse was scanned before and after IL-2 treatment, serving as its own control. Image analysis was performed as previously described (38).

Statistical analysis. All data are expressed as mean±standard error of the mean (SEM). Statistics of the immunohistochemistry data were analyzed using 3-factor analysis of variance (ANOVA) including treatment group, mouse type, and brain region as sources of variation. The Auto-track data were analyzed as repeated measures using linear mixed models. Fixed factors included in the model were the baseline covariate, group (either mouse type or treatment group), time, and the group by time interaction. A random factor for mouse was included to account for within animal correlation. Between and within group comparisons were tested at the alpha = 0.05 significance level. MRI and rotor rod data were analyzed using paired Student's 2-tailed t-test using GraphPad PRISM software (GraphPad Software, La Jolla, CA), unless otherwise indicated. A p-value ≤ 0.05 was considered significant.

Results

IL-2 induced behavioral changes in mice. Changes in spontaneous behavior of mice were quantified following daily treatment with IL-2 (n = 3) using the Opto-Varimex apparatus and Auto-Track software (Columbus Instruments, Columbus, OH). Spontaneous mobility over 60 min was significantly decreased by 50% after only 4 doses of 150,000 IU IL-2 (day 2 measurement; p = 0.0005) and further decreased over 5 days of IL-2 treatment (Fig. 3.1a). Rearing and grooming behavior were also significantly

reduced by day 2 of IL-2 treatment. On day 2, control mice reared 125±16% baseline vs. IL-2 treated 49±16% baseline, $p = 0.0041$ (Fig. 3.1b). Grooming activities of control mice on day 2 were 106±12% baseline vs. IL-2 treated 64±12% baseline, $p = 0.0218$ (Fig. 3.1c). Rearing and grooming activities of the IL-2 treated mice consistently decreased after day 2. These data establish that IL-2 induced substantial behavioral changes in mice.

To evaluate physical strength and coordination, mice were tested by rotor rod during IL-2 treatment ($n = 5$). The results showed that motor impairment in the mice did not occur until day 4 of IL-2 treatment. The ability of mice to balance on the rotor rod decreased to 18.6±3.5 seconds on day 4 and further decreased to 5.7±0.7 seconds on day 5, compared to the normal mice (> 180 seconds), $p < 0.0001$ (Fig. 3.1d). These data suggest that changes in spontaneous behavior induced by IL-2 treatment occurred well before the onset of motor impairment, which was observed on day 4 or 5 when IL-2 treated mice are known to be profoundly hypotensive (39).

Vasodilation of brain blood vessels in IL-2 treated mice. NO derived from endothelial cells or pharmacologic donors induces peripheral vasodilation by causing relaxation of endothelial smooth muscle cells (40-42). Hibbs et al. have shown that IL-2 treatment increases systemic NO production (28). We evaluated whether IL-2 induces vasodilation of brain blood vessels in IL-2 treated mice ($n = 3$) using immunohistochemistry. Frozen sections (6 µm) were carefully prepared from a defined anatomic region of the mouse mid-brain, as previously described (38). This region was chosen to reflect highly vascular areas based on a detailed mouse brain anatomy study by Dorr et al. (43). Sections were dual-stained with Isolectin GS-IB_4 (Iso-B4) to identify

Figure 3.1

IL-2 induced behavioral changes in mice. Spontaneous nocturnal activity of C3H/HeN mice (n = 3) was measured using the Auto-Track system for 60 min each day. Mice were evaluated prior to treatment and daily during treatment with 150,000 IU IL-2 or same volume of PBS i.p., b.i.d. for 5 days. The post-IL-2 data were expressed as % of pre-IL-2 (baseline) for each mouse and averaged for each day. In Panel (a) total distance travelled in 1h is shown on a daily basis. Panel (b) vertical activity/rearing and (c) stereotypical activity/grooming are also shown. In panel (d) a rotor rod study was used to evaluate physical strength and coordination of C3H/HeN mice (n = 5) prior to and during IL-2 treatment. Results are expressed as mean±SEM. The p-values for between group comparisons at specific time points are shown.

a

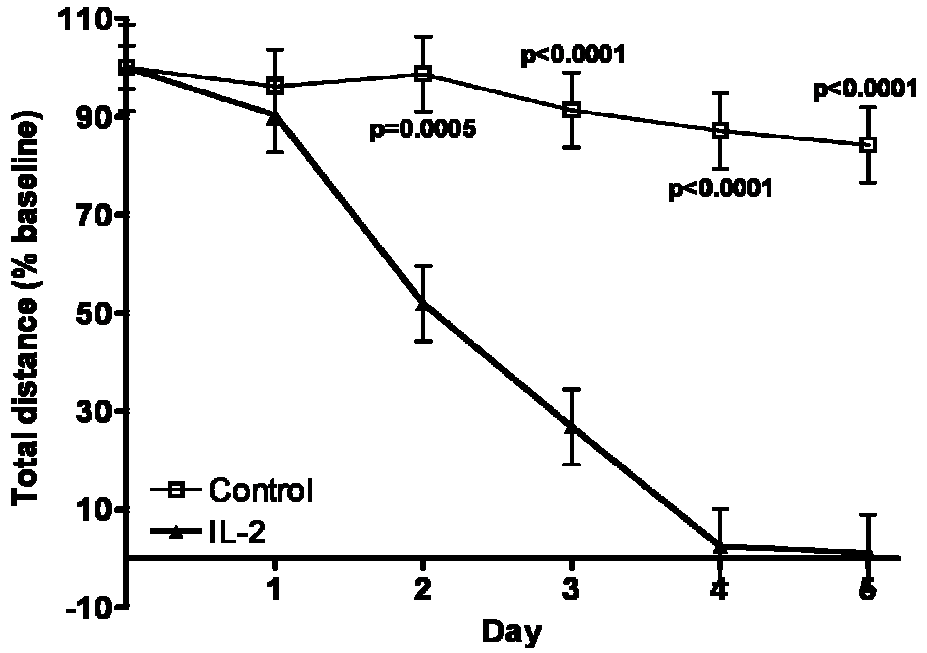
110
90
70
50
30
10
-10
Total distance (% baseline)
p=0.0005
p<0.0001
p<0.0001
p<0.0001
Control
IL-2
1
2
3
4
5
Day

b

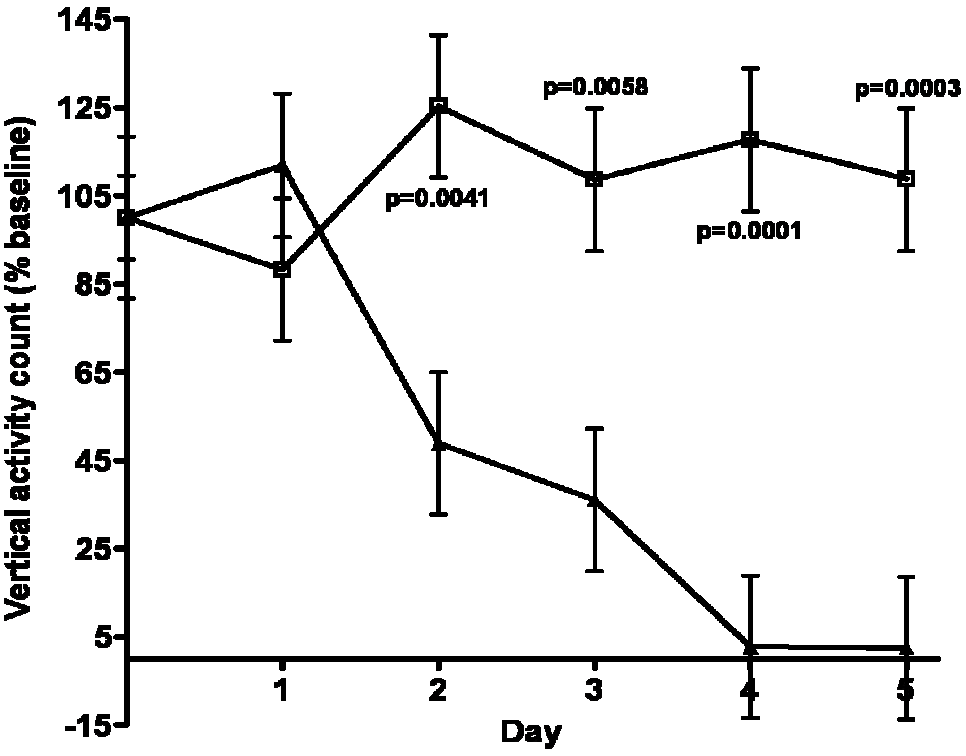
145
125
105
85
65
45
25
5
-15
Vertical activity count (% baseline)
p=0.0041
p=0.0058
p=0.0001
p=0.0003
1
2
3
4
5
Day

c

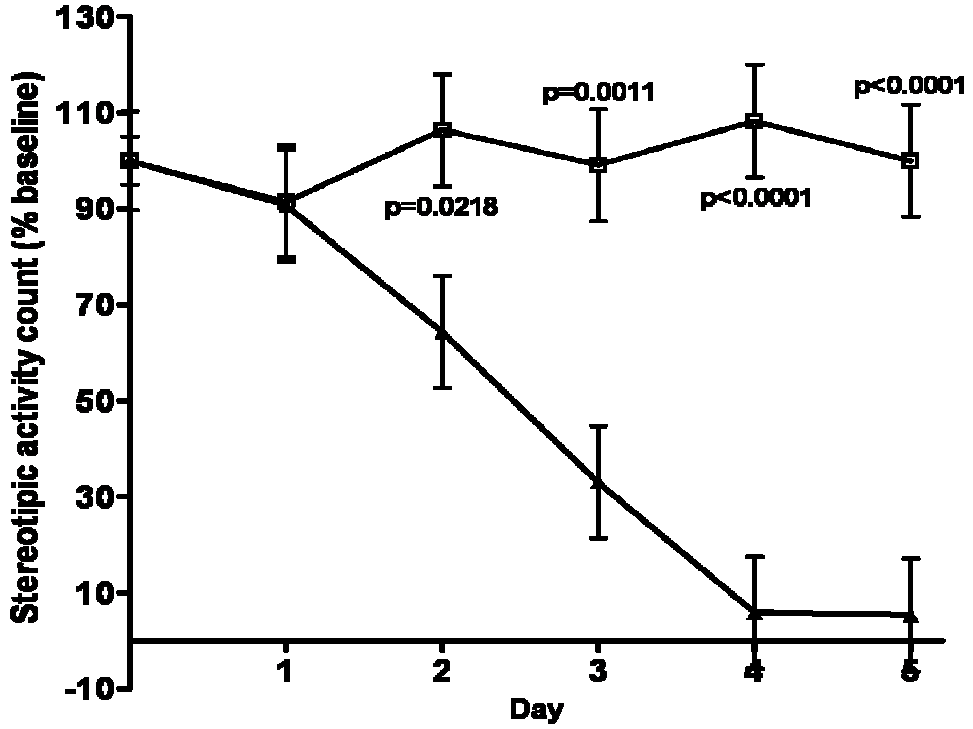
130
110
90
70
50
30
10
-10
Stereotipic activity count (% baseline)
p=0.0218
p=0.0011
p<0.0001
p<0.0001
1
2
3
4
5
Day

d

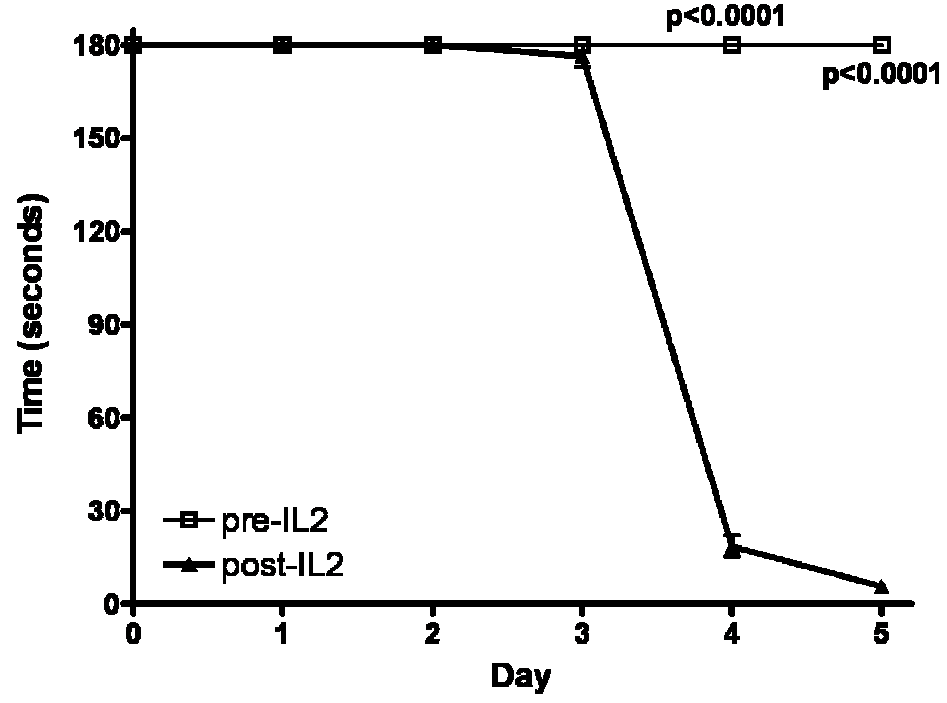
180
150
120
90
60
30
0
Time (seconds)
p<0.0001
p<0.0001
pre-IL2
post-IL2
0
1
2
3
4
5
Day

vascular pericytes and antibody to von Willebrand Factor (anti-vWF) to identify endothelial cells. Staining was evaluated in twenty 20x magnification digital images of the areas selected, which include the cortex, the cerebral fissure, and the striatum. Each image was analyzed for the numbers and average size of dual-stained blood vessels. The results showed that the average size of vessels in the brain of IL-2 treated mice (131±19 mm^2) was almost 2-fold more dilated than in control mice (71±19 mm^2), p = 0.0389 (Fig. 3.2a), while the number of vessels in the brain were not significantly different between the IL-2 treated (8±2) and control mice (7±2), p = 0.7765 (Fig. 3.2b). These results suggest that IL-2 induces substantial vasodilation of the brain blood vessels.

Effects of IL-2 on brain microvasculature permeability. We evaluated possible IL-2 induced changes in the mouse brain microvasculature permeability using dynamic contrast enhanced (DCE) MRI (magnetic resonance imaging). This technique has been used to assess tumor vascular permeability in patients and animal models (44-45). We developed a protocol to evaluate the brain microvasculature of IL-2 treated mice by DCE MRI (38). This technique was used to quantify 3 vascular parameters: 1) fractional plasma volume (f^{PV}) describes the plasma volume of the blood vessels in the tissue (mouse brain), 2) endothelium transfer coefficient (K^{PS}) reflects the permeability of the contrast agent from the blood vessels to the extravascular and extracellular space (EES) of the tissue, and 3) permeability surface area product (PS), which is the product of f^{PV} and K^{PS}, describes the permeability of the vasculature in the tissue to the contrast agent (46-47). Our experimental results demonstrated a 2-fold increase of f^{PV} in the mice brain (n = 5) after receiving IL-2 treatment for 4 days (0.016±0.002 pre-IL-2 vs. 0.031±0.006 post-IL-2), p = 0.0285 (Fig. 3.3a). A significant increase in the brain microvasculature

Figure 3.2

Vasodilation of brain blood vessels in IL-2 treated mice. C3H/HeN mice were treated with IL-2 (150,000 U i.p., b.i.d. for 5 days). Immediately following completion of IL-2 treatment, mice were sacrificed and the brains excised. The brain was embedded and frozen. Frozen sections (6 µm) were prepared and blood vessels were identified by dual-staining with Iso-B4 and anti-vWF. ImageJ software was used to analyze the area and numbers of blood vessels that were manually outlined on digitized fluorescence images of 4 different areas in the left and right cortex, left and right striatum, and the cerebral fissure (20 regions of interest/n). In panel (a) representative images of a specific area of the brain section. Arrow indicates a dual-stained blood vessel. (b) IL-2 treatment significantly increased the average area of blood vessels in matched 6 µm-thick mid-brain sections from IL-2 treated and control mice (n = 3). (c) The number of blood vessels in the brain was not significantly changed by IL-2. Results are expressed as mean±SEM. NS, not significant.

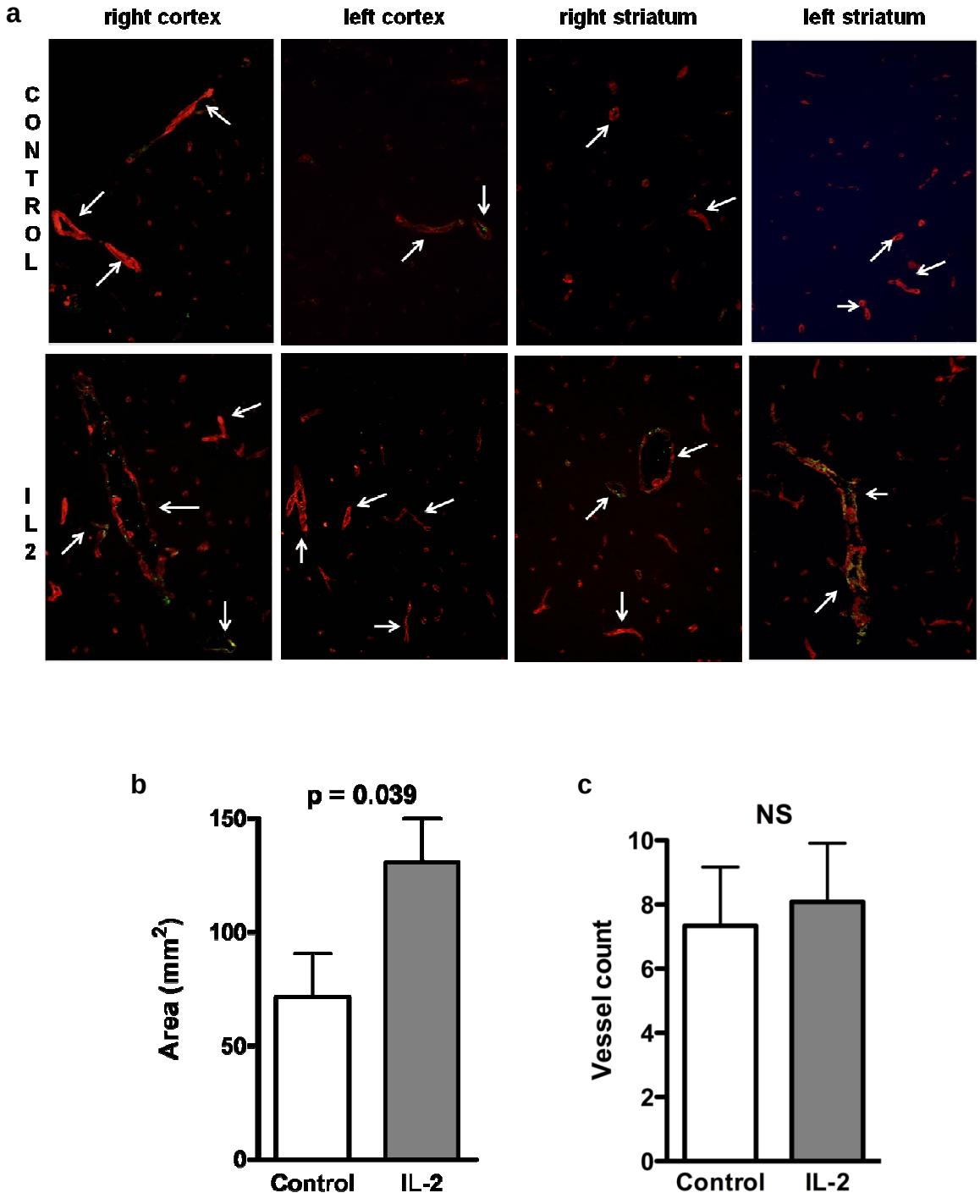
a
right cortex
left cortex
right striatum
left striatum
CONTROL
IL2
b
p = 0.039
Area (mm2)
150
100
50
0
Control
IL-2
c
NS
Vessel count
10
8
6
4
2
0
Control
IL-2

permeability (K^{PS}) to the contrast agent was also seen following IL-2 treatment (0.204±0.039 ml/min/100 cm^3 pre-IL-2 vs. 0.431±0.052 ml/min/100 cm^3 following IL-2 treatment), p = 0.0079 (Fig. 3.3b). Finally, the PS was 0.003±0.0005 ml/min/100 cm^3 in the mice prior to the IL-2 treatment and increased to 0.013±0.0022 ml/min/100 cm^3 after receiving IL-2 (Fig. 3.3c). These data suggested a 2-fold increase in the plasma volume and permeability of the brain blood vessels, which yielded a 4-fold increase in the blood vessel surface area in the mouse brain that became "leaky" to the contrast agent after IL-2 treatment (p = 0.0083).

Roles of NO in IL-2 induced CNS effects. Our previous laboratory data suggest that NO production derived from eNOS, rather than iNOS, contributes to IL-2 induced systemic VLS (29 and manuscript submitted). We therefore utilized eNOS knockout ($eNOS^{-/-}$) mice to determine the role of eNOS-derived NO in IL-2 induced neurotoxicity, by evaluating vasodilation and microvascular permeability in the brain. Immunohistochemistry of $eNOS^{-/-}$ brain blood vessels (n = 3, 20 digital images/n) using Iso-B4 and anti-vWF dual staining (as previously described (38)) showed that $eNOS^{-/-}$ developed only an attenuated and statistically insignificant vasodilation in the brain following IL-2 treatment (average vessel size of 42±19 mm^2 vs. control 27±19 mm^2), p = 0.5827 (Fig. 3.4a). DCE MRI data further showed that the f^{PV} value in $eNOS^{-/-}$ mice did not significantly increase following IL-2 treatment (p = 0.173) as it did in wild-type (WT) and $iNOS^{-/-}$ mice (p < 0.001 and 0.029, respectively; Fig. 3.4b). Similar to C3H/HeN mice, IL-2 treatment also increased K^{PS} and PS values in WT C57/Bl6 mice (Fig. 3.4c and 3.4d). Surprisingly, IL-2 treatment induced negative changes in K^{PS} and PS values (ΔK^{PS} and ΔPS, respectively) in $eNOS^{-/-}$ and $iNOS^{-/-}$ mice (Fig. 3.4c and 3.4d), although

Figure 3.3

Effects of IL-2 on brain plasma volume and microvascular permeability in mice evaluated by DCE MRI. C3H/HeN mice (n = 5) were scanned with a 7T MRI scanner using a T_1-weighted 2D-FLASH MRI sequence before and after 4 days of IL-2 treatment (150,000 U i.p., b.i.d.). Signal intensity from a manually drawn ROI on a selected 1-mm mid brain section of each mouse was calculated using customized MATLAB programs. The contrast agent concentration in the blood pool was derived by averaging the signal intensities of the left and right maxillary veins. A two-compartment model was used to calculate the vascular parameters. In panel (a) IL-2 increased the fractional plasma volume (f^{PV}) in the brain by 2-fold. (b) IL-2 increased the permeability of contrast agent from the blood vessels to the brain EES (K^{PS}) by 2-fold. (c) The surface of the brain blood vessels that becomes permeable to the contrast agent (PS) increased by 4-fold after IL-2 treatment. Results are expressed as mean±SEM.

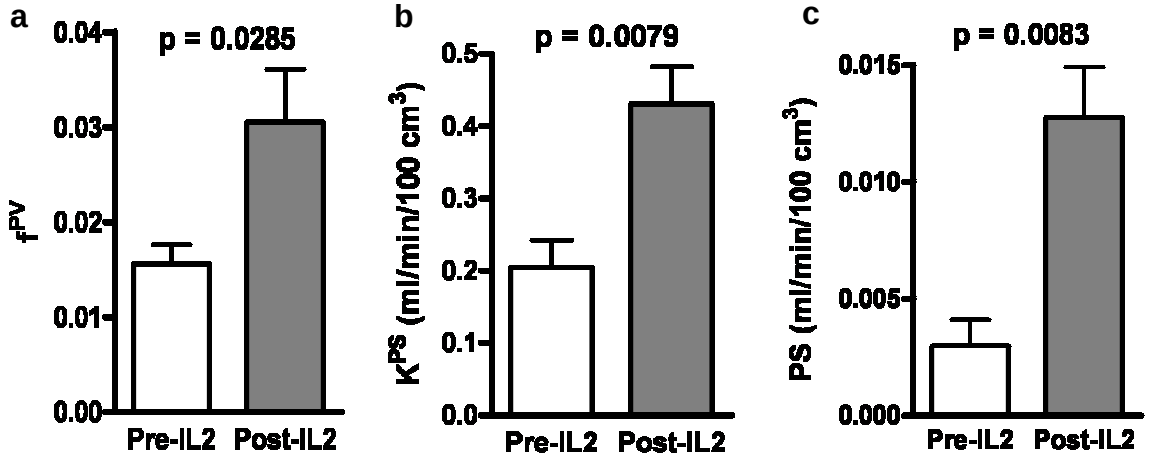
a
p = 0.0285
0.04
0.03
0.02
0.01
0.00
f_t^{PV}
Pre-IL2
Post-IL2
b
p = 0.0079
0.5
0.4
0.3
0.2
0.1
0.0
K^{PS} (ml/min/100 cm^3)
Pre-IL2
Post-IL2
c
p = 0.0083
0.015
0.010
0.005
0.000
PS (ml/min/100 cm^3)
Pre-IL2
Post-IL2

Figure 3.4

IL-2 induced vasodilation and microvascular permeability in the brain are abrogated in $eNOS^{-/-}$ mice. (a) Brain blood vessels immunohistochemistry of $eNOS^{-/-}$ mice did not show vasodilation following IL-2 treatment (800,000 U i.p., b.i.d. for 5 days). Matched 6-µm frozen mid-brain sections of IL-2 treated and control $eNOS^{-/-}$ mice (n = 3) were dual-stained with Iso-B4 and anti-vWF to identify blood vessels. ImageJ software was used to analyze the area of blood vessels that were manually outlined on digitized fluorescence images of 4 different areas in the left and right cortex, left and right striatum, and the cerebral fissure (20 regions of interest/n). (b, c, d) $eNOS^{-/-}$ mice do not show positive cerebrovascular changes following IL-2 treatment evaluated using DCE MRI. The f^{PV}, K^{PS}, and PS values of WT C57/Bl6, $eNOS^{-/-}$, and $iNOS^{-/-}$ mice (n = 4) were obtained as previously described before and after 5 days of IL-2 treatment (800,000U i.p., b.i.d.) and the values following IL-2 treatment were subtracted with the values prior to IL-2 treatment for each mouse. The differences (Δf^{PV}, ΔK^{PS}, and ΔPS) were then analyzed using analysis of variance (ANOVA) techniques. A single-factor ANOVA using the mouse type (WT, $eNOS^{-/-}$, and $iNOS^{-/-}$) as the source of variation was conducted. Comparisons between groups were tested at the alpha = 0.05 significance level using Turkey's multiple comparisons method. Within each group changes were tested for each group separately using t-tests. Results are expressed as mean±SEM. NS, not significant.

a

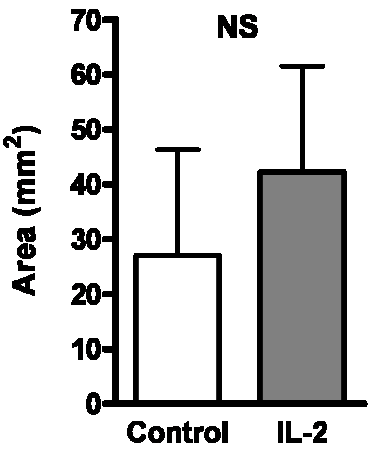
NS
70
60
50
40
30
20
10
0
Area (mm2)
Control
IL-2

b

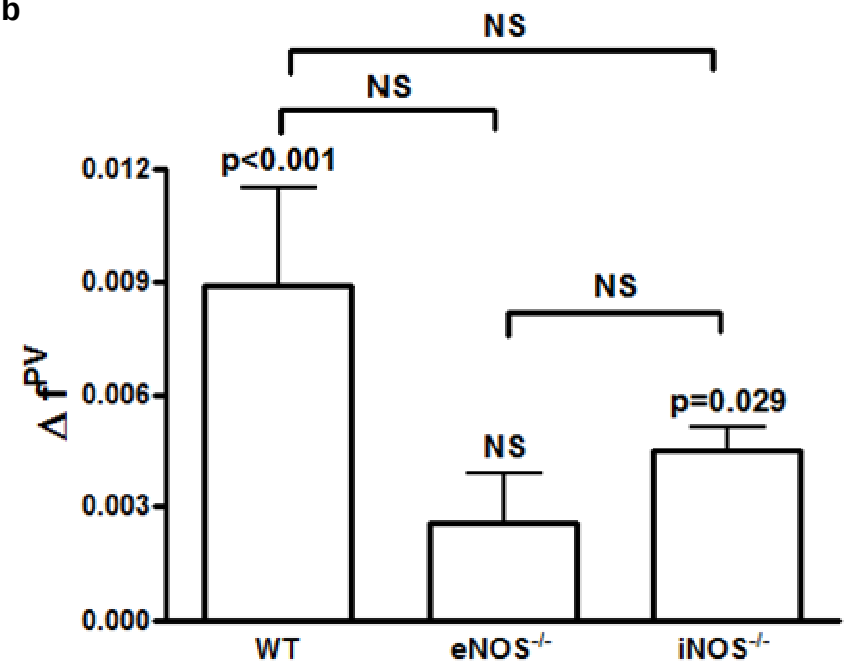
NS
NS
p<0.001
NS
NS
p=0.029
0.012
0.009
0.006
0.003
0.000
Δ fPV
WT
eNOS-/-
iNOS-/-

c

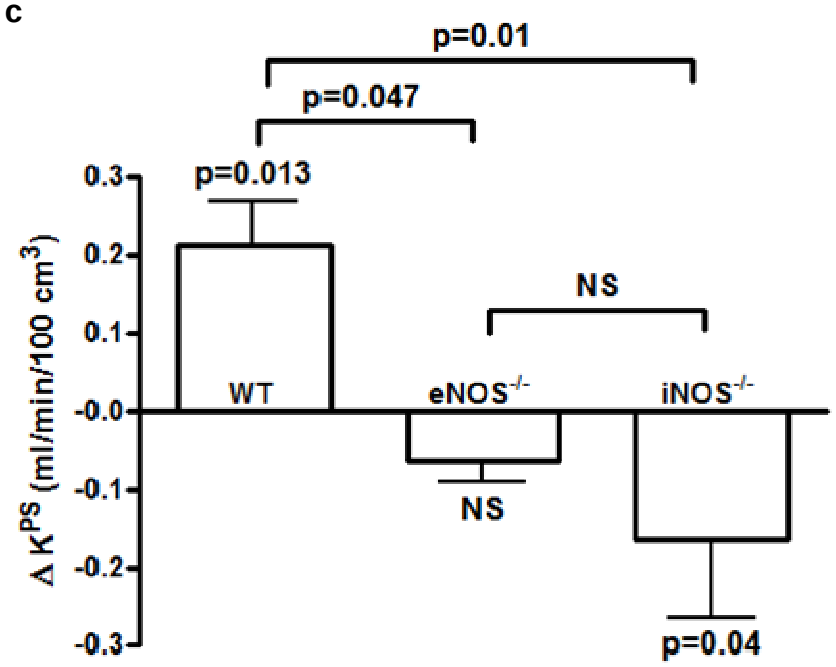
p=0.01
p=0.047
p=0.013
NS
0.3
0.2
0.1
-0.0
-0.1
-0.2
-0.3
ΔK^PS (ml/min/100 cm^3)
WT
eNOS-/-
iNOS-/-
NS
p=0.04

d

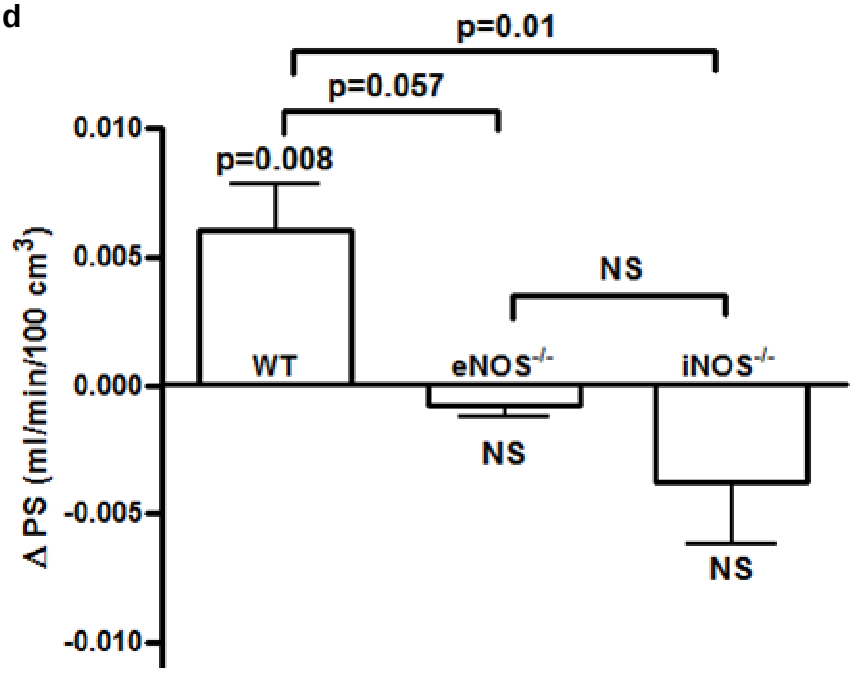
p=0.01
p=0.057
p=0.008
NS
0.010
0.005
0.000
-0.005
-0.010
ΔPS (ml/min/100 cm^3)
WT
eNOS-/-
iNOS-/-
NS
NS

only ΔK^{PS} of $iNOS^{-/-}$ mice showed significance ($p = 0.04$). Both ΔK^{PS} and ΔPS of $eNOS^{-/-}$ and $iNOS^{-/-}$ mice are statistically different compared to the WT mice. These data indicate that eNOS-derived NO plays a major role in IL-2 induced vasodilation and microvascular permeability in the brain, while iNOS-derived NO may also contribute to brain microvascular permeability but not vasodilation.

Unexpectedly, there were no significant differences in behavior changes between WT, $eNOS^{-/-}$, and $iNOS^{-/-}$ mice ($n = 4$). All mice showed decreased spontaneous mobility over 60 min (Fig. 3.5a), rearing (Fig. 3.5b), and grooming (Fig. 3.5c) following IL-2 treatment. However, when we compared the post-IL-2 vs. pre-IL-2 (averaged over 4 days prior to the onset of IL-2 treatment as day 0 value = 100%) data within each group, the results showed that the spontaneous behaviors of WT and $iNOS^{-/-}$ mice were significantly reduced by day 3 of IL-2 treatment whereas the $eNOS^{-/-}$ mice did not show significant decreases in all 3 activities measured until day 4. Furthermore, WT and $eNOS^{-/-}$ mice were able to stay on the rotor rod for 180 seconds for the whole period of IL-2 administration, while 2 out of 4 $iNOS^{-/-}$ mice could not complete this test by day 5, $p = 0.089$ (Fig. 3.5d), and eventually died of IL-2 toxicity on day 6. There was no IL-2 induced mortality in eNOS knockout mice. These data suggest that IL-2 induced behavioral changes were markedly attenuated in $eNOS^{-/-}$ mice compared to WT and $iNOS^{-/-}$ mice.

Discussion

In mice, the therapeutic effectiveness is closely related to the dose of the drug (48). A recent phase II randomized study has suggested that high-dose IL-2 produces a

Figure 3.5

IL-2 induced behavioral changes were attenuated in $eNOS^{-/-}$ mice. Spontaneous nocturnal activities of WT C57/Bl6, $eNOS^{-/-}$, and $iNOS^{-/-}$ mice (n = 4) were measured using the Auto-Track system (as previously described) prior to and daily during treatment with 800,000 IU IL-2 i.p., b.i.d. for 5 days and expressed as % of baseline. In Panel (a) total distance travelled in 1h is shown on a daily basis. Panel (b) vertical activity/rearing and (c) stereotypical activity/grooming are also shown. In Panel (d) a rotor rod study was used to evaluate physical strength and coordination prior to and during IL-2 treatment of these mice. Results are expressed as mean±SEM.

a

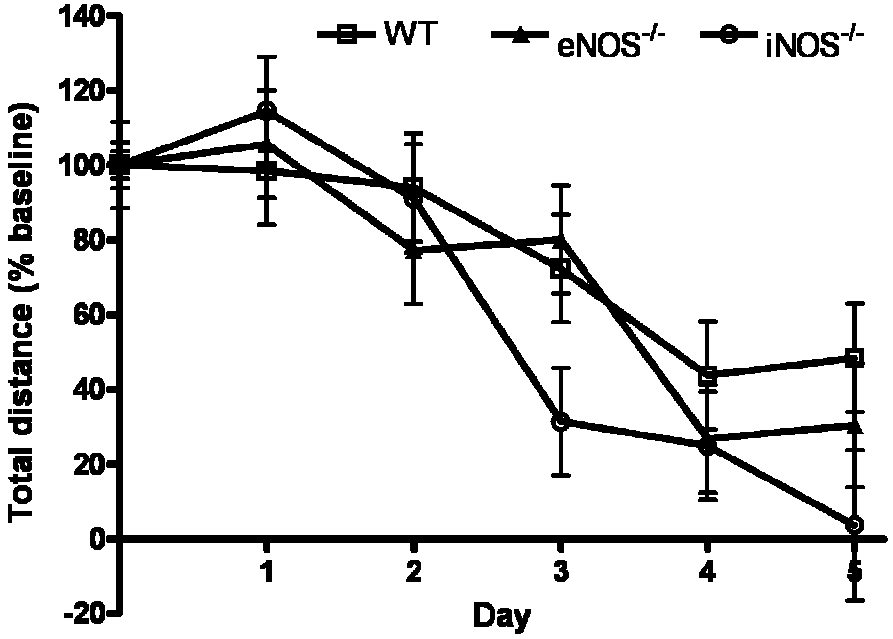
WT
eNOS-/-
iNOS-/-
Total distance (% baseline)
140
120
100
80
60
40
20
0
-20
1
2
3
4
5
Day

b

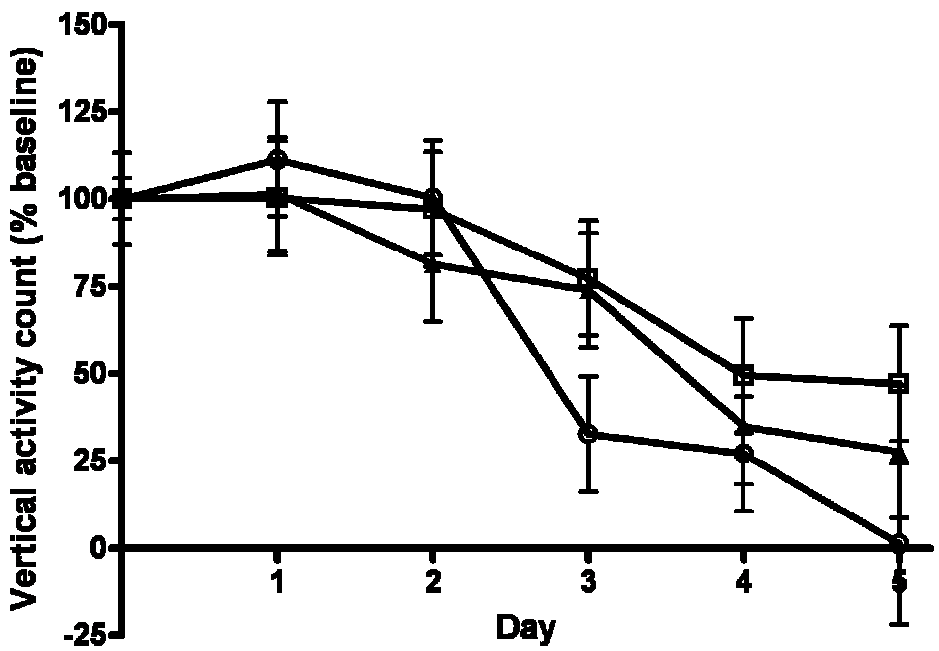
Vertical activity count (% baseline)
150
125
100
75
50
25
0
-25
1
2
3
4
5
Day

c

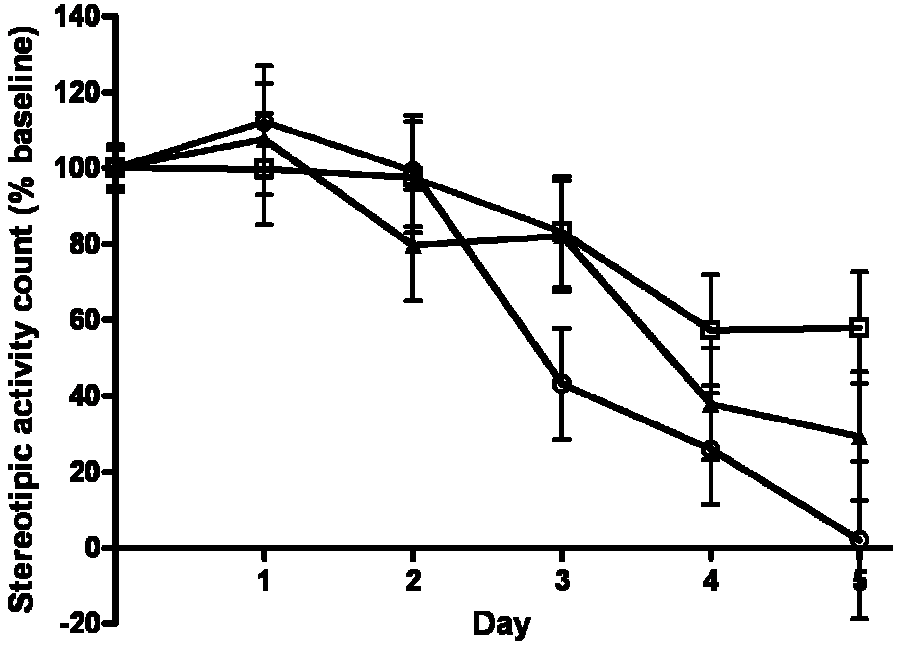
Stereotipic activity count (% baseline)
140
120
100
80
60
40
20
0
-20
1
2
3
4
5
Day

d

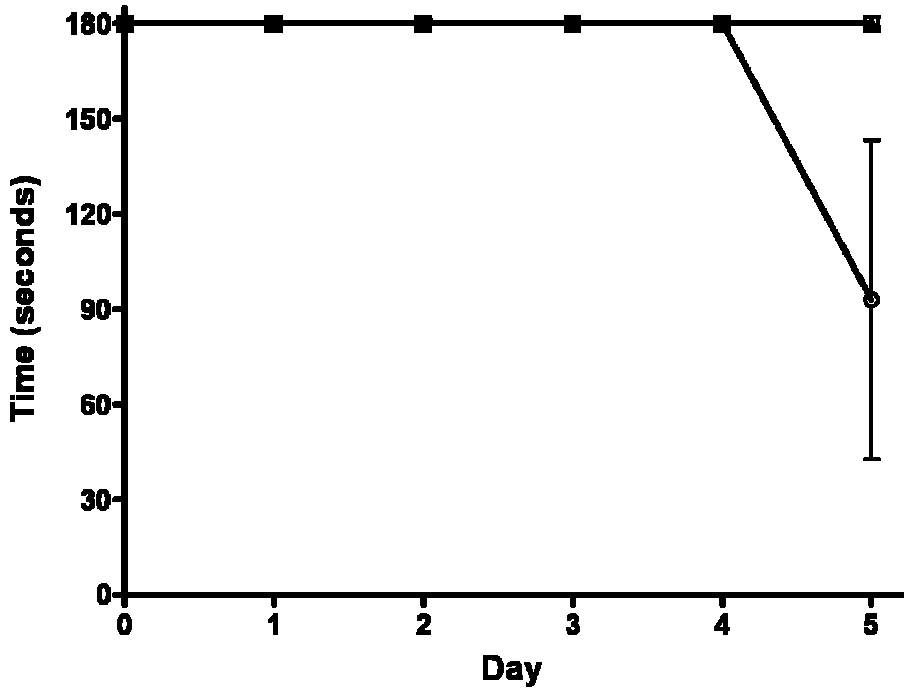
Time (seconds)
180
150
120
90
60
30
0
0
1
2
3
4
5
Day

higher response and complete response rate than intermediate dose or low dose IL-2 (49). The effectiveness of IL-2 therapy as a human cancer treatment is, however, markedly limited by cardiovascular and neuropsychiatric toxicities (13-14, 31). While the cardiovascular toxicities can be managed with pressor agents and fluid administration, the neuropsychiatric toxicity is the least predictable and controllable. This toxicity invariably leads to treatment discontinuation. Approximately 10–20% of patients receiving IL-2 therapy become agitated, sometimes with delusions or hallucinations, and at least 30–50% have more subtle CNS changes, such as mental slowing or confusion. The pathophysiology of this toxicity remains poorly understood.

Studies attempted to delineate IL-2-induced neuropsychiatric toxicity have been limited by the availability of suitable experimental techniques, as well as the technical challenges of performing DCE MRI studies in critically ill patients. A previous study looking at the effects of IL-2 in the brain of patients with extracranial cancer without evidence of intracranial metastases using T_2-weighted MRI suggested a massive increase of cerebral water content in both the gray matter (12.6±7.3%) and white matter (17±6.2%) after IL-2 therapy (50). However, only 3 out of these 7 patients were mildly lethargic, and the range of these measurements varied from 3–48%, raising questions concerning the accuracy of these results. The magnitudes of these apparent cerebral water content increases are also difficult to believe as they are far greater than the magnitude of VLS measured in any other organ or even compared to the overall weight changes in the intact IL-2 treated animals or patients (approximately 6–8%). Studies in cats and rats have shown that a single intravenous injection of recombinant IL-2 increased the permeability of horseradish peroxidase into the brain, suggesting that IL-2 disrupted the

blood-brain barrier (BBB) and cerebrovascular morphological integrity (51-52). Another study on the effect of IL-2 on the CNS in rat gliosarcoma model suggested that IL-2 increased the transfer constant of carbon-14-labeled aminoisobutyric acid from the BBB into the brain of tumor-bearing rat brains, but not in normal brains (53). The significance of this finding is uncertain, since brain tumors are known to have abnormal blood vessel permeability and consequently could have contributed to the increased brain edema following IL-2 treatment. We therefore evaluated behavioral and CNS changes induced by IL-2 treatment in the normal brain using a well-characterized murine model (30, 54).

In the current study, behavioral changes were observed as early as day 2 following the onset of IL-2 treatment (Fig. 3.1a–c), well before the onset of motor impairment. Motor impairment occurred on day 4 of IL-2 treatment (Fig. 3.1d), when the mice are known to be profoundly hypotensive (39). These results indicate that the decreases in the spontaneous behavior of these mice were not due to the mice being too sick to move. Instead, these data suggest that IL-2 affects the CNS in a manner distinct from the dose-limiting systemic cardiovascular effects of IL-2.

We have evaluated a number of approaches to assess cerebrovascular changes in IL-2 treated mice (38). We analyzed vascular regions of the mid-brain section, which includes the striatum and cerebral cortex. Both of these brain regions are within the gray matter, consisting of the glial cells (astroglia and oligodendrocyte), neuronal cell bodies, neuropil (dendrites and axons), and capillary blood vessels. We also assessed the regions of interest in the striatum, which is best known for its role in cognitive processes, and the cerebral cortex, which plays an essential role in attention, memory, thought, perceptual awareness, and consciousness. Using immunohistochemistry, we demonstrated that IL-2

induced vasodilation of the blood vessels in these regions (Fig. 3.2). This was confirmed by DCE MRI, which showed both vasodilation and increased permeability of blood vessels in these specific anatomic regions in mice that appeared to correlate with behavioral changes (Fig. 3.3).

NO has been shown to mediate IL-2-induced VLS (55), presumably via alterations of the tight junctions between endothelial cells. Our previous studies in iNOS$^{-/-}$ and eNOS$^{-/-}$ mice have further demonstrated that NO production via the eNOS isoform, rather than the iNOS isoform, in the systemic circulation is necessary for VLS (29 and manuscript submitted). The role of NO in the IL-2-induced CNS effects has not previously been evaluated. Since we showed that IL-2 induces vasodilation of the brain blood vessels, we evaluated whether eNOS- or iNOS-derived NO contributes to IL-2 induced neurologic changes. Our current results show that eNOS$^{-/-}$ mice exhibited decreased vasodilation and microvascular permeability following IL-2 treatment (Fig. 3.4), indicating a key role of this enzyme in IL-2 induced brain microvasculature changes. On the other hand, iNOS-derived NO seems to contribute to IL-2 induced microvascular permeability in the brain (Fig. 3.4c–d). Further analyses of these DCE MRI data indicate that eNOS$^{-/-}$ and iNOS$^{-/-}$ mice develop leaky brain blood vessels prior to IL-2 treatment, and this permeability is decreased following IL-2 treatment (Fig. 3.4c–d). This phenomenon is very intriguing. These knockout mice develop normally and it is not previously known that they have leaky blood vessels. Although they seem to be more aggressive than the WT mice, their behavioral studies prior to IL-2 show similar data as the WT mice (Fig. 3.5). One possible explanation is that IL-2 synthesis strongly induces nitric oxide and vasodilation. Compensatory pathways may also be induced by IL-2. In

mice without NO production (due to knockout of eNOS or iNOS), the compensatory pathway may still be strongly induced, decreasing microvascular permeability in the brain. The mechanisms that appear to decrease vascular permeability in $eNOS^{-/-}$ or $iNOS^{-/-}$ mice will require further investigation.

Unexpectedly, $eNOS^{-/-}$ mice still showed measurable behavioral changes following IL-2 treatment (Fig. 3.5a–c) although these changes were attenuated compared to the WT and $iNOS^{-/-}$ mice. We considered that NO produced by the iNOS isoform might contribute to some of these behavioral changes. This possibility appears unlikely as administration of L-N^6-(1-Imminoethyl)lysine (L-NIL, a relatively specific inhibitor of iNOS (56)) to $eNOS^{-/-}$ mice failed to prevent IL-2 induced behavioral changes (data not shown). These results suggest that there may be additional mechanisms involved in IL-2-induced neurologic changes in mice. This may be similar to the observations in thiamine-deficient mice, where the eNOS gene knockout prevented blood brain barrier disruption but not neuronal cell loss (57). It should also be noted that our DCE MRI data on C3H/HeN mice indicated no significant changes in f^{PV}, K^{PS}, and PS values on day 3 of IL-2 treatment (data not shown), whereas the behavioral changes were observed as early as day 2. These data suggest that IL-2 induced behavior and cognitive changes occurred before detectable IL-2 induced vasodilation and microvascular permeability. We therefore hypothesize that other mechanisms, such as the release of excitatory neurotransmitters, may contribute to the changes in behavior and cognitive functions observed at early time points during IL-2 treatment while the eNOS-mediated vasodilation and microvascular permeability in the CNS contribute to neuropsychiatric toxicities observed on days 4 and 5.

It should be noted that there are striking similarities in the pattern of IL-2 induced VLS, hypotension, and delirium (neuropsychiatric toxicity) with the initial phase of septic shock (16). This is also associated with the rapid onset of a similar “cytokine storm” and pathophysiologic features (58-60). Sepsis progresses rapidly (in hours) to a refractory shock, associated with organ failure and a high mortality rate. IL-2 treatment may be a convenient model to study the cardiovascular and neurologic mechanisms involved in the acute and reversible phase of sepsis, as the onset is more gradual and is dose dependent.

Acknowledgments

We thank the generous support of Novartis for providing IL-2 used in these studies.

References

1. Weiss A. 1993. T lymphocyte activation. In *Fundamental Immunology.*, ed. WE Paul, pp. 467-504. New York: Raven Press.

2. Lotze MT, Grimm EA, Mazumder A, Strausser JL, Rosenberg SA. 1981. Lysis of fresh and cultured autologous tumor by human lymphocytes cultured in T-cell growth factor. *Cancer Res.* 41: 4420-5.

3. Grimm EA, Wilson DJ. 1985. The human lymphokine-activated killer cell system. V. Purified recombinant interleukin 2 activates cytotoxic lymphocytes which lyse both natural killer-resistant autologous and allogeneic tumors and trinitrophenyl-modified autologous peripheral blood lymphocytes. *Cell Immunol* 94: 568-78.

4. Rayner AA, Grimm EA, Lotze MT, Wilson DJ, Rosenberg SA. 1985. Lymphokine-activated killer (LAK) cell phenomenon. IV. Lysis by LAK cell clones of fresh human tumor cells from autologous and multiple allogeneic tumors. *J. Natl. Cancer Inst.* 75: 67-75.

5. Hank JA, Kohler PC, Weil-Hillman G, Rosenthal N, Moore KH, Storer B, Minkoff D, Bradshaw J, Bechhofer R, Sondel PM. 1988. In vivo induction of the lymphokine-activated killer phenomenon: interleukin 2-dependent human non-major histocompatibility complex-restricted cytotoxicity generated in vivo during administration of human recombinant interleukin 2. *Cancer Res.* 48: 1965-71.

6. Harker WG, Tom C, McGregor JR, Slade L, Samlowski WE. 1990. Human tumor cell line resistance to chemotherapeutic agents does not predict resistance to natural killer or lymphokine-activated killer cell-mediated cytolysis. *Cancer Res.* 50: 5931-6.

7. Rosenberg SA, Mule JJ, Spiess PJ, Reichert CM, Schwarz SL. 1985. Regression of established pulmonary metastases and subcutaneous tumor mediated by the systemic administration of high-dose recombinant interleukin 2. *J Exp Med* 161: 1169-88.

8. Rosenberg SA, Yang JC, Topalian SL, Schwartzentruber DJ, Weber JS, Parkinson DR, Seipp CA, Einhorn JH, White DE. 1994. Treatment of 283 consecutive patients with metastatic melanoma or renal cell cancer using high-dose bolus interleukin 2. *Jama* 271: 907-13.

9. Samlowski WE, Wong B, Vogelzang NJ. 2008. Management of renal cancer in the tyrosine kinase inhibitor era: a view from 3 years on. *BJU Int* 102: 162-5.

10. Menard D, Niculescu-Duvaz I, Dijkstra HP, Niculescu-Duvaz D, Suijkerbuijk BM, Zambon A, Nourry A, Roman E, Davies L, Manne HA, Friedlos F, Kirk R, Whittaker S, Gill A, Taylor RD, Marais R, Springer CJ. 2009. Novel potent BRAF inhibitors: toward 1 nM compounds through optimization of the central phenyl ring. *J Med Chem* 52: 3881-91.

11. Fisher RI, Rosenberg SA, Sznol M, Parkinson DR, Fyfe G. 1997. High-dose aldesleukin in renal cell carcinoma: long-term survival update. *Cancer J Sci Am* 3 Suppl 1: S70-2.

12. Atkins MB, Kunkel L, Sznol M, Rosenberg SA. 2000. High-dose recombinant interleukin-2 therapy in patients with metastatic melanoma: long-term survival update. *Cancer J. Sci. Am.* 6 Suppl 1: S11-4.

13. Margolin KA, Rayner AA, Hawkins MJ, Atkins MB, Dutcher JP, Fisher RI, Weiss GR, Doroshow JH, Jaffe HS, Roper M, et al. 1989. Interleukin-2 and lymphokine-activated killer cell therapy of solid tumors: analysis of toxicity and management guidelines. *J Clin Oncol* 7: 486-98.

14. Siegel JP, Puri RK. 1991. Interleukin-2 toxicity. *J Clin Oncol* 9: 694-704.

15. Mann H, Ward JH, Samlowski WE. 1990. Vascular leak syndrome associated with interleukin-2: chest radiographic manifestations. *Radiology* 176: 191-4.

16. Ognibene FP, Rosenberg SA, Lotze M, Skibber J, Parker MM, Shelhamer JH, Parrillo JE. 1988. Interleukin-2 administration causes reversible hemodynamic changes and left ventricular dysfunction similar to those seen in septic shock. *Chest* 94: 750-4.

17. Panelli MC, White R, Foster M, Martin B, Wang E, Smith K, Marincola FM. 2004. Forecasting the cytokine storm following systemic interleukin (IL)-2 administration. *J Transl Med* 2: 17.

18. Gemlo BT, Palladino MA, Jr., Jaffe HS, Espevik TP, Rayner AA. 1988. Circulating cytokines in patients with metastatic cancer treated with recombinant interleukin 2 and lymphokine-activated killer cells. *Cancer Res* 48: 5864-7.

19. Jablons DM, Mule JJ, McIntosh JK, Sehgal PB, May LT, Huang CM, Rosenberg SA, Lotze MT. 1989. IL-6/IFN-beta-2 as a circulating hormone. Induction by cytokine administration in humans. *J Immunol* 142: 1542-7.

20. Mier JW, Vachino G, van der Meer JW, Numerof RP, Adams S, Cannon JG, Bernheim HA, Atkins MB, Parkinson DR, Dinarello CA. 1988. Induction of circulating tumor necrosis factor (TNF alpha) as the mechanism for the febrile response to interleukin-2 (IL-2) in cancer patients. *J Clin Immunol* 8: 426-36.

21. Schaafsma MR, Falkenburg JH, Landegent JE, Duinkerken N, Osanto S, Ralph P, Kaushansky K, Wagemaker G, Van Damme J, Willemze R, et al. 1991. In vivo production of interleukin-5, granulocyte-macrophage colony-stimulating factor, macrophages colony-stimulating factor, and interleukin-6 during intravenous administration of high-dose interleukin-2 in cancer patients. *Blood* 78: 1981-7.

22. Papa MZ, Vetto JT, Ettinghausen SE, Mule JJ, Rosenberg SA. 1986. Effect of corticosteroid on the antitumor activity of lymphokine-activated killer cells and interleukin 2 in mice. *Cancer Res* 46: 5618-23.

23. Drapier JC, Wietzerbin J, Hibbs JB, Jr. 1988. Interferon-gamma and tumor necrosis factor induce the L-arginine-dependent cytotoxic effector mechanism in murine macrophages. *Eur J Immunol* 18: 1587-92.

24. Amber IJ, Hibbs JB, Jr., Taintor RR, Vavrin Z. 1988. Cytokines induce an L-arginine-dependent effector system in nonmacrophage cells. *J Leukoc Biol* 44: 58-65.

25. Amber IJ, Hibbs JB, Jr., Taintor RR, Vavrin Z. 1988. The L-arginine dependent effector mechanism is induced in murine adenocarcinoma cells by culture supernatant from cytotoxic activated macrophages. *J Leukoc Biol* 43: 187-92.

26. Hibbs JB, Jr., Taintor RR, Vavrin Z. 1987. Macrophage cytotoxicity: role for L-arginine deiminase and imino nitrogen oxidation to nitrite. *Science* 235: 473-6.

27. Marletta MA, Yoon PS, Iyengar R, Leaf CD, Wishnok JS. 1988. Macrophage oxidation of L-arginine to nitrite and nitrate: nitric oxide is an intermediate. *Biochemistry* 27: 8706-11.

28. Hibbs JB, Jr., Westenfelder C, Taintor R, Vavrin Z, Kablitz C, Baranowski RL, Ward JH, Menlove RL, McMurry MP, Kushner JP, et al. 1992. Evidence for cytokine-inducible nitric oxide synthesis from L-arginine in patients receiving interleukin-2 therapy. *J Clin Invest* 89: 867-77.

29. Kondapaneni M, McGregor JR, Salvemini D, Laubach VE, Samlowski WE. 2008. Inducible nitric oxide synthase (iNOS) is not required for IL-2-induced hypotension and vascular leak syndrome in mice. *J Immunother* 31: 325-33.

30. Samlowski WE, Petersen R, Cuzzocrea S, Macarthur H, Burton D, McGregor JR, Salvemini D. 2003. A nonpeptidyl mimic of superoxide dismutase, M40403, inhibits dose-limiting hypotension associated with interleukin-2 and increases its antitumor effects. *Nat Med* 9: 750-5.

31. Denicoff KD, Rubinow DR, Papa MZ, Simpson C, Seipp CA, Lotze MT, Chang AE, Rosenstein D, Rosenberg SA. 1987. The neuropsychiatric effects of treatment with interleukin-2 and lymphokine-activated killer cells. *Ann Intern Med* 107: 293-300.

32. Laubach VE, Shesely EG, Smithies O, Sherman PA. 1995. Mice lacking inducible nitric oxide synthase are not resistant to lipopolysaccharide-induced death. *Proc Natl Acad Sci U S A* 92: 10688-92.

33. Shesely EG, Maeda N, Kim HS, Desai KM, Krege JH, Laubach VE, Sherman PA, Sessa WC, Smithies O. 1996. Elevated blood pressures in mice lacking endothelial nitric oxide synthase. *Proc Natl Acad Sci U S A* 93: 13176-81.

34. Wedzony K, Mackowiak M, Zajaczkowski W, Fijal K, Chocyk A, Czyrak A. 2000. WAY 100135, an antagonist of 5-HT1A serotonin receptors, attenuates psychotomimetic effects of MK-801. *Neuropsychopharmacology* 23: 547-59.

35. Dunham NW, Miya TS. 1957. A note on a simple apparatus for detecting neurological deficit in rats and mice. *J Am Pharm Assoc Am Pharm Assoc (Baltim)* 46: 208-9.

36. Dar MS, Bowman ER, Li C. 1994. Intracerebellar nicotinic-cholinergic participation in the cerebellar adenosinergic modulation of ethanol-induced motor incoordination in mice. *Brain Res* 644: 117-27.

37. Dar MS. 2000. Cerebellar CB(1) receptor mediation of Delta(9)-THC-induced motor incoordination and its potentiation by ethanol and modulation by the cerebellar adenosinergic A(1) receptor in the mouse. *Brain Res* 864: 186-94.

38. Irwan YY, Feng Y, Gach HM, Symanowski JT, McGregor JR, Veni G, Schabel M, Samlowski WE. 2009. Quantitative analysis of cytokine-induced vascular toxicity and vascular leak in the mouse brain. *J Immunol Methods*

39. Samlowski WE, Petersen R, McGregor JR, Kondapaneni M, Salvemini D. 2005. Evaluation of a Superoxide Dismutase Mimetic As an Adjunct to Interleukin 2 Based Cancer Therapy. In *Therapeutic Application of Superoxide Dismutase (SOD)*, ed. D Salvemini, S Cuzzocrea, pp. 1-20: Eurekah.com.

40. Brenner BM, Troy JL, Ballermann BJ. 1989. Endothelium-dependent vascular responses. Mediators and mechanisms. *J Clin Invest* 84: 1373-8.

41. Vallance P, Collier J, Moncada S. 1989. Effects of endothelium-derived nitric oxide on peripheral arteriolar tone in man. *Lancet* 2: 997-1000.

42. Torfgard KE, Ahlner J. 1994. Mechanisms of action of nitrates. *Cardiovasc Drugs Ther* 8: 701-17.

43. Dorr A, Sled JG, Kabani N. 2007. Three-dimensional cerebral vasculature of the CBA mouse brain: a magnetic resonance imaging and micro computed tomography study. *Neuroimage* 35: 1409-23.

44. Knopp MV, Giesel FL, Marcos H, von Tengg-Kobligk H, Choyke P. 2001. Dynamic contrast-enhanced magnetic resonance imaging in oncology. *Top Magn Reson Imaging* 12: 301-8.

45. Padhani AR. 2003. MRI for assessing antivascular cancer treatments. *Br J Radiol* 76 Spec No 1: S60-80.

46. Daldrup H, Shames DM, Wendland M, Okuhata Y, Link TM, Rosenau W, Lu Y, Brasch RC. 1998. Correlation of dynamic contrast-enhanced magnetic resonance imaging with histologic tumor grade: comparison of macromolecular and small-molecular contrast media. *Pediatr Radiol* 28: 67-78.

47. Feng Y, Jeong EK, Mohs AM, Emerson L, Lu ZR. 2008. Characterization of tumor angiogenesis with dynamic contrast-enhanced MRI and biodegradable macromolecular contrast agents in mice. *Magn Reson Med* 60: 1347-52.

48. Ettinghausen SE, Rosenberg SA. 1986. Immunotherapy of murine sarcomas using lymphokine activated killer cells: optimization of the schedule and route of administration of recombinant interleukin-2. *Cancer Res* 46: 2784-92.

49. Yang JC, Sherry RM, Steinberg SM, Topalian SL, Schwartzentruber DJ, Hwu P, Seipp CA, Rogers-Freezer L, Morton KE, White DE, Liewehr DJ, Merino MJ, Rosenberg SA. 2003. Randomized study of high-dose and low-dose interleukin-2 in patients with metastatic renal cancer. *J Clin Oncol* 21: 3127-32.

50. Saris SC, Patronas NJ, Rosenberg SA, Alexander JT, Frank J, Schwartzentruber DJ, Rubin JT, Barba D, Oldfield EH. 1989. The effect of intravenous interleukin-2 on brain water content. *J Neurosurg* 71: 169-74.

51. Ellison MD, Povlishock JT, Merchant RE. 1987. Blood-brain barrier dysfunction in cats following recombinant interleukin-2 infusion. *Cancer Res* 47: 5765-70.

52. Watts RG, Wright JL, Atkinson LL, Merchant RE. 1989. Histopathological and blood-brain barrier changes in rats induced by an intracerebral injection of human recombinant interleukin 2. *Neurosurgery* 25: 202-8.

53. Alexander JT, Saris SC, Oldfield EH. 1989. The effect of interleukin-2 on the blood-brain barrier in the 9L gliosarcoma rat model. *J Neurosurg* 70: 92-6.

54. Yim CY, McGregor JR, Kwon OD, Bastian NR, Rees M, Mori M, Hibbs JB, Jr., Samlowski WE. 1995. Nitric oxide synthesis contributes to IL-2-induced antitumor responses against intraperitoneal Meth A tumor. *J Immunol* 155: 4382-90.

55. Samlowski WE. 2001. Nitric oxide as a mediator of interleukin-2 induced cardiovascular toxicity and antitumor activity. In *Nitric Oxide and Inflammation*, ed. D Salvemini, TR Billiar, Y Vodovotz, pp. 249-72. Basel/Switzerland: Birkhäuser Verlag.

56. Moore WM, Webber RK, Jerome GM, Tjoeng FS, Misko TP, Currie MG. 1994. L-N6-(1-iminoethyl)lysine: a selective inhibitor of inducible nitric oxide synthase. *J Med Chem* 37: 3886-8.

57. Beauchesne E, Desjardins P, Hazell AS, Butterworth RF. 2009. eNOS gene deletion restores blood-brain barrier integrity and attenuates neurodegeneration in the thiamine-deficient mouse brain. *J Neurochem*

58. Martin S, Maruta K, Burkart V, Gillis S, Kolb H. 1988. IL-1 and IFN-gamma increase vascular permeability. *Immunology* 64: 301-5.

59. Maruo N, Morita I, Shirao M, Murota S. 1992. IL-6 increases endothelial permeability in vitro. *Endocrinology* 131: 710-4.

60. Nooteboom A, Van Der Linden CJ, Hendriks T. 2002. Tumor necrosis factor-alpha and interleukin-1beta mediate endothelial permeability induced by lipopolysaccharide-stimulated whole blood. *Crit Care Med* 30: 2063-8.

CHAPTER 4

DISCUSSION

Despite other currently available chemotherapy for metastatic melanoma and renal cell carcinoma (1-2), IL-2 is the only agent that can induce durable complete remissions in approximately 5-10% of patients with these cancers (3-4). Unfortunately, IL-2-induced cardiovascular and neuropsychiatric toxicities (5-7) limit the administration of high dose IL-2 required to achieve complete remissions. While the cardiovascular toxicities can be attenuated in patients by administration of pressor agents and fluid, the neuropsychiatric toxicity can only be managed by holding further doses of IL-2. Studies using a nonpeptidyl mimic of O_2^- dismutase, NOS inhibitors, and NOS knockout mice have shed some light on the mechanisms involved in IL-2-induced hypotension and VLS (8-10). On the other hand, the pathophysiology of IL-2-induced neuropsychiatric toxicity was previously unclear.

Previous studies attempting to look at the effects of IL-2 in the CNS have suggested an increase in BBB permeability and therefore brain edema (11-14). However, some of these results are questionable. Further attempts to delineate IL-2-induced neuropsychiatric toxicity have been limited mostly by the availability of suitable experimental techniques. Therefore, we first evaluated and developed a number of potential experimental methods that could quantify cerebrovascular changes in an established murine IL-2 treatment model (8, 15). Our evaluations showed that assays quantifying changes in the mouse brain interstitial fluid following IL-2 treatment (i.e. wet versus dry brain weight, MRI proton density measurement, and quantification of radioactive labeled [^{125}I]-bovine serum albumin, tritiated water, or fluorescence marker), were not informative due to lack of sensitivity to accurately measure the small changes in the mouse brain water content. Two successful methods identified include DCE MRI and

quantitative analysis of the mouse brain blood vessels dual-stained with isolectin GS-IB_4 and an antibody to von Willebrand factor. The data demonstrated that IL-2 induced vasodilation and microvascular permeability in the mid-brain section containing the cerebral cortex and striatum, which correlate with cognitive and behavioral changes.

Previous data in our lab have shown that by day 4 and 5 following IL-2 treatment, IL-2 treated mice have a blood pressure of < 40 mmHg (16) and a significantly decreased serum albumin (unpublished), resulting in low hydrostatic and osmotic pressures within the vasculature. Thus, the increase of contrast agent in the IL-2 treated mouse brain detected by DCE MRI is not likely due to a hydrostatic pressure-induced filtration, as decreased systolic pressure should decrease these forces. In the presence of decreased hydrostatic pressure, the only way to fully account for the identified changes is an increase in BBB permeability acting in concert with decreased osmotic forces. As the contrast agent was injected gently by hand during all DCE MRI procedures through a thin bore tube that is not amenable to high injection pressures, artifact changes seem unlikely. A high-pressure automatic injector device (pump), such as usually used in patients, was not used.

Using a behavior monitoring system, we established that IL-2 treated mice exhibited behavioral changes, suggesting that IL-2 affects the CNS in a similar fashion in the murine model as in IL-2 treated patients. The behavioral changes in C3H/HeN mice were observed as early as day 2 (after 4 doses of 180,000 IU IL-2 i.p., b.i.d) following IL-2 treatment. This occurred long before the onset of severe motor impairment observed on day 4 when IL-2 treated mice are known to be profoundly hypotensive (16). These data indicate that decreases in the spontaneous behavior of these mice are not due to the

mice being too sick to move and that IL-2 affects the CNS via a different time course than the systemic cardiovascular toxicities of IL-2.

As NO derived from endothelial cells or pharmacologic donors is known to induce peripheral vasodilation and is thought to contribute to vascular permeability changes (17-19), we evaluated its role in the IL-2-induced vasodilation and microvascular permeability in the CNS using the immunohistochemistry and DCE MRI techniques. The results of these experiments established that IL-2-induced vasodilation and microvascular permeability were abrogated in $eNOS^{-/-}$ mice, demonstrating a causal role of this enzyme in IL-2-induced brain vasculature changes. These data are consistent with the crucial role of eNOS in IL-2-induced systemic cardiovascular toxicities (10). Interestingly, $iNOS^{-/-}$ mice still developed vasodilation following IL-2 treatment, but not microvascular permeability, suggesting that iNOS also plays a role in IL-2 induced microvascular permeability in the brain.

IL-2 is unique as it induces a transient autocrine feedback loop in T and NK lymphocytes, further increasing IL-2 synthesis. This result in a marked induction of a 'cytokine storm' (20), which is thought to mediate IL-2-induced dose-limiting toxicities. However, questions remain whether IL-2 induces effects on the vasculature by binding directly onto IL-2 receptor (IL-2R) on the endothelial cells or indirectly via IL-2R on the leukocytes. There are several studies that suggest low level expression of IL-2R on endothelial cells. The functional relevance is currently poorly understood. We have performed preliminary experiments employing mice with homologous recombination in the IL-2Rα ($CD25^{-/-}$). These mice are resistant to induction of IL-2 induced hypotension (Fig. 4.1). These data do not explain whether this is a result of a decrease in the cytokine

Figure 4.1

Assessment of whether IL-2 induces hypotension via IL-2 receptor (IL-2R) expression on endothelial cells or leukocytes. C57/Bl6 WT and IL-2R$\alpha^{-/-}$ mice (back-crossed onto a C57/Bl6 background, not 100% chimeras) were treated with 1 mg Ciprofloxacin i.p. once a day for 2 days followed by 25 mg/kg Busulfan i.p. once a day for 6 days to ablate endogenous bone marrow. Ciprofloxacin (0.18 mg/ml) was also added into the drinking water during the duration of the experiment. Two days after the last dose of Busulfan, $2x10^6$ syngeneic bone marrow cells were transferred into each mouse i.v. via the tail vein. Mice were allowed to reconstitute normal bone marrow function for 1 month. At this time, the hemato-immune cells in transplant recipient were predominantly of bone marrow donor origin, while the endothelium was of host derivation. C57/Bl6 WT, IL-2R$\alpha^{-/-}$, WT mice transplanted with bone marrow (BM) from either WT (WT/WTBM) or IL-2R$\alpha^{-/-}$ mice (WT/KOBM), and IL-2R$\alpha^{-/-}$ mice transplanted with WT bone marrow (KO/WTBM) (n = 3) were treated with 800,000 IU IL-2 i.p., b.i.d. for 5 days. On day 5, the blood pressure of each mouse was measured via tail cuff method (Stoelting, Wood Dell, IL) using PowerLab digital signal transducer (AD instruments, Mountain View, CA). Pulse and blood pressures were recorded onto a computer and analyzed using Chart 3.6.1 software (AD instruments) to obtain systolic blood pressure of each mouse. Results are expressed as mean±SEM. The statistics were analyzed using 2-sample Student's 2-tailed t-test. A p-value ≤ 0.05 was considered significant and is indicated on the graph.

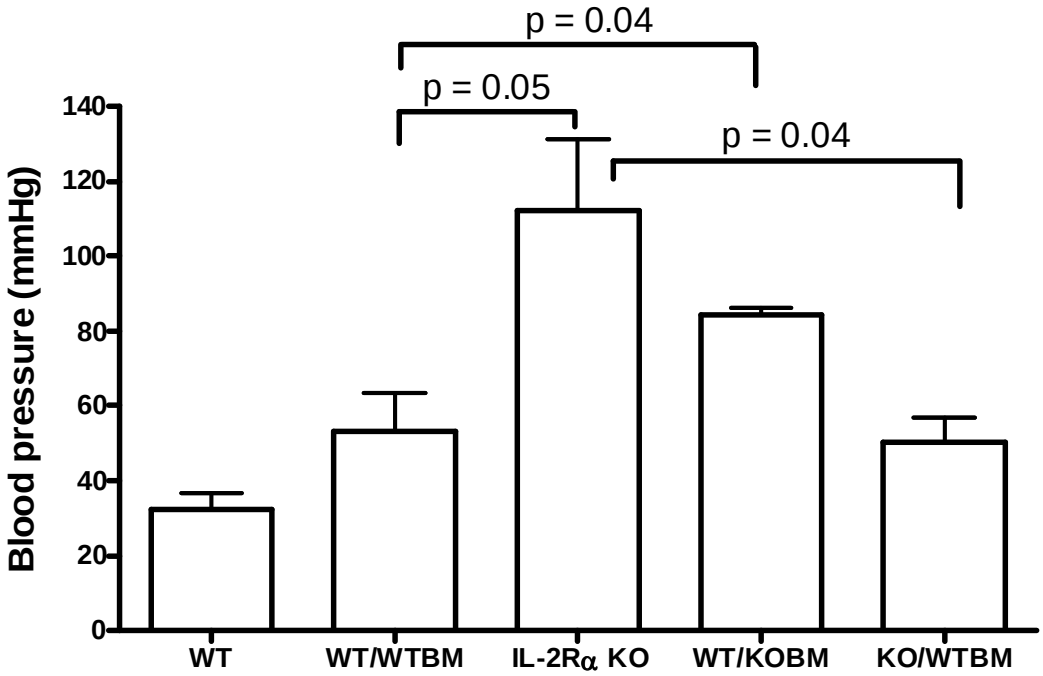
p = 0.04
p = 0.05
p = 0.04
Blood pressure (mmHg)
140
120
100
80
60
40
20
0
WT
WT/WTBM
IL-2Rα KO
WT/KOBM
KO/WTBM

storm or in endothelial responsiveness. We therefore performed a transplant experiment to create chimeric mice. The results suggest that the presence of IL-2Rα on the immune cells, but not endothelial cells, is essential for IL-2-induced hypotension in mice (Fig. 4.1).

Surprisingly, $eNOS^{-/-}$ mice still exhibited substantial behavioral changes following IL-2 treatment although these changes were attenuated compared to the WT and $iNOS^{-/-}$ mice. Administration of LNIL, a specific inhibitor of iNOS (21), to $eNOS^{-/-}$ failed to prevent IL-2-induced behavioral changes, indicating an additional mechanisms are likely to be involved in IL-2-induced neuropsychiatric changes. Furthermore, our DCE MRI data showed no significant changes in f^{PV}, K^{PS}, and PS values in C3H/HeN mice on day 3 of IL-2 treatment (Fig. 4.2), whereas the behavioral changes were observed as early as day 2 in these mice. These data suggest that IL-2-induced behavior and cognitive changes occurred before detectable IL-2 induced vasodilation and microvascular permeability. We hypothesize that excitatory neurotransmitters may also be increased in the brain following IL-2 treatment and may contribute to the neuropsychiatric toxicity observed at early time points during IL-2 treatment while the eNOS-mediated vasodilation and microvascular permeability in the CNS are likely to exacerbate this toxicity by days 4 and 5. The excitatory neurotransmitters may account for the frequent agitation, hallucinations, and delusions seen in human IL-2 treated patients. This possibility will require further investigation.

Collectively, this study provides the tools to evaluate other situations that result in cytokine-induced neuropsychiatric toxicity, i.e., sepsis or therapy with other inflammatory cytokines (i.e. IFNγ or TNFα). Further delineation of the signaling

Figure 4.2

DCE MRI following 3 days of IL-2 treatment (6 doses of 150,000 IU i.p., b.i.d.) to evaluate early changes in vasodilation and microvascular permeability induced by IL-2 in the brain. C3H/HeN mice (n = 5) were scanned both before and after 3 days of IL-2 treatment using T_1-weighted 2D-FLASH MRI sequence (TE/TR = 3.06 ms/84.992 ms, flip angle = 40º, slice thickness = 1 mm, number of slices = 10, field of view = 2 x 2 cm, matrix = 128 x 128 pixels, a single scan time = 8.159 s, number of repetitions = 60). After baseline imaging, 0.1 mmol/kg of gadobenate dimeglumine (MultiHance®, Bracco) was administered by bolus injection via tail vein catheterization. Customized MATLAB programs were used to measure signal intensities from manually drawn ROI on a selected 1-mm mid-brain section of each mouse. The left and right maxillary veins were averaged to derive the contrast agent concentration in the blood pool and a two-compartment model was used to calculate A) fractional plasma volume (f^{PV}), B) endothelium transfer coefficient (K^{PS}), and C) permeability surface area product (PS). Results are expressed as mean±SEM. Statistical analysis was performed using paired Student's 2-tailed t-test using GraphPad PRISM software and the p-values are shown. A p-value ≤ 0.05 was considered significant.

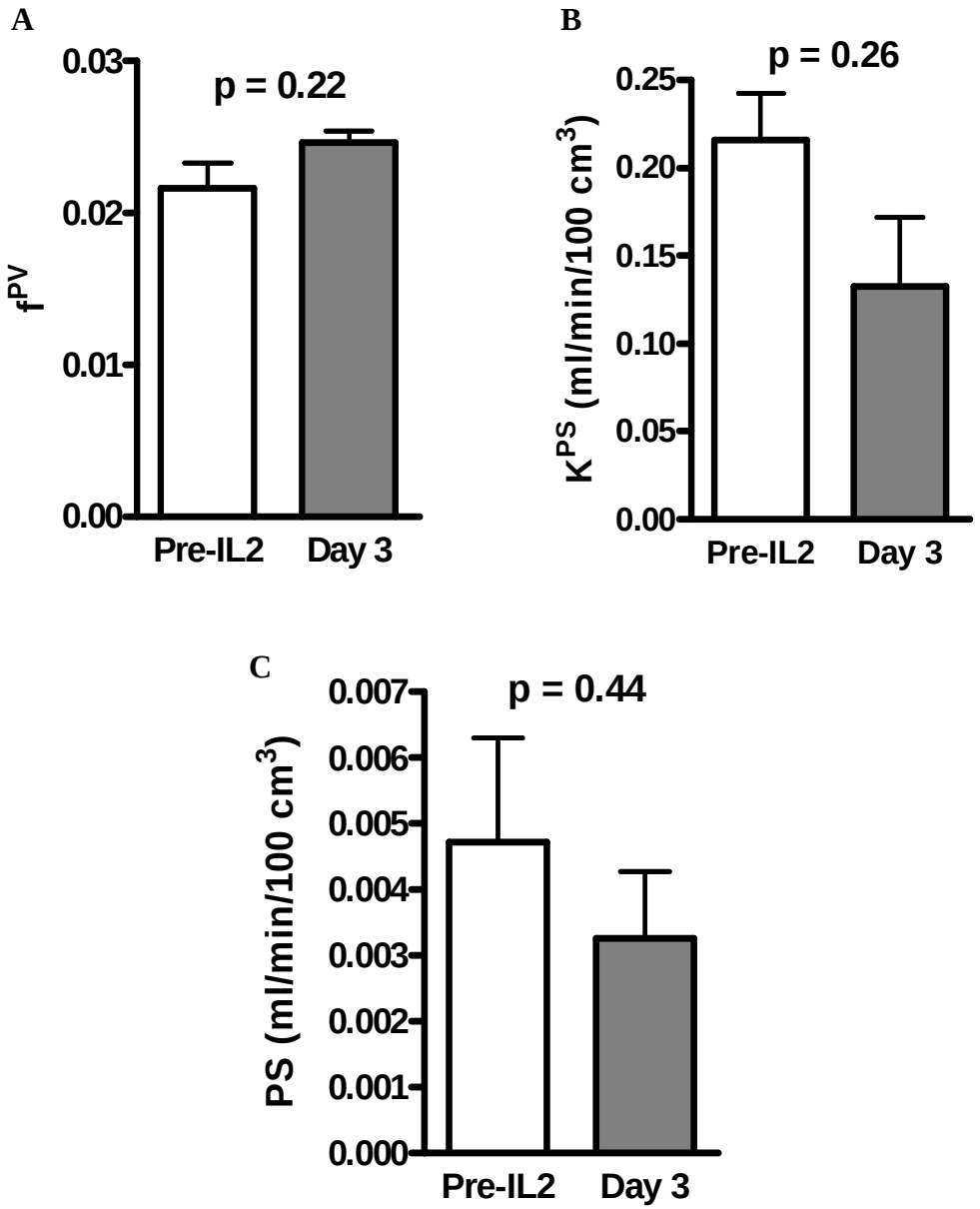
A
p = 0.22
0.03
0.02
0.01
0.00
f^{PV}
Pre-IL2
Day 3
B
p = 0.26
0.25
0.20
0.15
0.10
0.05
0.00
K^{PS} (ml/min/100 cm^3)
Pre-IL2
Day 3
C
p = 0.44
0.007
0.006
0.005
0.004
0.003
0.002
0.001
0.000
PS (ml/min/100 cm^3)
Pre-IL2
Day 3

pathways upstream or downstream of eNOS that contribute to IL-2-induced vasodilation and microvascular permeability in the CNS is also feasible using these experimental methods. A longer-term goal of this line of investigation is to develop a more complete understanding of the mechanisms involved in IL-2-induced neuropsychiatric toxicity. This will be important to allow identification of pharmacologic inhibitors that block this toxicity in patients. Blockade of IL-2 induced cardiovascular and neurologic toxicities may enable dose escalation of IL-2 in human patients and may allow more patients to achieve complete and long-term remissions of otherwise incurable cancers.

References

1. Menard D, Niculescu-Duvaz I, Dijkstra HP, Niculescu-Duvaz D, Suijkerbuijk BM, Zambon A, Nourry A, Roman E, Davies L, Manne HA, Friedlos F, Kirk R, Whittaker S, Gill A, Taylor RD, Marais R, Springer CJ. 2009. Novel potent BRAF inhibitors: toward 1 nM compounds through optimization of the central phenyl ring. *J Med Chem* 52: 3881-91.

2. Samlowski WE, Wong B, Vogelzang NJ. 2008. Management of renal cancer in the tyrosine kinase inhibitor era: a view from 3 years on. *BJU Int* 102: 162-5.

3. Atkins MB, Kunkel L, Sznol M, Rosenberg SA. 2000. High-dose recombinant interleukin-2 therapy in patients with metastatic melanoma: long-term survival update. *Cancer J. Sci. Am.* 6 Suppl 1: S11-4.

4. Fisher RI, Rosenberg SA, Sznol M, Parkinson DR, Fyfe G. 1997. High-dose aldesleukin in renal cell carcinoma: long-term survival update. *Cancer J Sci Am* 3 Suppl 1: S70-2.

5. Siegel JP, Puri RK. 1991. Interleukin-2 toxicity. *J Clin Oncol* 9: 694-704.

6. Margolin KA, Rayner AA, Hawkins MJ, Atkins MB, Dutcher JP, Fisher RI, Weiss GR, Doroshow JH, Jaffe HS, Roper M, et al. 1989. Interleukin-2 and lymphokine-activated killer cell therapy of solid tumors: analysis of toxicity and management guidelines. *J Clin Oncol* 7: 486-98.

7. Denicoff KD, Rubinow DR, Papa MZ, Simpson C, Seipp CA, Lotze MT, Chang AE, Rosenstein D, Rosenberg SA. 1987. The neuropsychiatric effects of treatment

with interleukin-2 and lymphokine-activated killer cells. *Ann Intern Med* 107: 293-300.

8. Samlowski WE, Petersen R, Cuzzocrea S, Macarthur H, Burton D, McGregor JR, Salvemini D. 2003. A nonpeptidyl mimic of superoxide dismutase, M40403, inhibits dose-limiting hypotension associated with interleukin-2 and increases its antitumor effects. *Nat Med* 9: 750-5.

9. Samlowski WE. 2001. Nitric oxide as a mediator of interleukin-2 induced cardiovascular toxicity and antitumor activity. In *Nitric Oxide and Inflammation*, ed. D Salvemini, TR Billiar, Y Vodovotz, pp. 249-72. Basel/Switzerland: Birkhäuser Verlag.

10. Kondapaneni M, McGregor JR, Salvemini D, Laubach VE, Samlowski WE. 2008. Inducible nitric oxide synthase (iNOS) is not required for IL-2-induced hypotension and vascular leak syndrome in mice. *J Immunother* 31: 325-33.

11. Ellison MD, Povlishock JT, Merchant RE. 1987. Blood-brain barrier dysfunction in cats following recombinant interleukin-2 infusion. *Cancer Res* 47: 5765-70.

12. Saris SC, Patronas NJ, Rosenberg SA, Alexander JT, Frank J, Schwartzentruber DJ, Rubin JT, Barba D, Oldfield EH. 1989. The effect of intravenous interleukin-2 on brain water content. *J. Neurosurg.* 71: 169-74.

13. Watts RG, Wright JL, Atkinson LL, Merchant RE. 1989. Histopathological and blood-brain barrier changes in rats induced by an intracerebral injection of human recombinant interleukin 2. *Neurosurgery* 25: 202-8.

14. Alexander JT, Saris SC, Oldfield EH. 1989. The effect of interleukin-2 on the blood-brain barrier in the 9L gliosarcoma rat model. *J Neurosurg* 70: 92-6.

15. Yim CY, McGregor JR, Kwon OD, Bastian NR, Rees M, Mori M, Hibbs JB, Jr., Samlowski WE. 1995. Nitric oxide synthesis contributes to IL-2-induced antitumor responses against intraperitoneal Meth A tumor. *J Immunol* 155: 4382-90.

16. Samlowski WE, Petersen R, McGregor JR, Kondapaneni M, Salvemini D. 2005. Evaluation of a Superoxide Dismutase Mimetic As an Adjunct to Interleukin 2 Based Cancer Therapy. In *Therapeutic Application of Superoxide Dismutase (SOD)*, ed. D Salvemini, S Cuzzocrea, pp. 1-20: Eurekah.com.

17. Brenner BM, Troy JL, Ballermann BJ. 1989. Endothelium-dependent vascular responses. Mediators and mechanisms. *J Clin Invest* 84: 1373-8.

18. Vallance P, Collier J, Moncada S. 1989. Effects of endothelium-derived nitric oxide on peripheral arteriolar tone in man. *Lancet* 2: 997-1000.

19. Torfgard KE, Ahlner J. 1994. Mechanisms of action of nitrates. *Cardiovasc Drugs Ther* 8: 701-17.

20. Panelli MC, White R, Foster M, Martin B, Wang E, Smith K, Marincola FM. 2004. Forecasting the cytokine storm following systemic interleukin (IL)-2 administration. *J Transl Med* 2: 17.

21. Moore WM, Webber RK, Jerome GM, Tjoeng FS, Misko TP, Currie MG. 1994. L-N6-(1-iminoethyl)lysine: a selective inhibitor of inducible nitric oxide synthase. *J Med Chem* 37: 3886-8.